LIGHT-INDUCED MASS MOTION: AN ATOMIC FORCE MICROSCOPY STUDY AND A RANDOM-WALK MODEL

Boris Bellini

UNIVERSITE DE LA MEDITERRANEE – AIX-MARSEILLE II

CENTRE DE RECHERCHE EN MATIERE CONDENSEE ET NANOSCIENCES

MOUVEMENT PHOTO-INDUIT : ETUDE EN MICROSCOPIE A FORCE ATOMIQUE ET MODELISATION PAR UNE MARCHE ALEATOIRE

THESE

présentée par

BORIS BELLINI

en vue d'obtenir le grade de

Docteur de l'Université de la Méditerranée

Spécialité : Sciences des Matériaux

Soutenue le 11 juillet 2005 devant le jury composé de :

Directeur de thèse : M. PHILIPPE DUMAS, Professeur

Président du jury : M. MICHEL DYAKONOV, Professeur

Rapporteur : M. YANNICK DE WILDE, Chargé de Recherche

Rapporteur : M. TOMAS LOPEZ-RIOS, Directeur de Recherche

Rapporteur : M. JACQUES PERETTI, Chargé de Recherche

Abstract. First evidenced in 1995, the light-induced mass motion in layers of azobenzene-containing molecules remains partly unexplained. Although it is agreed that the isomerization of the azobenzene function triggers the phenomenon, it has led to diverging interpretations: some view it as an individual process where each molecule is independently put in motion, others as a collective one.
In this memoir, as a contribution to the study of this mass motion, we discuss a light-driven random-walk model where each moving azobenzene function drags the molecule to which it is grafted.
The experimental part of this work lies on atomic force microscopy measurements of the light-induced deformations and on the study of the evolution of the absorption properties of the layers of azobenzene-containing molecules. These results allow us to draw the main characteristics of the phenomenon. We also evidence the bleaching of the azobenzene chromophores which is bound to limit the mass motion.
The theoretical section that follows starts with a presentation of the hypotheses of the model. It consists in a diffusion motion of the azobenzene functions where each random step follows an isomerising absorption
Applied to the environment of layers, as resorted to experimentally, this model provides a suitable description of the light-induced surface deformations experimentally observed.
In the frame of this model, we assess the distance over which an azobenzene-containing molecule can be dragged. We also estimate the energetic output of this dragging process.
Finally, we discuss the microscopic origin of these molecular motors and we compare it to the model of thermal ratchets which are extensively resorted to in Biology nowadays.

Key words: light-induced mass motion, azobenzene, molecular motors, atomic force microscopy, photo-bleaching, random-walk.

Résumé. Mis en évidence en 1995, le mouvement de matière photo-induit qui est observé dans des couches de molécules contenant la fonction azobenzène reste en partie mal compris. Bien que tous s'accordent à penser que l'isomérisation de la fonction azobenzène en est le facteur déclencheur, son interprétation suscite des interprétations divergentes : certains l'envisagent comme un mouvement individuel, d'autres comme un phénomène collectif.
Dans ce mémoire de thèse, nous proposons et discutons un modèle de marche aléatoire piloté par la lumière dans lequel la fonction azobenzène entraîne dans son mouvement la molécule à laquelle elle est attachée.
La partie expérimentale de ce travail repose sur des mesures en microscopie à force atomique des déformations photo-induites et sur l'étude de l'évolution des propriétés d'absorption des azo-molécules. Elle permet ainsi de dégager les principales caractéristiques du mouvement. Nous mettons également en évidence le phénomène de photo-blanchiment des fonctions azobenzène
La partie théorique commence par une présentation des hypothèses du modèle. Il s'agit d'un mouvement de diffusion pour lequel chaque pas de la marche aléatoire de la fonction azobenzène est induit par une absorption. Appliqué aux conditions expérimentales utilisées, c'est-à-dire à des couches de molécules, ce modèle rend compte de façon satisfaisante des déformations photo-induites observées.
Dans le cadre de ce modèle, et tenant compte de la durée d'activité optique des chromophores, nous estimons la distance sur laquelle peut être déplacée une molécule dotée d'une fonction azobenzène.
Nous discutons également l'origine microscopique de ce moteur moléculaire en le comparant au cliquet thermique largement utilisé par les biologistes.

Mots clés: mouvement de matière photo-induit, azobenzène, moteur moléculaire, microscopie à force atomique, photo-blanchiment, marche aléatoire.

REMERCIEMENTS

Je souhaite d'abord exprimer toute ma reconnaissance à mon directeur de thèse, le Professeur Philippe Dumas, pour l'attention avec laquelle il a encadré ce travail, les nombreux conseils qu'il m'a dispensés, ainsi que pour sa grande disponibilité.
Sa prodigalité à partager sa culture scientifique et ses grandes qualités humaines ont fait des années que j'ai passées dans son équipe une experience des plus enrichissantes.
Je remercie les membres du jury d'avoir accepté de juger ce travail. Ainsi, j'adresse l'expression de ma respectueuse reconnaissance au Professeur Michel Dyakonov du Laboratoire de Physique Théorique et Astroparticules de l'Université de Montpellier II ; au Docteur Yannick de Wilde, Chargé de Recherche au Laboratoire d'Optique Physique de l'Ecole Supérieure de Physique et de Chimie Industrielles ; au Docteur Tomás Lopez-Rios, Directeur de Recherche au Laboratoire d'Etudes des Propriétés Electroniques des Solides de Grenoble ainsi qu'au Docteur Jacques Peretti, Chargé de Recherches au Laboratoire de Physique de la Matière Condensée de l'Ecole Polytechnique.
Je tiens à remercier le Professeur Viatcheslav Safarov de m'avoir accueilli au sein du Centre de Recherches en Matière Condensée et Nanomatériaux dont il assure la direction. Je lui sais également gré de l'intérêt qu'il a porté au déroulement de mon travail de thèse.
Un grand merci, également, au Docteur Carole Fauquet, Maître de Conférences, qui a été mon tuteur d'enseignement au cours de mes trois années de Monitorat. Ses conseils ainsi que son engagement dans son activité d'enseignement sont pour moi des modèles précieux pour ma future carrière d'enseignant.
Je tiens également à exprimer ma reconnaissance aux Docteurs Hubert Klein et Petar Vidakovic pour le temps qu'ils ont accordé à toutes mes questions.
Je remercie chaleureusement les Docteurs Jorg Ackermann et Christian Grave qui ont successivement travaillé dans l'équipe du Professeur Philippe Dumas en qualité de post-doctorants. Ce travail doit beaucoup à leurs compétences d'expérimentateurs.
Toute l'expression de ma gratitude va également aux Docteurs Wladimir Marine et Bernard Tinland pour le materiel prêté dans un moment de transition où l'attente de commandes aurait ralenti ce travail.
Je tiens à remercier Monsieur Philippe Bindzi ainsi que les membres de l'atelier, Messieurs Gérard Incerti et Marcel Fernandez pour leur disponibilité et la qualité de leur travail.
Les dispositifs expérimentaux sur lesquels nous avons travaillé et leur exploitation doivent aussi beaucoup aux réalisations d'électronique de Messieurs Franck Jandard et Mohammed Cherriguène ainsi qu'aux compétences en informatique de Monsieur Bruno Gély.
Plus largement, j'adresse mes remerciements à tous les membres du CRMCN pour leur accueil et la sympathie dont ils ont fait montre au cours de ces années passées parmi eux.

AVERTISSEMENT

Ce mémoire de thèse a été rédigé en langue anglaise.

Il est précédé d'un résumé de trente quatre pages en langue française.

TABLE OF CONTENTS

RESUME.

Le mouvement photo-induit de certaines familles de molécules à été mis en évidence il y a une dizaine d'années[1,2].
En effet, des couches plates de quelques centaines de nanomètres d'épaisseur éclairées par une longueur d'onde appropriée se déforment de façon significative : la corrugation peut atteindre une amplitude de plus de la moitié de l'épaisseur initiale.
Ce déplacement de molécules, contrôlé par la lumière, présente un intérêt tant fondamental que pratique.
En effet, d'un point de vue théorique, le déplacement photo-induit de matière est encore mal compris, tant par le mécanisme qui le régit que dans sa nature même : ces molécules sont elles mues individuellement ou collectivement ?
Quant aux applications ambitionnées, elles sont de taille : le développement des nanotechnologies, qui met en œuvre une architecture complexe à des échelles où la manipulation de molécules est délicate, s'enrichirait d'une telle perspective de contrôle de ses constituants ainsi que de la possibilité de stocker, à l'échelle d'une molécule, une information lumineuse reçue.

Mon travail de thèse s'inscrit dans le cadre d'une coopération européenne sur le thème du mouvement photo-induit : LIMM (Light Induced Molecular Motion). Il repose sur l'étude expérimentale et la modélisation du déplacement de matière induit par la raie à λ=473 nm d'un laser à faible intensité (15 mW / 10 mm^2) dans des couches de polymères ou de dendrimères dotés de fonctions azobenzène.
Si les premiers ont été largement étudiés depuis une dizaine d'années, les seconds n'ont fait l'objet que de quelques études de déplacement de matière[3]. Néanmoins, permettant de s'affranchir de phénomènes parasites rencontrés avec les polymères, les dendrimères permettent d'envisager à terme une meilleure compréhension des phénomènes.
Ces couches se déforment sous l'effet d'un laser de faible intensité et témoignent d'un mouvement de masse des zones les plus éclairées vers les plus sombres.
Dix ans après la mise en évidence de ce phénomène, son origine est encore mal comprise. L'intensité étant faible, les hypothèses d'ablation ou d'élévation de température doivent être écartés. Comme nous allons le voir, certains modèles le décrivent comme un processus individuel, d'autres comme un processus collectif. En revanche, tous s'accordent sur le facteur déclenchant de ce déplacement : il s'agit de l'isomérisation de la fonction azobenzène sous l'effet de la longueur d'onde appropriée.

A travers ce mémoire, nous proposons et discutons une interprétation de ce phénomène qui s'appuie sur un travail expérimental.
Cette interprétation repose sur l'hypothèse d'un mouvement individuel, perspective s'inscrivant dans l'actualité de l'activité de recherche de l'équipe dans laquelle j'ai travaillé.

Pour présenter le travail effectué et les résultats obtenus, nous nous proposons de suivre le cheminement qui suit.
Avant toute hypothèse sur la nature du mouvement, il convient de consacrer un premier chapitre aux différentes interprétations proposées, en distinguant entre celles de type « mouvement individuel » et celles de type « mouvement collectif ».
Puis nous exposons nos choix expérimentaux : les molécules étudiées déposées en couches fines par spin-coating ainsi que les dispositifs permettant de suivre le mouvement de matière.
Nous présentons ensuite nos résultats expérimentaux qui permettent de dégager les caractéristiques essentielles du phénomène et les paramètres pertinents qui le régissent.

---

[1] Rochon, P. ; Mao, J. ; Natansohn, A. ; Batalla E. *Polymer. Prepr.* **1994**, *35*, 154.
[2] Rochon, P. ; Batalla E.; Natansohn, A. *Appl. Phys. Lett.* **1995**, *66*, 136.
[3] Archut, A. ; Vogtle, F. ; Cola, L. D. ; Azzellini, G. C. ; Balzani, V. ; Ramanujam, P. S. ; Berg, R. *Chem. Eur. J.* **1998**, *4*, 169.

Ainsi, dans un quatrième chapitre, nous pouvons proposer un modèle de mouvement photo-induit et le confronter aux résultats expérimentaux afin de discuter la possibilité d'un mouvement individuel.
Enfin, il convient de conclure en soulignant la complexité du phénomène étudié que nous n'avions pas soupçonnée en commençant le travail présenté ici: nous avions entrepris les premières expériences avec l'ambition de reproduire ce qui était rapporté dans la littérature puis d'obtenir une série de résultats quantitatifs. Progressivement, nos observations expérimentales nous ont conduit à redéfinir les limites de notre compréhension du (des) phénomène(s) à l'œuvre. Elles nous amènent ainsi à repenser le modèle et à suggérer des pistes de recherche.

I. Mécanisme du mouvement photo-induit : des points de vue divergents.

L'orientation photo-induite des chromophores d'azobenzène dans les azo-polymères a été observée pour la première fois dans les années 1960[4] et a conduit à de nombreux travaux pratiques et théoriques sur l'anisotropie photo-induite.

I.1. Modèles de type « mouvement collectif ».

Barret et al, qui ont été parmi les premiers[1] à rendre compte du mouvement photo-induit dans certaines couches d'azopolymères, ont proposé une interprétation fondée sur le changement du volume libre nécessaire à l'endroit où la lumière induit l'isomérisation des azobenzène[5]. Le passage de la forme trans à la forme cis s'accompagne d'une augmentation du volume libre requis autour du chromophore. L'insuffisance de volume libre conduit à une augmentation de la pression locale qui dépasse la pression de rupture. La couche de polymère est alors décrite comme un fluide visqueux, siège d'un mouvement de matière sous l'effet d'un gradient de pression.
Dans ce mécanisme, le mouvement est déclenché par l'isomérisation mais il ne se produit que parce qu'il y a un ensemble de molécules et une variation des propriétés mésoscopiques de la couche. Barret[6] et al ont ensuite rendu le modèle quantitatif par le recours aux équations de l'hydrodynamique. S'il permet de rendre compte de l'effet de la plupart des paramètres de l'éclairage qui induit le mouvement, il ne permet pas d'expliquer l'effet pourtant remarquable de la polarisation de la lumière: comme nous le verrons au paragraphe III.2.b., l'état de polarisation est déterminant dans la possibilité d'induire un mouvement de masse.

Pedersen et al décrivent le mouvement de masse dans le cadre d'une théorie de champ moyen[7]. Selon eux, les chromophores s'orientent au cours de la photo-isomérisation, définissant un ordre local. Chaque chromophore est alors soumis au champ moyen des chromophores voisins qui tendent à l'orienter selon la direction privilégiée locale. Dans ce modèle, c'est le gradient d'ordre local qui pilote le mouvement de matière : les molécules tendent à migrer vers les zones les plus ordonnées où la pression est moindre.
Si ce modèle rend compte des effets de la polarisation, il prévoit une accumulation de matière dans les zones les plus éclairées. Or, à faible puissance, il a été montré que la matière fuit la lumière, sauf dans le cas des polymères qui sont des cristaux liquides[8]. Cette description est également adaptée aux intensités élevées où l'on rend compte d'un mouvement vers les zones

[4] Neporent, N. S. ;Stolbova, O. V. *Opt. Spectrosc.* **1961**, *10*, 146.
[5] Barrett, C. J.; Natansohn, A. L.; Rochon, P.L. *J. Phys. Chem.* **1996**, *100*, 8836.
[6] Barrett, C. J. ; Rochon, P. L. ; Natansohn, A. *J. Chem. Phys.* **1998**, *109*, 1505.
[7] Pedersen, T. G. ; Johansen, P.M. ; Holme, N.C.R. ; Ramanujam, P.S. *Phys.Rev.Lett.* **1998**, *80*, 89.
[8] Bublitz, D.; Helgert, M. ; Fleck, B. ; Wenke, L. ; Hvilsted, S. ; Ramanujam,P.S. *Appl. Phys. B* **2000**, *70*, 863.

les plus lumineuses. En revanche, il ne correspond pas à nos conditions expérimentales que nous présentons au chapitre II.

D'autres équipes proposent un mécanisme de structuration de la couche sous l'effet de l'orientation de la chaîne principale su polymère. En effet, comme nous le préciserons au paragraphe III.1.b., les chromophores azobenzène s'orientent statistiquement au cours du temps perpendiculairement à la (aux) direction(s) du champ électrique. En supposant qu'il existe une rigidité entre la chaîne principale et les chaînes latérales contenant la fonction azobenzène, l'orientation de celle-ci conduit à une orientation de la chaîne principale selon la direction du cham électrique. Enfin, la couche est décrite comme un milieu élastique qui s'étire dans la direction du champ électrique.
Si cette description convient aux azo-polymères, elle est cependant moins adaptée aux dendrimères qui ne présentent pas d'axe principal privilégié.

I.2. Modèles de type « mouvement individuel ».

Kumar et al expliquent le mouvement de masse photo-induit observé dans les couches d'azopolymères par une interaction du champ électrique avec le dipôle induit de chaque chromophore[9,10]. Pour justifier que, parmi tous les polymères contenant des groupements dipolaires, seuls les azopolymères manifestent ce comportement, ils associent à l'isomérisation répétée des azo-chromophores une plastification de la couche.
Si ce modèle rend compte des effets de la polarisation, il prévoit une accumulation de matière dans les zones les plus éclairées, là où l'énergie d'interaction dipolaire est minimum, à moins de définir une susceptibilité négative.

Le mécanisme proposé par Nunzi et al. repose sur l'hypothèse d'une marche aléatoire unidimensionnelle des azobenzène[11,12] : l'isomérisation du chromophore s'accompagne d'un déplacement selon la direction de polarisation du champ électrique. C'est cette description du mouvement photo-induit que nous retenons pour développer le modèle proposé au chapitre IV.

II. Matériaux, dispositifs et méthodes.

II. 1. Quelles molécules pour mettre en évidence le mouvement photo-induit ?

Nous avons effectué l'étude expérimentale du mouvement photo-induit sur deux familles molécules contenant la fonction azobenzène déposées par spin coating sur du verre en couches d'épaisseur variant de 0,1 à 1 µm.
La première molécule utilisée est le **PMMA DR1**, polymère présentant un mélange statistique d'unités PMMA (30%) et DR1 (70%), ces dernières présentant un azobenzène substitué en chaîne latérale. Son choix a été motivé par les travaux que d'autres équipes ont déjà effectués sur elle, et pour laquelle de nombreuses informations sont déjà disponibles[13,14]. D'autre part, le PMMA est disponible commercialement.

Néanmoins, nous avons élargi notre étude aux **dendrimères de POPAM fonctionnalisés méthly-orange** (azobenzène substitué), de générations 2, 3 et 4 dans la

---

[9] Kumar, J. ; Li, L. ; Liang, X. L. ; Kim, D.Y. ; Lee, T.S. ; Tripathy, S.K., *Appl. Phys. Lett.* **1998**, *72*, 2096.
[10] Viswanathan, N.K. ; Balasubramanian, S. ; Li, L. ; Kumar, J. ; Tripathy, S.K. *J. Phys. Chem. B*. **1998**, *72*, 2096.
[11] Lefin, P. ; Fiorini, C. ; Nunzi, J. M. *Pure Appl. Opt.* **1998**, *7*, 71.
[12] Lefin P.; Fiorini, C.; Nunzi, J. M. *Opt. Mater.* **1998**, *9*, 323.
[13] Delaire, J. A. ; Nakatani, K. *Chem. Rev.* **2000**, *100*, 1817.
[14] Natansohn, A. ; Rochon, P. *Chem. Rev.* **2002**, *102*, 4139.

mesure où, contrairement aux polymères, ils ne possèdent pas de chaîne principale imposant une direction caractéristique qui introduit une brisure de symétrie parasite. De plus, l'étude du déplacement de masse de ces molécules dans la configuration expérimentale proposée a fait l'objet – à notre connaissance - de peu de publications.
Nous avons également utilisé des **molécules dendritiques dites « de Fréchet »**.
Ces molécules, qui ne sont pas disponibles commercialement, ont été synthétisées par l'équipe du Professeur Vögtle du Kekulé-Institut für Organische Chemie und Biochemie de Bonn, avec laquelle nous collaborons dans le cadre du projet européen LIMM.

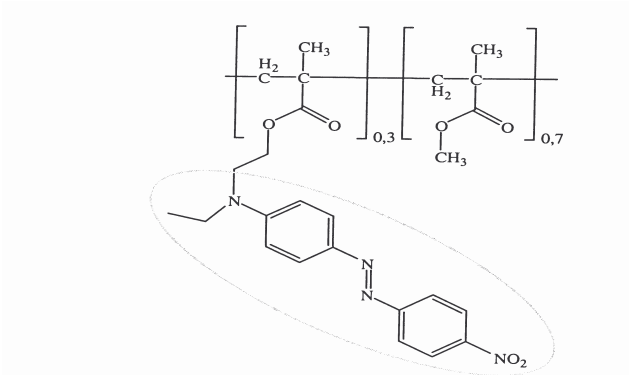

Fig. 1. Unité statistique élémentaire de PMMA DR1

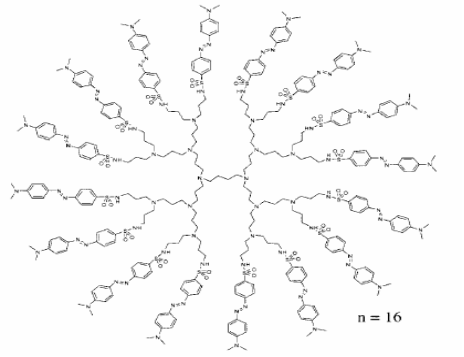

Fig. 2. Dendrimère POPAM MO G3

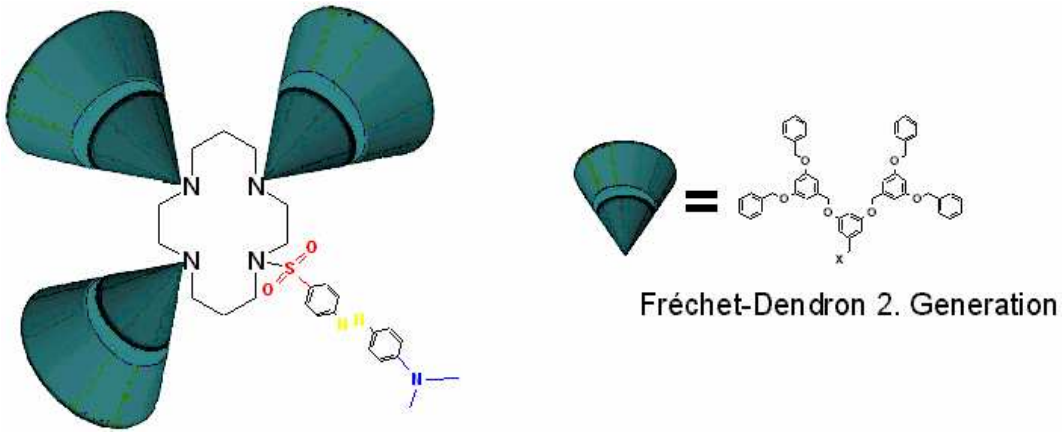

Fig.3. Azo-molécule de Fréchet utilisée : méthyl orange et dendrons de Frechet

II. 2. Quel environnement pour les molécules ?

Les molécules sont dissoutes dans du dichlorométhane puis déposées par **spin-coating** sur du verre. On obtient ainsi des couches d'épaisseur comprise entre 0,1 µm et 1 µm.
Ces couches constituent un milieu dense : nous estimons qu'il y a 10^{21} molécules par millimètre cube.
Le choix de couches pour mettre en évidence le déplacement de matière peut apparaître paradoxal dans une étude qui propose une interprétation en termes de mouvement individuel.
Cependant, l'étude de molécules isolées, déposées en « sub-monolayers », est difficile à mettre en œuvre. Observer un mouvement individuel suppose d'abord de maîtriser l'interaction molécule – substrat : elle doit être suffisante pour que la molécule soit couplée de façon significative à la surface (dans l'hypothèse d'une nano-friction que nous présenterons

au paragraphe IV.4.) mais elle ne doit pas être trop forte afin de permettre le mouvement. La recherche d'un protocole de préparation d'échantillons et la tentative d'observation d'un mouvement individuel ont été entreprises au laboratoire, parallèlement à mon travail de thèse. Jusqu'à présent aucun déplacement de molécules individuelles n'a été observé mais cela n'infirme pas nécessairement l'hypothèse de son existence : nous verrons plus bas que le temps d'observation et la durée d'activité optique du chromophore se sont avérés être des paramètres critiques.
Aussi, l'étude de couches nous a paru une méthode plus efficace, à condition de faire par la suite le lien avec le comportement attendu pour ces couches dans l'hypothèse d'un mouvement individuel.

II.3. Comment induire le déplacement de matière ?

Pour mettre en évidence le phénomène, **ces couches doivent être exposées à un motif lumineux modulé spatialement à l'échelle du micromètre**. Le choix d'une figure de franges d'interférences à deux ondes, obtenues par division du front d'onde d'un laser bleu, obéit à plusieurs motivations.
D'une part, son pas micrométrique, obtenu pour un angle α d'une trentaine de degrés entre les deux faisceaux interférents, permet une modulation spatiale à l'échelle à laquelle nous souhaitons observer le déplacement de matière. De plus, la périodicité du motif sur plusieurs centaines de micromètres le rend beaucoup plus facilement repérable qu'une figure de même gradient d'intensité. Enfin, parce qu'utilisée par plusieurs équipes, cette configuration se prête a priori à la comparaison avec des travaux antérieurs.
Il convient de souligner la nécessité de disposer d'un laser de bonne cohérence pour disposer d'un nombre suffisant (plus d'une centaine) de franges d'interférence. La grande cohérence (plusieurs dizaines de centimètres) du laser solide à 473 nm que nous avons utilisé nous a permis,outre d'obtenir une figure d'interférences suffisamment étendue, de ne pas nous préoccuper de l'égalité des deux voies interférentes, qui est sinon un paramètre critique.
Nous avons utilisé **trois motifs lumineux distincts** :
-Si la direction de polarisation des faisceaux interférant est linéaire il convient de distinguer deux cas : pour une direction de polarisation située dans le plan défini par les faisceaux, la distribution de l'intensité lumineuse le long de l'axe (Ox) perpendiculaire aux franges suit une loi sinusoïdale du type $I(x) = 2I_0 (1+ v \cos Kx)$ **où** $v = \cos \alpha$ est le facteur de visibilité tenant compte de l'angle α entre les deux faisceaux qui interfèrent. En revanche, si la direction de polarisation des faisceaux est perpendiculaire au plan que ceux-ci définissent, alors la visibilité v est égale à 1.
- Si les faisceaux interférant sont polarisés circulairement et dans le même sens, la modulation d'intensité est de la forme $I(x) = 2I_0 (1+\cos^2\alpha/2. \cos Kx)$ mais la polarisation résultante dans le plan de la couche est pratiquement circulaire.
- Enfin, si les faisceaux interférant sont polarisés circulairement mais en sens contraire, l'intensité résultant est presque uniforme. C'est la polarisation qui est modulée spatialement : elle tourne périodiquement dans l'espace, avec un pas identique à celui des franges d'intensité obtenues pour un même angle α entre faisceaux interférents.
Si **nous avons largement utilisé le premier motif**, les deux suivants ont fait l'objet d'observations essentiellement qualitatives.

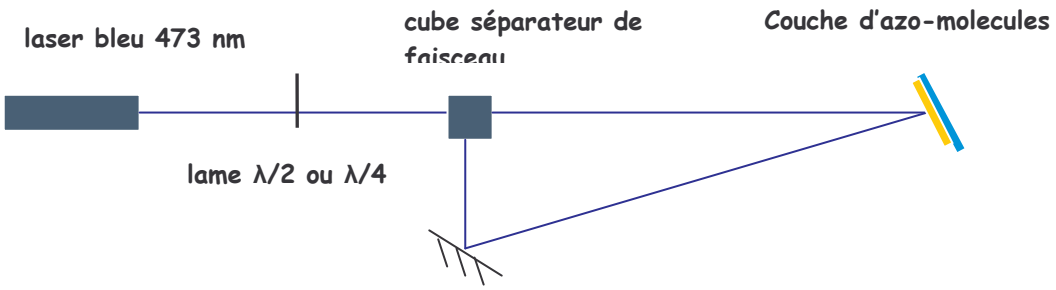

Fig.4. Exposition d'une couche d'azo-molécules à un motif de franges d'interférence.

II. 4. Observation du déplacement de matière : choix de l'AFM.

Sous l'effet de ces différentes modulations de la lumière, les couches se structurent en surface.
Nous observons et quantifions cette déformation de surface à l'aide d'un **microscope à force atomique (AFM)** en mode « contact intermittent ». Les pointes AFM choisies pour scanner la surface sont les plus souples possibles afin d'interagir aussi peu que possible avec la surface imagée. Quant à l'amplitude de balayage de l'AFM, qui est de 60 µm × 60 µm, elle permet d'observer la déformation induite en surface des couches par le motif de pas micrométrique.
Pour une couche exposée à un motif de franges d'interférence, **l'image AFM révèle une déformation périodique, a priori sinusoïdale, de même pas que les franges lumineuses et de plusieurs dizaines de nanomètres d'amplitude.**

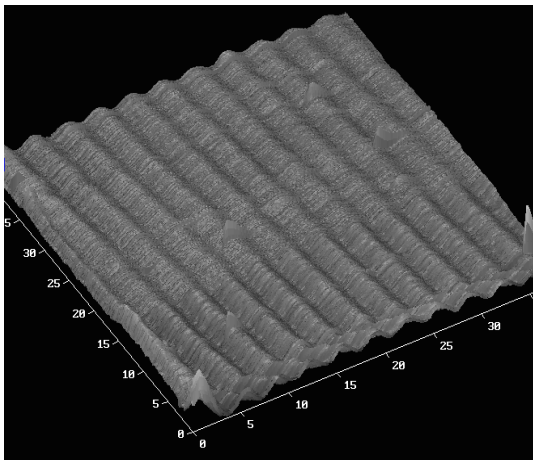

Fig. 5. Image AFM d'un réseau de surface obtenu sur une couche de PMMA DR1 après quelques minutes d'exposition à un motif de franges d'interférence.

On pourrait objecter qu'il existe une méthode de détermination optique de la rugosité d'une surface périodique, rapide à mettre en œuvre et permettant de rendre compte facilement de l'évolution au cours du temps. Cette méthode consiste à étudier l'évolution des propriétés de diffraction de la couche au cours de sa déformation[15]. Elle repose sur l'hypothèse d'une relation de proportionnalité entre l'amplitude du réseau périodique de surface et l'intensité du premier pic de diffraction généré par le réseau.
Néanmoins, dans le cadre d'une étude qui se propose de rendre compte d'un mouvement individuel, le choix de l'AFM semble judicieux en ce qu'il permet une observation directe de la surface alors qu'une méthode optique repose sur une propriété d'ensemble du matériau. De

[15] Natansohn, A. ; Rochon, P. *Chem. Rev.* **2002**, *102*, 4139.

plus, un calcul de l'intensité du premier pic de diffraction, même après simplifications, conduit à une relation non linéaire entre celui-ci et l'amplitude de déformation, remettant en question l'utilisation de cette méthode pour une étude quantitative de la dynamique de formation du réseau de surface.
Plus encore, l'orientation des chromophores dans les zones éclairées conduit à une modulation spatiale de l'indice de réfraction de la couche, de même périodicité que le réseau de surface, qui participe au phénomène de diffraction observé[16].
Enfin, a posteriori **l'observation directe de la surface avec un AFM** s'est avérée riche en enseignements : nous verrons au chapitre V qu'elle **met en évidence des phénomène encore plus riches.**
D'autres configurations, inspirées de la nanolithographie ont été envisagées pour observer le mouvement photo-induit mais n'ont pas encore été mises en œuvre : avec un microscope optique, il est possible de projeter un masque à l'échelle de la dizaine de micromètres sur une couche, dans le champ de balayage d'un AFM.

II. 5. Protocoles d'étude : temps réel et ex-situ.

Pour les expériences effectuées, on peut distinguer entre protocole ex-situ et protocole in-situ ou « temps réel ».

II.5.a. Expériences ex-situ.

Dans le cadre de manipulations ex-situ, **la couche est d'abord exposée face avant** au(x) faisceau(x) laser.

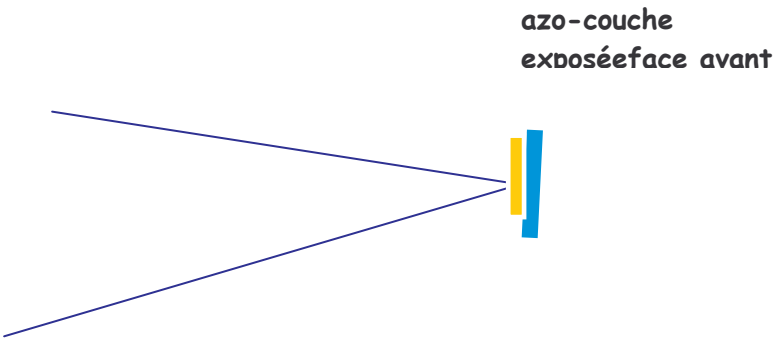

Fig. 6. Dispositif d'inscription ex-situ d'un réseau de surface : la couche est éclairée face avant

Une fois la déformation induite, et la position de la tache repérée face arrière, on observe la topographie de la couche en plaçant celle-ci sous la pointe de l'AFM. L'intensité du faisceau laser présentant un profil gaussien, avec une largeur d'une centaine de micromètres, il est nécessaire de placer la pointe de l'AFM dans la zone où l'intensité était la plus élevée. Aussi, après un repérage grossier effectué grâce au marquage préalable du spot, on utilise une platine translatable X-Y afin de rechercher de proche en proche la zone où l'amplitude de déformation est la plus grande. Typiquement, il s'agit d'une zone de 200µm×200µm. Cette recherche du maximum, quelque laborieuse qu'elle soit, est **une étape essentielle à toute approche quantitative**. Cependant, les observations AFM rapportées dans la littérature n'en font pas mention.
Deux types d'observations AFM ex situ ont été effectués.

[16] Labarthet, F. ; Buffeteau, T. ; Sourisseau C. *J. Phys. Chem. B.* **1998**, *102*, 2654.

-Les premières consistent à établir point par point l'évolution de l'amplitude de déformation de surface en fonction du temps d'exposition à un motif de franges d'interférences, chaque valeur de l'amplitude correspondant à une expérience pendant laquelle la couche a été exposée face (surface libre de l'azo-couche) avant au motif d'interférence.
-Les secondes ont pour but d'étudier la possibilité d'effacer un réseau de surface. Elles consistent à exposer un réseau, préalablement inscrit et d'amplitude déterminée, à un seul faisceau laser, puis à l'observer en AFM afin de voir si l'amplitude de modulation a changé de façon significative.

II.5.a. Expériences in situ ou « temps réel »..

Les observations réalisées in situ consistent à **étudier l'évolution de la surface à l'AFM au cours de l'exposition à un motif lumineux**. La surface libre de la couche, c'est-à-dire la face avant, étant stériquement occupée par le dispositif AFM, la zone étudiée doit être **éclairée par la face arrière**, à travers le substrat de verre.

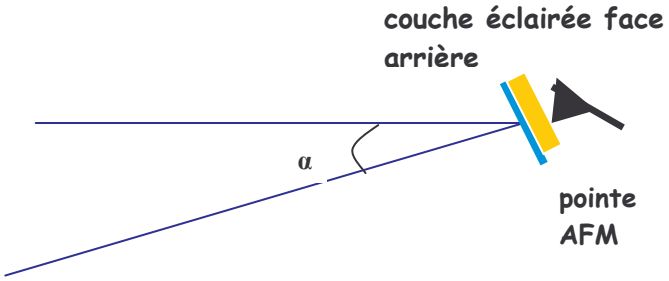

Fig.7. Dispositif d'inscription et d'observation in-situ ou « temps réel » du réseau.

L'image AFM, qui fait apparaître une croissance de l'amplitude du réseau au cours du balayage, est ensuite **analysée par un programme que nous avons écrit en Labview** et qui permet d'établir la courbe d'évolution de l'amplitude de déformation. Cependant, cette méthode qui repose sur un éclairage par la face arrière fait apparaître après quelques secondes des phénomènes parasites qui limitent la pertinence des informations apportées. Ceci sera précisé au paragraphe III.3.

III. Résultats expérimentaux.

Les résultats expérimentaux que nous présentons dans ce mémoire permettent de dégager certaines caractéristiques du mouvement et les paramètres essentiels qui y président.

III.1. Etude des propriétés d'absorption du PMMA DR1.

De manière unanime[13,14], le déclenchement du déplacement photo-induit est associé à **l'isomérisation trans / cis des fonctions azobenzène** présentes dans les molécules considérées.

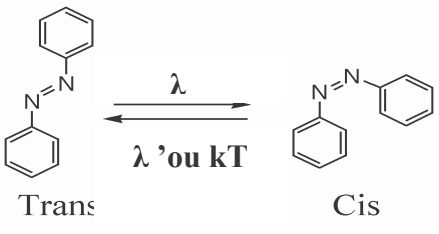

Fig. 8. Isomérisation de la fonction azobenzène.

Aussi il convient de s'intéresser à la propriété d'absorption des milieux étudiés et à son évolution dans le temps.

III.1.a. Spectre d'absorption des couches de PMMA DR1.

Nous avons commencé par une étude en spectroscopie visible des couches de PMMA DR1 et de dendrimères.

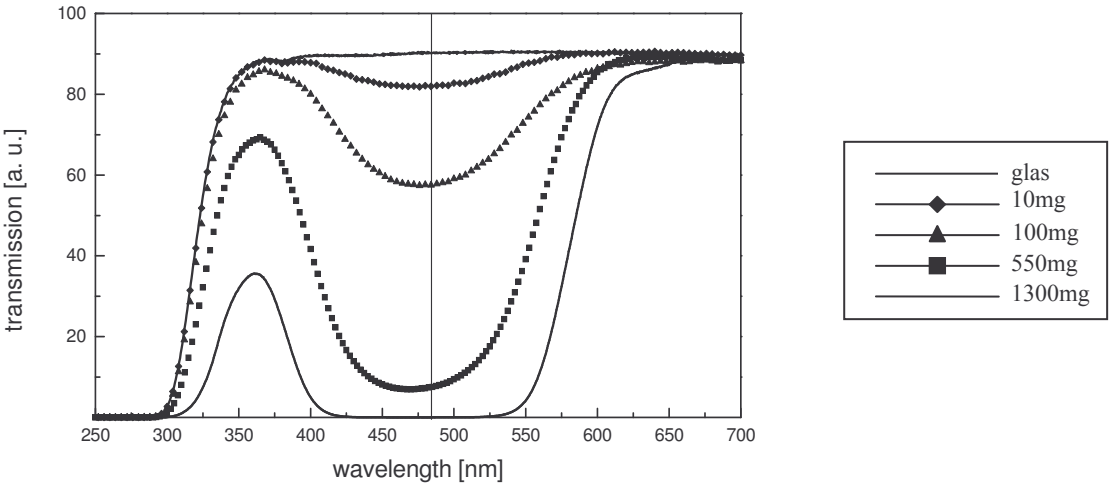

Fig. 9. Spectre de transmission pour des couches de PMMA DR1 d'épaisseurs différentes.

Il apparaît que la bande d'absorption dans le bleu-vert des azo-molécules étudiées se caractérise par sa largeur. Le PMMA DR1 et les dendrimères POPAM fonctionnalisés méthyl-orange présentent des fonctions azobenzène de type pseudostilbène selon la classification de Rau[17]. Pour celles-ci, la fonction azobenzène est dotée d'un groupement électro-donneur et d'un groupement électro-attracteur qui conduisent à une inversion des bandes d'absorption π-π^* et n-π^* ce qui assure à la fois l'isomérisation trans-cis et le retour cis-trans de la fonction par photo-activation autour de 400-500 nm ainsi que par un retour thermique rapide (de l'ordre de la seconde). Si à forte intensité c'est le premier mécanisme de retour qui préside, le retour thermique est certainement prépondérant à faible intensité lumineuse. Les chromophores peuvent, dans les deux cas, effectuer des cycles répétés d'isomérisation trans-cis-trans. Ces cycles semblent être une condition nécessaire à l'observation d'un déplacement de matière. En effet, nous vérifions au paragraphe III plus bas qu'aucune modification structurale n'est observée pour une couche constituée de molécules d'azobenzène non substituées.

[17] Rau, H. in *Photochemistry and Photophysics*; Rabek J.K., Ed; CRC Press: Boca Raton, FL 1990; Vol. 2, p. 119.

Natansohn et Rochon[14] l'attribuent au retour par voie photonique.
Nous suggérons au chapitre IV que le retour par voie thermique (moins d'une seconde pour les pseudostilbènes) joue également un rôle.

III.1.b. Evaluation du coefficient d'absorption β des couches de PMMA DR1 à λ=473 nm.

Pour mesurer avec précision l'épaisseur des couches, nous utilisons un microscope électronique à balayage.

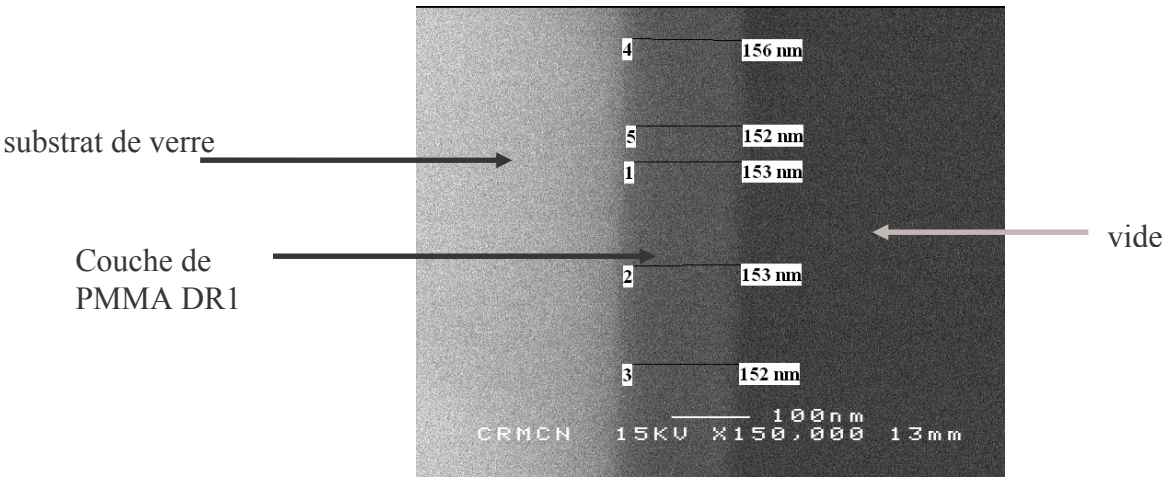

Fig. 10. Image au MEB d'une couche de PMMA DR1 préparée par spin coating à partir d'une solution de concentration 280 mg/10 mL.

On peut alors relier l'épaisseur attendue à la composition PMMA DR1 / dichlorométhane.

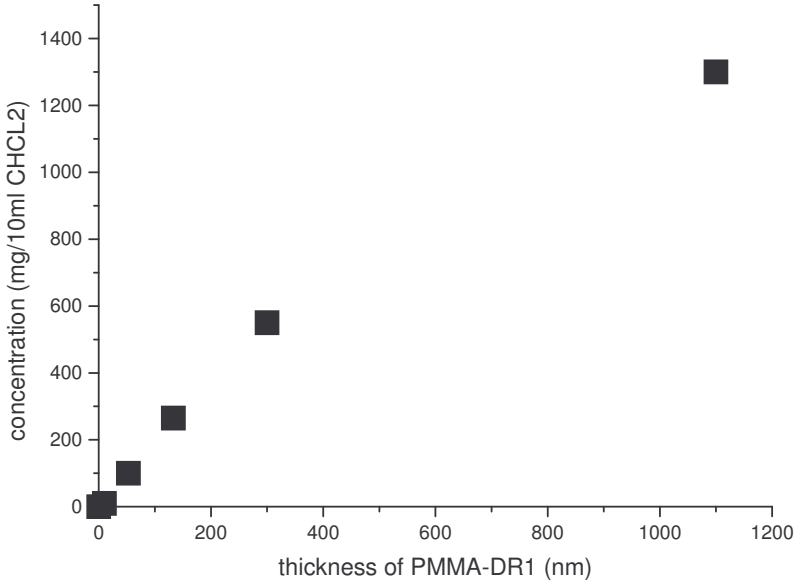

Fig. 11. Relation linéaire entre la concentration de la solution et l'épaisseur de la couche obtenue par spin-coating.

Quant à la transmission des différentes couches pour λ = 473 nm, on la détermine en lisant la valeur de la transmission sur le spectrogramme à cette longueur d'onde.

En supposant que l'absorption est linéaire en intensité, on peut appliquer la loi de Beer-Lambert : $I_t = I(0)\, e^{-\beta h0}$ qui relie l'épaisseur de la couche h_0 à l'intensité lumineuse I_t qu'elle transmet.
Deux mesures épaisseur/transmission permettent de **calculer le coefficient d'absorption au début de l'exposition : β = 8 µm^{-1}**. C'est dire que l'intensité lumineuse est atténuée d'un facteur e sur 120 nm. Comparées à cette valeur, les épaisseurs des couches obtenues par spin-coating sont grandes. Dans ce qui suit, nous ne pourrons pas formuler l'hypothèse de couches fines.
Connaissant β, il est possible de déterminer par absorption l'épaisseur locale d'une couche et ses variations à l'échelle du centimètre. Cette étude préalable de la topographie est essentielle car l'épaisseur est un paramètre du modèle proposé. Il en ressort que, pour une composition PMMA DR1 / dichlorométhane fixée, l'épaisseur est généralement maîtrisée à 10 % près, sauf pour quelques échantillons pour lesquels l'incertitude peut atteindre 30 %.
Mais la valeur de β évolue-t-elle au cours du temps ?

III.1.c. Détermination de la perte d'activité optique des chromophores : mise en évidence du photo-blanchiment.

Nous montrons qu'une couche de PMMA DR1, éclairée par un faisceau laser de puissance comparable à celle utilisée par la suite pour induire le mouvement, absorbe de moins en moins au cours du temps : ***β(t)* est une fonction décroissante du temps**. C'est dire qu'une partie des molécules devient optiquement inactive pendant l'exposition, et ne peut donc plus participer au mouvement de masse.
Pour évaluer cette diminution d'activité optique, nous avons étudié l'évolution au cours du temps de l'intensité transmise d'un faisceau laser polarisé linéairement, à différentes puissances, par une couche de PMMA DR1 d'épaisseur 150 nm.

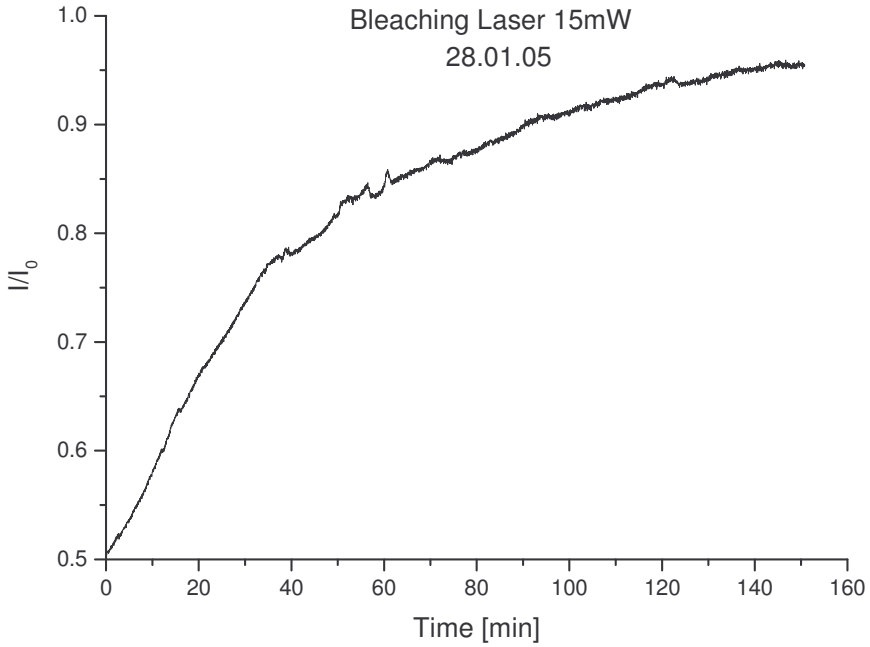

Fig. 12. Evolution de la transmission à λ=473 nm d'une couche de PMMADR1 d'épaisseur 150 nm.

On distingue deux régimes d'augmentation de la transmission: elle augmente rapidement, de 0,3 à 0,5, au cours des premières secondes puis avec une constante de temps caractéristique

τ_B beaucoup plus longue au cours de l'heure qui suit. La transmission de la couche de PMMA DR1 atteint une valeur de la transmission à saturation supérieure à 95 %. Or, en supposant que le coefficient de réflexion du système couche + verre représente 4 % de l'intensité incidente, nous en déduisons qu'à saturation de la transmission, la couche d'azopolymère n'absorbe plus.
Pour une intensité de I = 15 mW / 10 mm^2, nous estimons la durée d'activité optique à 40 minutes.
Une série d'expériences faites pour différentes intensités lumineuses montre que la durée de vie τ_B est reliée à l'intensité du faisceau incident I par une relation du type $I\,\tau_{B.} = \gamma$ où γ est une constante que nous calculons : $\gamma = 35$ W.s.
Le déplacement de matière, même s'il joue un rôle dans l'augmentation de la transmission, ne peut à lui expliquer cette observation. En effet, une étude en infrarouge montre qu'à l'endroit blanchi il reste de la matière. D'autre part, les réseaux de surface paraissent également blanchis à l'œil alors qu'il reste de la matière et qu'un calcul de la transmission donne une valeur bien inférieure à celle constatée pour les réseaux de surface.
C'est pourquoi nous proposons deux mécanismes pour rendre compte de ces résultats :
- **La diminution de l'activité optique à l'échelle de l'heure est irréversible.** Nous l'attribuons à une dénaturation irréversible des molécules par oxydation. A l'endroit exposé pendant plus d'une dizaine de minute, on observe, à l'œil, une zone devenue presque transparente : on parle, à cet égard, d'un phénomène de photo-blanchiment, la couche ayant été blanchie.
- **La diminution rapide de l'activité optique qui se produit au cours des premières secondes est réversible.** Si l'on arrête d'éclairer après quelques secondes, la transmission de la couche retrouve sa valeur originelle. De plus, si l'on tourne de 90 degrés la direction de polarisation du laser, la transmission est toujours minimale. Aussi, nous attribuons l'évolution aux premières secondes à un **effet d'orientation de l'axe principal des chromophores** selon les directions où le champ électrique n'a pas de composante (le plan perpendiculaire à la direction de polarisation pour un champ polarisé linéairement ou l'axe perpendiculaire au plan de la polarisation circulaire). Ce mécanisme d'orientation des azobenzène dans un polymère amorphe (méthyl orange/polyvinyl alcool) a été décrit dès 1984 par Todorov et al[18]. La probabilité d'absorption d'une fonction azobenzène est proportionnelle au carré du cosinus de l'angle entre la direction de polarisation du champ électrique et celle du dipôle induit du chromophore azobenzène (presque confondu avec l'axe principal de la molécule). Aussi, celles dont le dipôle se retrouve perpendiculaire au champ électrique n'interagissent plus avec la lumière, conduisant à une orientation statistique d'une partie des dipôles et ainsi à une diminution de l'absorption.
Dans le premier cas, on peut envisager une réorientation thermique aléatoire. Dans le second cas, les chromophores qui étaient devenus inactifs après orientation perpendiculaire au champ électrique se retrouvent colinéaires à la nouvelle direction de polarisation.

III.2. Paramètres clés du déplacement de matière photo-induit.

III.2.a. Sens de migration et gradient d'intensité lumineuse.

Nous avons commencé par vérifier que, dans les conditions dans lesquelles nous travaillions, la matière fuyait la lumière pour aller dans les zones les moins éclairées. A cet effet, une couche de PMMA DR1 éclairée face arrière, c'est-à-dire à travers le substrat de verre, par un spot laser d'une puissance surfacique de quelques centaines de mW par cm^2, focalisé sur 100 micromètres carrés, pendant quelques minutes, se creuse, témoignant d'une **fuite de matière à l'endroit de la zone éclairée**.

[18] Todorov, T. ; Nikolova, L. ; Tomova, N. *Appl. Opt.* **1984**, *23*, 4309.

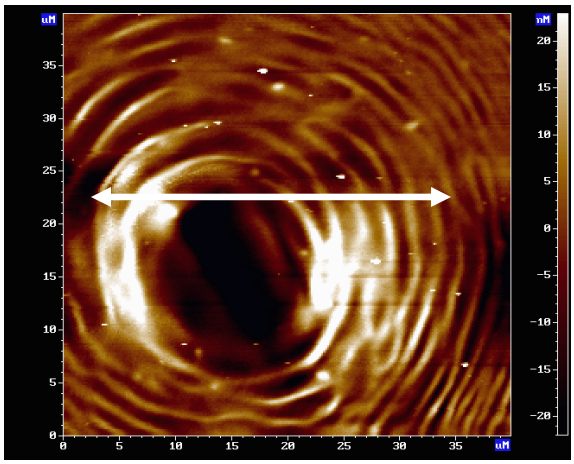

Fig. 13. Image AFM d'une couche de PMMA DR1 d'épaisseur 275 nm après quelques minutes d'exposition face arrière à un laser d'intensité 15 mW / cm^2 polarisé linéairement selon la direction indiquée par la flèche.

III.2.b. Mise en évidence du rôle de la polarisation : un phénomène qui ne peut se réduire à un effet thermique ou de changement de configuration.

Néanmoins, avant d'aller plus loin dans l'étude du mouvement photo-induit, il est nécessaire de s'assurer que celui-ci n'est pas simplement un phénomène d'ablation ou d'élévation de température de la couche au-delà de la température de transition vitreuse.
En résolvant l'équation de la chaleur pour un couche de PMMA DR1 considérée comme un demi-plan infini, nous estimons l'élévation maximum de température à une dizaine de degrés Kelvin après une trentaine de minutes. C'est dire qu'au cours de la formation du réseau, le polymère n'atteint pas sa température de transition vitreuse.

Une autre preuve que des phénomènes encore mal compris, et qui excluent un processus purement thermique, rentrent en jeu est apportée par l'effet de la polarisation de la lumière. Pour mettre cet effet en évidence, nous faisons varier la polarisation du motif lumineux éclairant la couche et nous comparons l'amplitude des réseaux de surface formés.
Ainsi, une polarisation parallèle aux franges lumineuses ne donne pas de déformation significative de la surface alors que, toutes conditions égales par ailleurs, une polarisation perpendiculaire aux franges d'interférence conduit à un réseau de surface d'amplitude notable. Ce résultat invite à penser que le déplacement de matière se produit dans la direction de polarisation de la lumière. C'est ce que mettent en évidence les résultats de Kumar et al. : alors qu'un faisceau laser polarisé circulairement donne lieu à un déplacement de matière de symétrie circulaire, un faisceau polarisé linéairement fait apparaître des bourrelets de matière dans la direction de polarisation.

Nous avons également mis en évidence cet effet de la polarisation : il apparaît sur la figure 13 du paragraphe précédent où l'on remarque **un bourrelet de part et d'autre du trou, suivant la direction de polarisation du champ électrique.**

Le rôle essentiel de la polarisation est confirmé par les expériences effectuées en configuration « réseau de polarisation » pour laquelle la couche est éclairée par un motif d'intensité lumineuse uniforme mais dont la direction de polarisation tourne périodiquement. Bien qu'il n'y ait pas de modulation notable de l'intensité lumineuse, on observe un réseau de surface comparable à celui obtenu avec une intensité modulée : pour un dispositif expérimental donné, la période est la même et l'amplitude de déformation est du même ordre de grandeur.

Ainsi, tout effet purement thermique, de changement d'état, ou encore de type « volume libre », qui ignore l'effet de la polarisation, est à exclure.

III.2.d. Un phénomène lié à la chaîne principale des polymères étudiés ?

Nous montrons que le mouvement de masse observé pour les PMMA DR1 ne résulte pas d'une orientation de la chaîne principale du polymère.
En effet, les azo-polymères ayant longtemps été le seul matériau étudié, le déplacement de matière pouvait être envisagé comme une conséquence de l'orientation des polymères.
Or, **nous montrons que les azo-dendrimères, qui ne présentent pas de direction privilégiée, manifestent un comportement semblable aux PMMA DR1**. Dans des conditions d'éclairement comparables par un motif de franges d'interférence, des couches d'azo dendrimères méthyl orange de générations 2, 3 et 4 se structurent également en un réseau de surface de mêmes caractéristiques. C'est ce qu'illustre l'image AFM ci-dessous d'une couche de G2MO d'épaisseur 500 nm éclairée face avant pendant 5 minutes par un motif d'interférence obtenu pour λ = 473 nm à 15 mW.

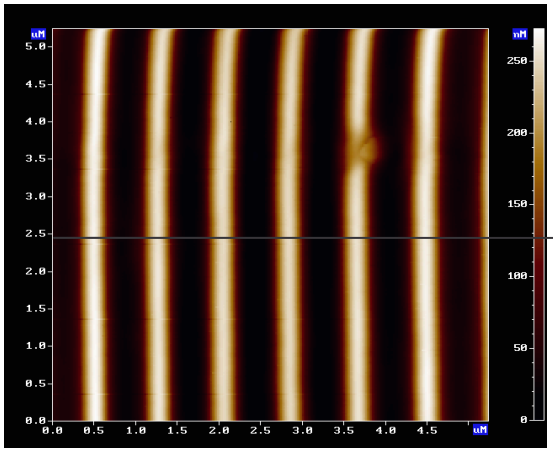

Fig. 14. Réseau de surface obtenu par exposition d'une couche de G2MO pendant 1 minute à un motif de frange de 15 mW

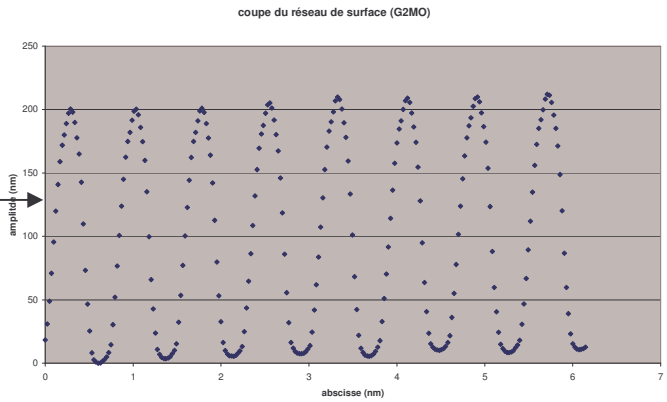

Fig. 15. Coupe mettant en évidence un déplacement de matière notable pour la couche de G2MO.

III.2.e. Importance de la substitution des chromophores.

Pour des **molécules azobenzène seules**, que nous avons déposées en couches par spin coating et éclairées dans les mêmes conditions que les azo-polymères et azo-dendrimère, nous n'avons observé **aucun déplacement de matière**.
Le paragraphe précédent apportant la preuve que l'absence de chaîne principale ne peut être invoquée, nous sommes conduit à penser que c'est l'environnement des azo-chromophores qui est en jeu. Comme nous l'avons évoqué plus haut, les azobenzène dotés d'un groupement électro-attracteur et d'un groupement électrodonneur (comme c'est le cas pour le PMMA DR1 ou les dendrimères de méthyl-orange) constituent des systèmes de type pseudostilbène pour lesquels les bandes d'absorption π-π^* et n-π^* sont inversées. Ils peuvent effectuer des cycles d'isomérisation trans-cis-trans répétés sous l'effet d'une lumière bleue et par un retour thermique rapide. Cette propriété joue un rôle clé dans le mouvement photo-induit comme l'ont souligné plusieurs équipes. Nous proposons une interprétation dans le chapitre qui suit.

III.3. Etude de la dynamique du déplacement de matière.

III.3.a. Forme générale des courbes d'évolution de l'amplitude du réseau.

Une fois ces points essentiels vérifiés, l'étude de la dynamique de formation du réseau de surface, telle qu'elle a été décrite ci-dessus, permet de dégager les caractéristiques et les paramètres clés du mouvement photo-induit.
Les images AFM révèlent une déformation induite de même périodicité que le motif de franges d'interférence qui a servi à l'éclairer. Au cours des premières minutes de sa formation, ce réseau de surface est sinusoïdal. En revanche, pour des temps plus long, le profil s'écarte d'une sinusoïde tout en conservant sa périodicité.
Toutes les courbes décrivant l'amplitude (distance pic-pic divisée par deux) de modulation du réseau de surface en fonction du temps, et obtenues avec la méthode ex-situ, ont la même forme : concaves, elles mettent en évidence **deux caractéristiques** : une **saturation** du phénomène à l'amplitude h_{sat} et une **vitesse de formation du réseau** maximale à l'origine $dh_1(0)/dt$.

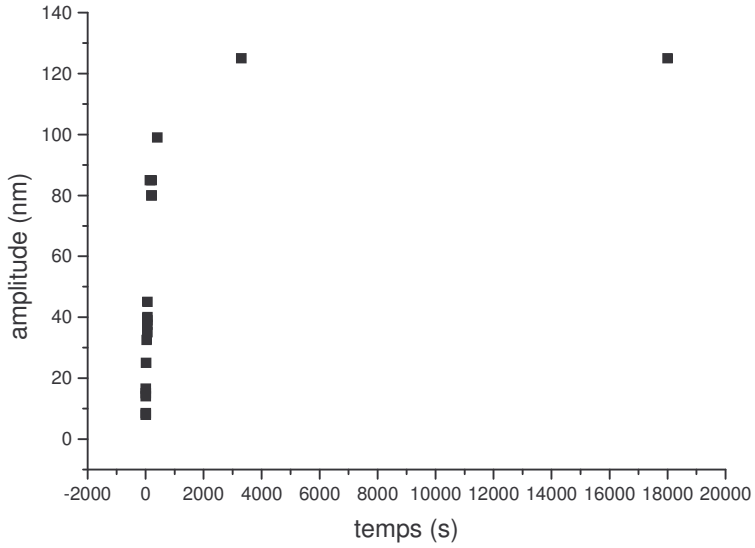

Fig. 16. Forme caractéristique de l'évolution de l'amplitude du réseau de surface observé face avant au cours de l'éclairement par un motif d'interférences.

En revanche, les courbes d'évolution de l'amplitude obtenues avec la méthode in-situ ou « temps réel » (éclairage face arrière et courbe obtenue en temps réel), si elles suivent la même évolution aux premières secondes, elles font ensuite apparaître un point de rupture puis **un signal brouillé**, inexploitable, aux grands temps. On peut justifier ce résultat parasite par un phénomène de déformation – contraintes mis en oeuvre dans la couche : le mouvement de matière, qui se produit essentiellement du côté éclairé, c'est-à-dire face arrière, est affecté par son environnement (d'un côté la lame de verre, de l'autre le reste de la couche) qui ne transmet pas la déformation de façon linéaire.

t

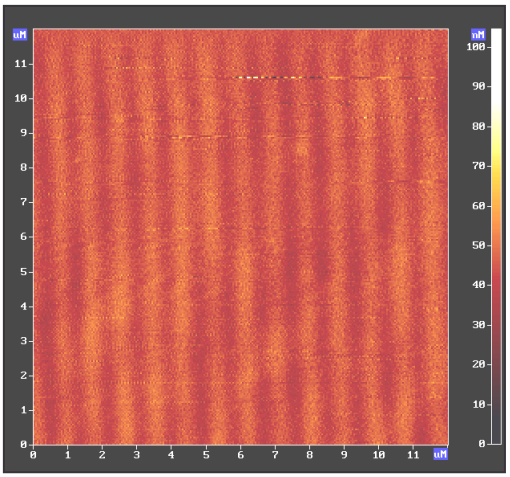

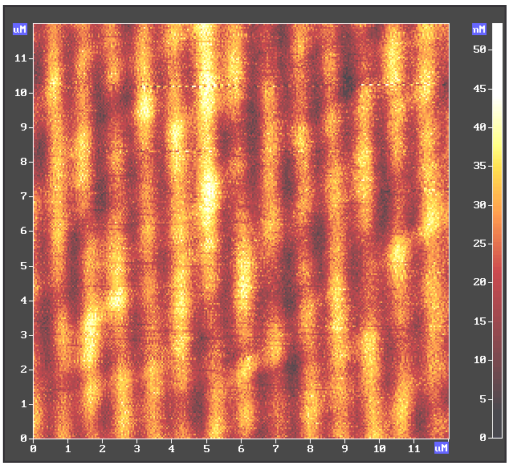

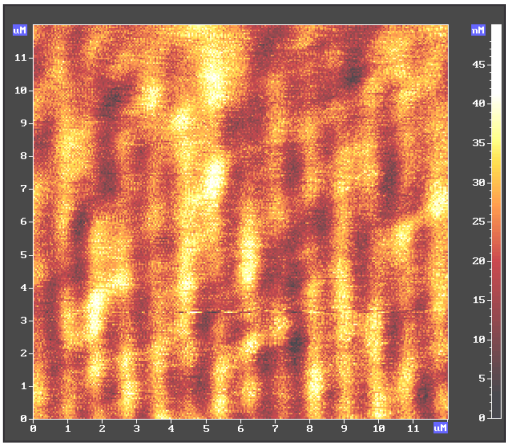

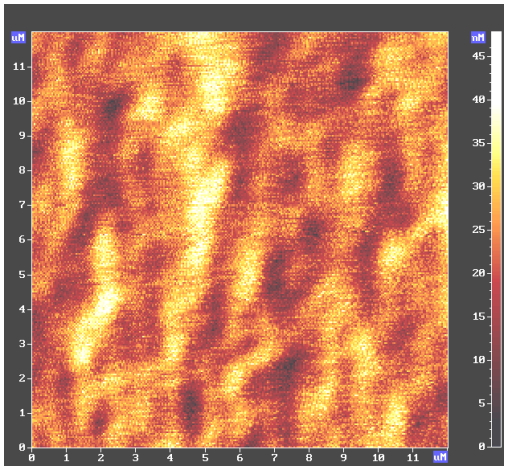

Néanmoins, les courbes obtenues en in-situ ou « temps réel » restent exploitables aux petits temps : si l'information sur l'amplitude à saturation h_{sat} est perdue, elles donnent néanmoins une valeur de la vitesse de croissance du réseau à l'origine.

Les deux caractéristiques dégagées jouent un rôle essentiel dans la compréhension du mécanisme :

-La vitesse de formation du réseau à l'origine se prête à une analyse quantitative que nous conduirons au chapitre suivant.

-Le phénomène de saturation est plus délicat à analyser quantitativement. Cependant, comprendre son origine est essentiel : est-elle due à un état d'équilibre entre zones de déplétion très éclairées et zones d'accumulation sombres ? S'explique-t-elle par la limitation dans le temps de l'activité optique évoquée au paragraphe III.1 ?
Dans tous les cas présentés ci-dessous, on notera sur que cette amplitude à saturation, quelque délicate qu'elle soit à déterminer dans le cas des grandes amplitudes (au-delà de 100 nm), est inférieure à l'épaisseur de la couche : elle vaut une trentaine de nanomètres pour une couche de PMMA d'environ 55 nm d'épaisseur, elle atteint 120 nm pour une couche de 250 nm de PMMA. C'est dire que la saturation est atteinte avant que la couche ne se creuse totalement.

Dans ce qui suit, nous étudions l'influence de différents paramètres sur ces deux grandeurs caractéristiques du mouvement photo-induit. Les valeurs numériques qui en découlent n'ont pas prétention à être quantitatives. La vitesse de formation du réseau aux premières secondes, par exemple, est entachée d'une incertitude liée au « bruit » d'au moins un nanomètre. Ces valeurs nous permettent néanmoins d'appréhender certains aspects du phénomène et de juger de la pertinence du modèle que nous proposerons au chapitre IV.

*III.3.b. Influence de l'épaisseur de la couche***.**

L'épaisseur de la couche influence la dynamique de formation du réseau.

L'influence de l'épaisseur de la couche h_0 apporte une information essentielle à la compréhension du phénomène. Nous comparons deux couches de PMMA DR1 d'épaisseur h_0 distincte, toutes deux éclairées par un motif de frange d'interférence en polarisation linp, avec une intensité de 15 mW / 10 mm^2 et un angle α entre les deux faisceaux de 32

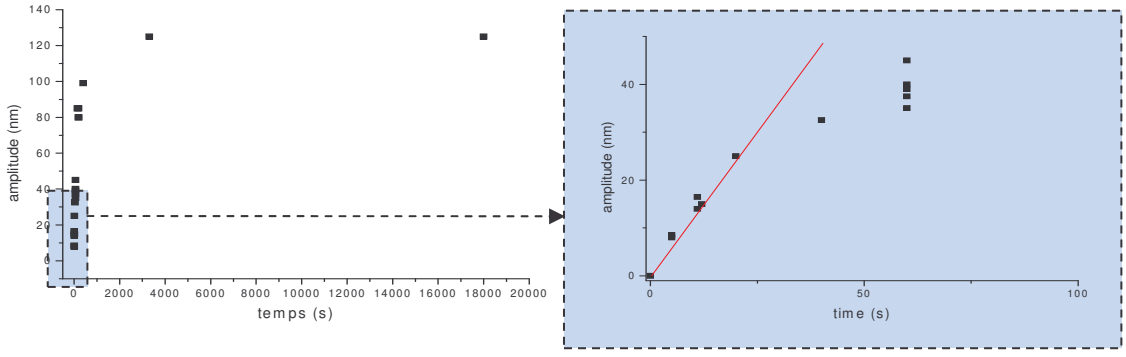

Fig. 18. Dynamique pour h_0 = 275

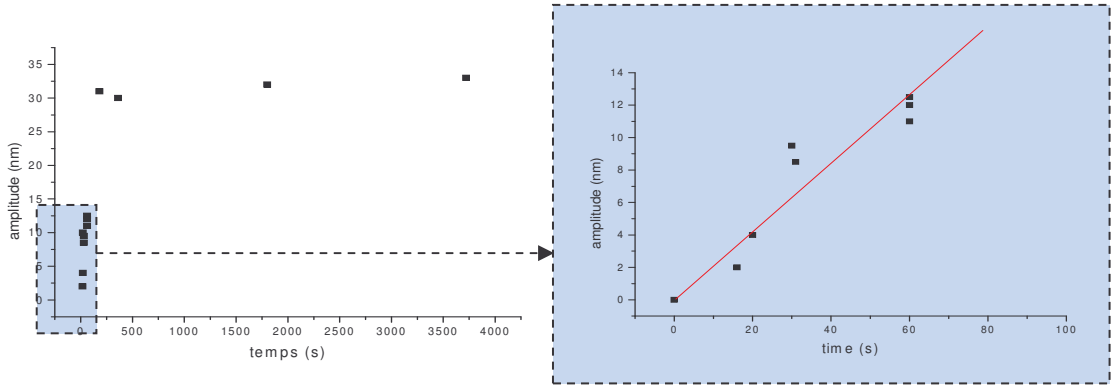

Fig. 19. Dynamique pour h_0 = 55

	h_0 = 275 nm	h_0 = 55 nm
initial growth rate	1 +/- 0,1 nm/s	0,3 +/-0,05 nm/s
saturation amplitude	120 +/- 7 nm	30 + / - 4 nm

Il apparaît que **les grandeurs caractéristiques de la formation du réseau sont d'autant plus grandes que la couche est épaisse.**
C'est dire que tout le volume de la couche est le siège du déplacement de matière : il ne s'agit pas d'un phénomène surfacique. Une plastification en surface de la couche, hypothèse parfois avancée, conduirait à des valeurs semblables pour des couches d'épaisseur radicalement différente.

Une dynamique semblable aux petits temps pour un éclairage face avant ou face arrière.

Pour une couche de PMMA DR1 d'épaisseur 55 nm **éclairée face arrière** dans des **conditions identiques** à celles du paragraphe ci-dessus, la vitesse de formation à l'origine est comprise entre 0,2 et 0,3 nm/s. Elle est donc compatible avec la gamme 0,2 – 0,5 nm/s pour une même couche éclairée face avant.

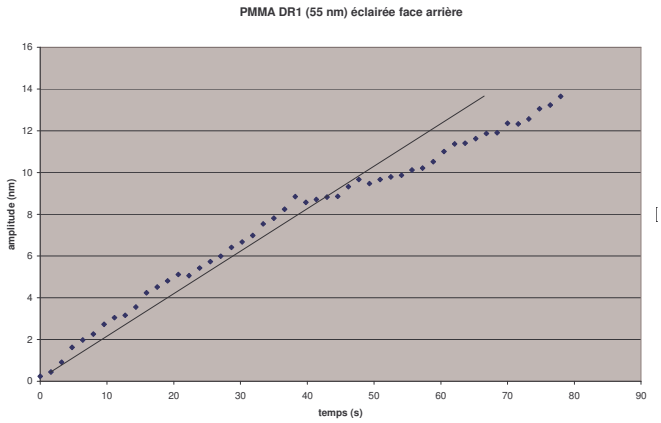

Fig. 20. Evolution aux premiers instants de l'amplitude d'un réseau inscrit face arrière sur une couche de PMMA DR1 d'épaisseur initiale 55 nm.

Là encore, un phénomène purement surfacique conduirait à un comportement différent pour un éclairage face arrière, même aux premiers instants de la formation du réseau

III.3.c. Effet de l'intensité lumineuse.

L'effet de l'intensité lumineuse incidente se manifeste sur la vitesse de formation du réseau à l'origine.
Pour une couche de PMMA DR1 d'épaisseur h_0 = 275 nm éclairée par un motif de franges d'interférence, en polarisation linéaire p, on note que :

	I_0 = 15 mW / 10 mm^2	I_0 = 1,5 mW / 10 mm^2
initial growth rate	1 +/- 0,1 nm/s	0,11 +/- 0,02 nm/s
saturation amplitude	120 nm à 15 % près	80 nm à 15 % près

La vitesse de formation du réseau est pratiquement divisée par 10 pour une intensité lumineuse incidente dix fois plus faible.
En revanche, l'amplitude atteinte par le réseau à saturation ne présente pas une différence si marquée.

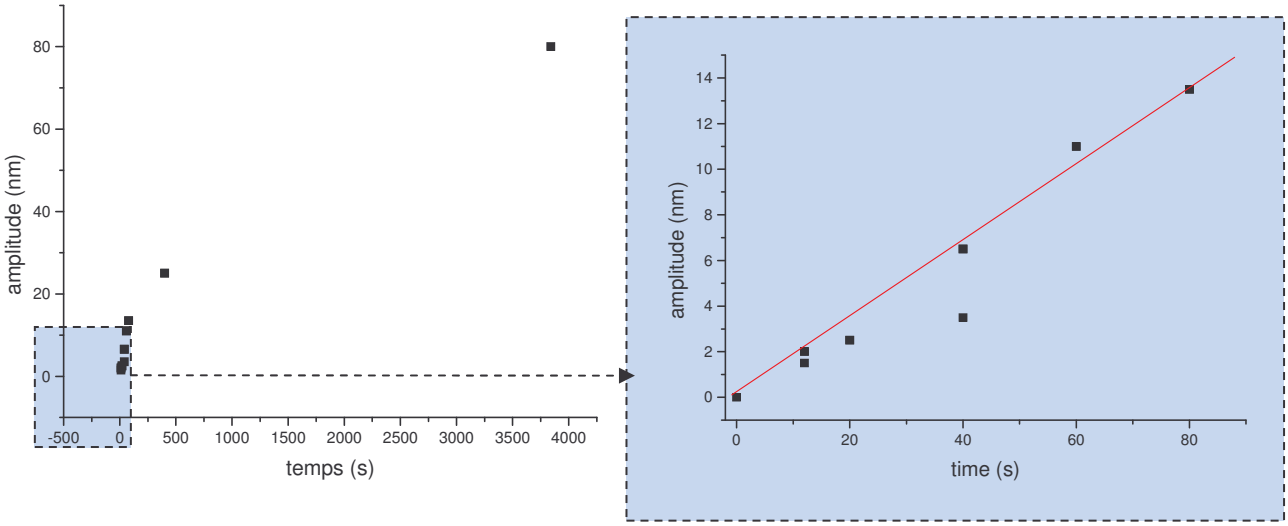

Fig. 22. Dynamique pour I_0 = 1,5 mW / 10 mm^2. On peut la comparer à la dynamique de croissance du réseau de surface obtenu pour I_0 = 15 mW / 10 mm^2 qui figure plus haut.

III.3.e. Nature de l'azo-molécule.

La nature de l'azo-molécule constituant la couche influence également les grandeurs caractéristiques de la dynamique de formation du réseau de surface.
Il apparaît que, pour les molécules dendritiques, la **vitesse de formation à l'origine est plus grande que pour les PMMA DR1.**
Pour une couche de **G2MO** de facteur d'absorption supérieur à 95 %, exposée à un motif de franges d'interférence, à une intensité de 15 mW / 10 mm^2, la vitesse de formation du réseau à l'origine est supérieure à 2,5 nm/s alors que les couches de PMMA DR1 les plus épaisses, qui absorbent 90 % de la lumière, donnent une vitesse au plus de 1,5 nm/s.

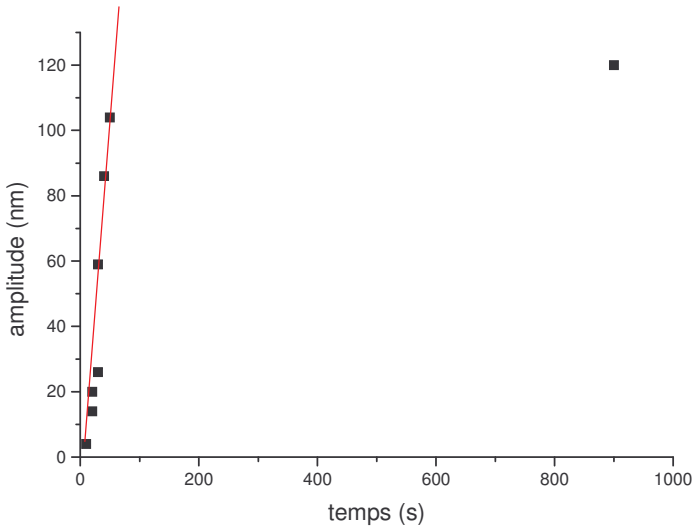

Fig. 23. Evolution de l'amplitude pour une couche de G2MO d'épaisseur 500 nm

III.4. Tentatives d'effacement d'un réseau préalablement formé.

Les tentatives d'effacement de réseaux de surface préalablement formés conduisent à plusieurs observations a priori antithétiques : dans la plupart des cas, un réseau de surface éclairé par un unique faisceau conserve sa structure. Cependant, dans des conditions semblables, nous avons parfois observé une diminution de l'amplitude du réseau et, plus rarement (deux fois), une augmentation significative de l'amplitude.
Ce résultat suggère que la distribution d'intensité lumineuse à l'intérieur de la couche est difficile à appréhender. Nous pensons que le faisceau destiné à effacer le réseau de surface est diffracté par ce dernier. Le profil d'intensité qui en résulte pourrait ainsi expliquer l'exaltation que nous avons remarquée.
Néanmoins, il se dégage une tendance en accord avec les observations de Bian et al[19] : nous avons noté une diminution significative de l'amplitude du réseau de surface seulement pour les couches les plus fines.
De plus, le réseaux nous ne sommes parvenus à effacer avaient été exposés quelques minutes seulement au laser.
Nous présentons une dynamique d'effacement d'un réseau de surface. La vitesse d'effacement à l'origine est très lente : environ 7.10^{-3} $nm.s^{-1}$. Nous en proposons une interprétation au chapitre IV.

IV. Modélisation, discussion et conséquences.

IV.1. Les hypothèses du modèle : une marche aléatoire pilotée par la lumière.

Le modèle que nous proposons pour rendre compte du déplacement photo-induit s'inspire du mécanisme proposé par Nunzi et al., evoqué au paragraphe I.2., et repose sur l'idée d'un mouvement individuel de nature probabiliste. Il se fonde sur cinq hypothèses :
- Lorsqu'elle absorbe un photon, la fonction azobenzène peut, avec une certaine efficacité quantique, être isomérisée de trans en cis. Dans un environnement de type pseudostilbène, le retour thermique de la forme cis à la forme trans s'effectue rapidement devant le temps entre deux isomérisations. Ce cycle isomérisation / retour thermique s'accompagne d'un déplacement de la fonction azobenzène d'un libre parcours moyen l. **(*H1*)**
- Ce déplacement du chromophore tend à entraîner avec lui la molécule (chaîne polymérique ou dendrimère) à laquelle il est greffé. Nous considérons dans les calculs qui suivent que le volume V déplacé par une fonction azobenzène est le volume du monomère de PMMA DR1 auquel il appartient. Nous estimons $V = 1$ nm^3. **(*H2*)**
- Ce déplacement de l s'effectue dans la direction du champ électrique, de part ou d'autre de façon équiprobable. **(*H3*)**
- Les chromophores exposés au laser ont une durée d'activité optique finie. En effet, nous avons mis en évidence, au paragraphe III.1.c., une diminution de l'activité optique des chromophores azobenzène au cours du temps. ***(H4)***
- Enfin, nous supposons que les fonctions azobenzène relatives à une même molécule ne sont pas optiquement activées simultanément. Cette hypothèse sera justifiée plus bas où nous comparons la durée d'un cycle et le temps entre deux cycles. **(H5)**

L'hypothèse **(*H1*)** permet d'exprimer le nombre n_d *d*e molécules par unités de temps et de volume qui subissent un déplacement. Il s'agit d'une fraction Φ des molécules absorbant un photon. Cette fraction tient compte de l'efficacité quantique d'isomérisation de la forme trans à la forme cis et de la probabilité de retour thermique à la forme trans stable.

[19] Bian, S. ; Williams, J. M. ; Kim, D. Y.; Li L.; Balasubramanian, S.; Kumar, J.; Tripathy, S. *Journ. Appl. Phys.* **1999**, *86*, 4498.

Or, on détermine le nombre de groupes azobenzène absorbant un photon en écrivant la variation d'intensité d'un faisceau traversant une couche d'épaisseur infinitésimale et de coefficient d'absorption β que nous déterminons au paragraphe III.1.b. Ainsi, on peut écrire :

$$n_d = (\Phi\, \beta\, \lambda / hc)\, I$$

λ est la longueur d'onde de la lumière incidente, h la constante de Planck et c la vitesse de la lumière.
Le nombre de molécules n_d par unités de volume et de temps qui se déplacent de l est donc proportionnel à l'intensité locale. De cette façon, les zones éclairées sont le siège de nombreux déplacements et se dépeuplent progressivement au profit des zones les plus sombres où la probabilité de déplacement, plus faible, conduit à une accumulation de matière.

IV.2. Application des hypothèses : évolution temporelle de l'amplitude d'une couche éclairée par un motif d'interférences en polarisation linéaire.

IV.2.a. Equation d'évolution de l'amplitude de la modulation de surface.

Comme nous l'avons souligné au chapitre II, il est nécessaire de faire le lien entre notre modèle de type « mouvement individuel » et nos résultats expérimentaux obtenus pour des couches, environnements à grand nombre de molécules. Aussi, nous appliquons les hypothèses *(H1)* et *(H2)* à une couche d'un azo-matériau, d'épaisseur supposée uniforme h_0 suivant la direction z de l'espace. Celle-ci est exposée, face avant ou face arrière, à une intensité lumineuse modulée selon l'axe x est qui s'atténue exponentiellement avec l'épaisseur de matière traversée, par absorption : $I(x)e^{-\beta(h-z)}$ pour une couche éclairée face avant ou $I(x)e^{-\beta z}$ pour une couche éclairée face arrière. Comme nous le montrons en annexe du paragraphe II.2., le profil d'intensité en polarisation linéaire de type p s'écrit :

$$I(x) = I_0 (1 + v \cos Kx)$$

Nous allons monter que l'équation d'évolution de la surface libre $h(x,t)$ vérifie une équation différentielle du type :

$$\frac{\partial h}{\partial t} = D \frac{\partial^2}{\partial x^2} [I(x).(1 - e^{-\beta h(x,t)})]$$

Le coefficient D sera explicité plus bas.

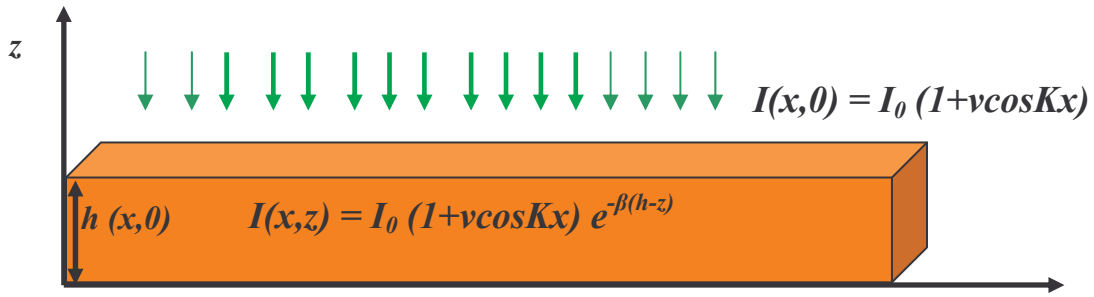

Fig. 24. Configuration d'étude pour une couche éclairée face avant.

Nous pouvons déterminer l'évolution de l'épaisseur locale $h(x,t)$ en fonction du temps en :

- **déterminant le flux algébrique *J(x,t)*** de molécules traversant, suivant la direction de l'axe (Ox), de la gauche vers la droite la surface de matière située à l'abscisse x.

- **puis en écrivant l'équation de conservation de la matière** pour une tranche d'épaisseur dx.
Par ailleurs, nous formulons l'**hypothèse simplificatrice** d'un temps caractéristique d'activité optique τ **uniforme**, tout en gardant à l'esprit qu'il dépend en fait de l'intensité locale de lumière.
Nous menons ci-dessous le calcul dans le cas d'une couche éclairée face avant. Néanmoins, le calcul mené face arrière conduit au même résultat, conformément aux hypothèses formulées.

- Le flux *J(x,t)* est égal à la moitié des molécules mises en mouvement dans le volume de matière compris entre (*x-l*) et *x*, à gauche de la surface considérée, auquel on retranche la moitié des molécules mises en mouvement dans le volume de la couche compris entre *x* et (*x+l*), à droite. Les molécules déplacées en dehors de ces éléments de volume n'atteignent pas la surface située à l'abscisse x, l correspondant au pas du déplacement.

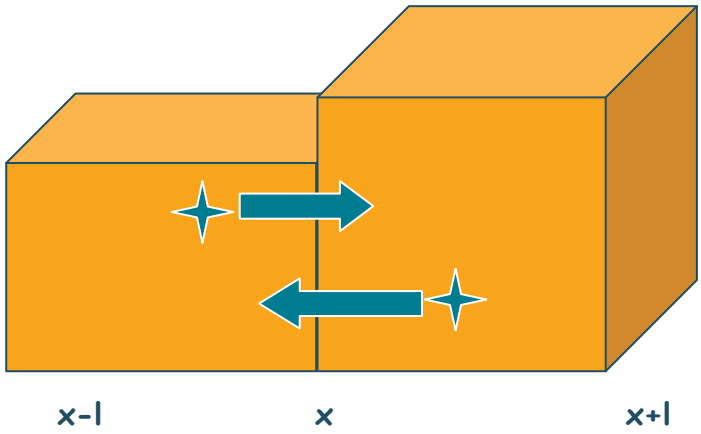

Fig. 25. Détermination du flux J(x,t) de molécules à travers la surface de matière située en x.

Ainsi, à travers la surface de matière de longueur *h(x,t)* suivant l'axe (*Oz*) et de largeur unité selon l'axe (*Oy*), le flux *J(x,t)* s'écrit :

J(x,t) = 1/2 molécules activées entre (x-l) et x- 1/2 molécules activées entre x et (x+l)

$$J(x,t) = \frac{1}{2}\int_0^1 dy \int_{x-l}^{x} dX \int_0^{h(X,t)} dz \cdot n_v(X,z,t) - \frac{1}{2}\int_0^1 dy \int_{x}^{x+l} dX \int_0^{h(X,t)} dz \cdot n_v(X,z,t)$$

$$J(x,t) = \frac{1}{2}\int_{x-l}^{x} dX \int_0^{h(X,t)} dz \cdot \phi\beta \frac{\lambda}{hc} I(X,z) - \frac{1}{2}\int_{x-l}^{x} dX \int_0^{h(X,t)} dz \cdot \phi\beta \frac{\lambda}{hc} I(X,z)$$

Si l'on suppose le pas de déplacement *l* petit devant les variations spatiales du profil d'intensité *I* selon *(Ox)*, l'intégrale sur cet axe peut être réécrite :

$$J(x,t) = \frac{1}{2} l \int_0^{h(x-l,t)} dz \cdot \phi\beta \frac{\lambda}{hc} I(x-l,z) - \frac{1}{2} l \int_0^{h(x+l,t)} dz \cdot \phi\beta \frac{\lambda}{hc} I(x+l,z)$$

Cette hypothèse permet également de développer au premier ordre selon x :

$$J(x,t) = \frac{1}{2} l.(-2l).\frac{\partial}{\partial x}(\int_0^{h(x,t)} dz \cdot \phi\beta \frac{\lambda}{hc} I(x,z))$$

Si l'on reprend l'expression $I(x,z) = I_0 (1+ \nu \cos Kx).e^{-\beta(h-z)}$, le flux total de molécules à

$$J(x,t) = -l^2 \phi\beta \frac{\lambda}{hc}.I_0 \frac{\partial}{\partial x}[(1+\nu\cos(Kx)) \int_0^{h(x,t)} dz \cdot e^{-\beta(h-z)}]$$

l'abscisse x devient :

$$J(x,t) = -l^2 \phi \frac{\lambda}{hc}.I_0 \frac{\partial}{\partial x}[(1+\nu\cos(Kx)).(1-e^{-\beta h(x,t)})]$$

On peut alors écrire la loi de conservation de la matière pour une tranche de couche d'épaisseur *dx*, de hauteur *h(x,t)* selon (*Oz*) et de largeur unité selon (*Oy*). En supposant constante la masse volumique du polymère, nous pouvons écrire la conservation du volume entre les instants *t* et *t+dt* sous la forme :

$$1.dx.[h(x,t+dt) - h(x,t)] = V.J(x,t).dt - V.J(x+dx,t).dt$$

J(x,t) étant le flux de chromophores, on multiplie par le volume *V* transporté. Dans l'hypothèse où chaque chromophore tend à entraîner dans son mouvement la chaîne de polymère à laquelle il est attaché, nous prenons pour *V* le volume du monomère de PMMA DR1 (ou la fraction de dendrimère) auquel est greffé une fonction azobenzène.

$$\frac{\partial h}{\partial t}.dt.dx = -V.\frac{\partial J}{\partial x}.dx.dt$$

En reprenant l'expression du flux de chromophores *J(x,t)*, il vient :

$$\frac{\partial h}{\partial t} = l^2 \phi \frac{\lambda}{hc}.I_0.V.\frac{\partial^2}{\partial x^2}.[(1+\nu\cos(Kx)).(1-e^{-\beta h(x,t)})]$$

Il convient de noter que, d'après l'hypothèse ***(H3)***, le libre parcours moyen *l* dépend de l'angle *α/2* que fait chaque faisceau avec la normale à la surface : $l=l_{max} \cos(\alpha/2)$.
Nous écrirons sous forme condensée :

$$\frac{\partial h}{\partial t} = D.\frac{\partial^2}{\partial x^2}[(1+\nu\cos(Kx)).(1-e^{-\beta h(x,t)})]$$

$\beta(t) = \beta_0 e^{-t/\tau} + \beta_\varepsilon$ est une fonction décroissante du temps.

IV.2.b. Résolution de l'équation d'évolution.

Une résolution complète de l'équation donnant *h(x,t)* suppose de recourir à une méthode numérique. Néanmoins, nous pouvons **déterminer analytiquement *h(x,t)* aux premiers instants** et ainsi obtenir une expression de la vitesse de formation du réseau à

l'origine *t=0*. Nous pouvons également dégager des **conséquences analytiques simples de l'équation pour l'amplitude à saturation.**

IV.2.b.α.Résolution analytique aux premiers instants de la formation du réseau : vitesse de croissance du réseau à l'origine.

Comme le montrent les images AFM, la déformation de surface présente un profil sinusoïdal pendant les premières secondes. De plus, la périodicité du réseau qui se forme est égale à celle des franges d'interférence. Aussi, près de l'origine des temps, on peut écrire $h(x,t)$ sous la forme $h_1(t).cos(Kx) + \varepsilon(x,t)$ où $\varepsilon(x,t) << h_1(t).cos(Kx)$ ainsi que pour leurs dérivées premières.
On peut alors introduire cette forme de $h(x,t)$ dans l'équation (X). En tenant compte du fait qu'aux premiers instants la déformation de surface induite est petite, on peut linéariser $e^{-\beta h1(t)}$ par $1-\beta h_1(t)$. Il vient :

$$dh_1(t)/dt\ cos(Kx) + \partial\varepsilon/\partial t = D\ \partial^2/\partial x^2\ ((1+v\ cos(Kx))(1-e^{-\beta(h0+h1(t)cos(Kx)+\varepsilon)}))$$

$$dh_1(t)/dt\ cos(Kx) = D\partial^2/\partial x^2\ ((1+v\ cos(Kx))(1-e^{-\beta h0}(1-\beta h_1(t)cos(Kx)+\varepsilon))$$

En identifiant les termes qui figurent devant $cos(Kx)$, pour lesquels $\partial^2/\partial x^2 = -K^2$, on obtient :

$$dh_1(t)/dt = -\ K^2D\ (\ e^{-\beta h0}\beta\ h_1(t) + v\ (1-\ e^{-\beta h0}))$$

La solution de cette équation différentielle est du type « charge de condensateur » et donne une valeur à saturation h_{sat}. Même s'il est tentant d'exploiter ce résultat, compte tenu de l'observation expérimentale d'une valeur de saturation, il convient cependant de garder à l'esprit que cette saturation concerne des valeurs de t grandes pour lesquelles la linéarisation est discutable et l'allure sinusoïdale remise en question par les images AFM.
En revanche, pour $t = 0$, on détermine l'expression de la vitesse de formation du réseau à l'origine :

$$dh_1(0)/dt = -\ K^2Dv\ (1-\ e^{-\beta h0})$$

Où:

$$D = l^2\phi\frac{\lambda}{hc}.I_0.V$$

On remarque que $dh_1(0)/dt < 0$, en accord avec le fait que la couche se creuse là où l'intensité de lumière est maximale ($cos(Kx) > 0$), et que l'épaisseur locale augmente dans les zones de faible intensité lumineuse ($cos(Kx) < 0$).
Cette expression de la vitesse à l'origine peut se réécrire en fonction du facteur d'absorption $A = (1-\ e^{-\beta h0})$ de la couche d'épaisseur h_0, à $t = 0$.

$$\boldsymbol{dh_1(0)/dt = -\ K^2D\ v\ A}$$

Dans le cadre du modèle présenté, une simple mesure donnant la fraction A d'intensité lumineuse absorbée à $\lambda = 473$ nm permet de comparer les vitesses à l'origine de deux couches de nature différente.

IV.2.b.β. Considérations sur l'amplitude à saturation.

Rôle de la diminution d'activité optique dans le phénomène de saturation observé.

Indépendamment d'une éventuelle diminution de l'activité optique des chromophores, le modèle de diffusion pilotée par la lumière que nous proposons ne semble pas exclure une saturation. En effet, on peut imaginer que les zones où la matière s'est accumulée et qui sont les moins éclairées sont le siège d'autant de mouvements de chromophores que les zones de déplétion où une intensité lumineuse plus forte induit davantage de mise en mouvement.
Cependant, nous montrons que, pour les conditions dans lesquelles nous avons travaillé ($v = 0,85$ et épaisseurs h_0 >55 nm), **si l'on ne tient pas compte du bleaching**, c'est-à-dire si le facteur d'absorption β_0 ne varie pas au cours du temps, **l'équation d'évolution de la surface libre *h(x,t)* n'admet pas de solution mathématique donnant une valeur à saturation.**
Or, comme nous l'avons souligné au paragraphe III.2.a., l'amplitude à saturation observée est toujours inférieure à l'épaisseur initiale de la couche. C'est dire qu'il y saturation avant que le réseau ne se creuse jusqu'à atteindre le substrat de verre.
Aussi, nous attribuons la saturation observée à la diminution d'activité optique.
Cependant, une résolution de l'équation d'évolution de $h(x,t)$ tenant compte de la dépendance en temps du facteur d'absorption $\beta = \beta_0 e^{-t/\tau} + \beta_\varepsilon$ est délicate. De plus, il faudrait tenir compte de ses variations spatiales puisque le produit du temps caractéristique d'activité optique τ par l'intensité $I(x,z)$ est une constante, comme nous l'avons montré au paragraphe III.1.c.

IV.3. Confrontation à l'expérience.

La confrontation des résultats dégagés aux observations expérimentales obéit à deux motivations. D'une part, il s'agit de voir si le modèle proposé rend qualitativement compte des phénomènes. Mais, au-delà d'un accord qualitatif, l'expression de la vitesse de formation à l'origine $dh_1(0)/dt$, permet d'accéder à un ordre de grandeur pour le pas l qui caractérise la marche au hasard du chromophore. Essentiel pour discuter le mouvement d'une molécule isolée, nous commençons ce chapitre par donner l'ordre de grandeur du pas l issu de notre modèle.

IV.3.1. Ordre de grandeur du pas l.

Considérons une couche de PMMA DR1 d'épaisseur 275 nm, éclairée en polarisation linéaire p un motif d'interférence d'interfrange proche de 0,85 µm, correspondant à un angle $\alpha = 32°$ entre les faisceaux qui interfèrent. La dynamique obtenue ex-situ donne pour la vitesse de formation à l'origine $dh_1(0)/dt$ une valeur voisine de 1 nm/s.
Or, nous avons établi au paragraphe IV.2.b.α. pour la vitesse à l'origine : $dh_1(0)/dt = - K^2 D\, v\, A$
Dans les conditions expérimentales mentionnées, on calcule :
$\boldsymbol{v = 0,85,\ K = 7,5.10^6\ m^{-1}}$ **et** $\boldsymbol{A = 1-e^{-\beta h0} = 0,75}$ (en tenant compte de l'orientation rapide des azobenzènes, conduisant à une diminution de l'absorption au cours des premières secondes).
On en déduit :

$$\boldsymbol{D = 5.10^{-23}\ U.S.I.}$$

En considérant, selon l'hypothèse **(H2)**, que le volume V qui figure dans l'expression de D est celui du monomère de PMMA DR1 (que nous estimons à 1 nm^3) auquel est greffé un azobenzène, alors on peut alors estimer la valeur du pas l de la marche au hasard des chromophores à quelques nanomètres.
Nous l'utiliserons par la suite pour discuter du mouvement d'une molécule isolée.
Il convient de noter que cette valeur est élevée : elle est de l'ordre de grandeur de la taille du monomère. Néanmoins, elle justifie a posteriori l'hypothèse d'un pas l petit devant les variations spatiales de l'intensité.

IV.3.2. Lien avec les paramètres influençant la dynamique de formation du réseau.

Influence de l'intensité lumineuse incidente sur la vitesse de formation à l'origine.

Le modèle prévoit une vitesse de formation à l'origine $dh_1(0)/dt = - K^2 D\, v\, A$ proportionnelle à l'intensité incidente I_0 par le truchement du facteur D.
Expérimentalement, nous avons mis en évidence l'effet de l'intensité sur la vitesse de formation du réseau, comme nous l'avons rapporté au paragraphe III.3.c.

	$I_0 = 15\ mW / 10\ mm^2$	$I_0 = 1{,}5\ mW / 10\ mm^2$
vitesse de formation à l'origine	1 +/- 0,1 nm/s	0,11 +/- 0,02 nm/s

Sans prétendre à une analyse quantitative, nous remarquons que, pour deux couches de PMMA DR1 d'épaisseur initiale $h_0 = 275$ nm et éclairées respectivement par 15 mW et 1,5 mW, les vitesses de formation à l'origine respectives sont dans un rapport voisin de 10.

Influence de l'épaisseur sur la vitesse à l'origine.

Par le facteur $(1-e^{-\beta h0})$, l'expression précédente conduit à une vitesse de formation à $t=0$ plus élevée pour une couche plus épaisse, ce qui est intuitif puisqu'il y a dans ce cas plus de protagonistes disponibles pour le mouvement. Cependant, comme nous l'avons noté au paragraphe III.1.b., la profondeur de pénétration caractéristique $1/\beta$ est de l'ordre de grandeur ou plus petite que l'épaisseur des couches réalisées. C'est dire que les couches avec lesquelles nous avons travaillées peuvent être considérées comme épaisses et que l'effet est largement sub-linéaire.
Expérimentalement, nous avons mis en évidence l'effet de l'épaisseur sur la vitesse de formation du réseau, comme nous l'avons rapporté au paragraphe III.3.c. Là encore, sans prétendre à une analyse quantitative, nous remarquons que, pour deux couches de PMMA DR1 d'épaisseurs initiales respectives $h_0 = 275$ nm et $h_0 = 55$ nm, éclairées par 15 mW, les vitesses de formation à l'origine respectives sont dans un rapport compris entre 1,5 et 2,5

	$h_0 = 275$ nm	$h_0 = 55$ nm
initial growth rate	1 +/- 0,1 nm/s	0,3 +/-0,05 nm/s

Soit β voisin de 4 μm^{-1} après la rapide perte d'activité optique, sous l'effet de ce que nous considérons être une orientation, déterminée au paragraphe III.1.b.
Par le truchement du facteur $(1-e^{-\beta h0})$, qui vaut pour $h_0 = 55$ nm et pour $h_0 = 275$ mn, le modèle prévoit, dans ces conditions, un rapport des vitesses proche de 3.

Influence de l'angle α entre les faisceaux incidents.

L'angle α est présent dans l'expression de la vitesse à l'origine $dh_1(0)/dt$ par le truchement du nombre d'onde K (proportionnel à $sin^2(\alpha/2)$), de A où figure l^2 (proportionnel à $cos^2(\alpha/2)$) et du facteur de visibilité V (proportionnel à cos α). La valeur du facteur angulaire $sin^2\alpha.\ cos^2\alpha$ qui en résulte est représenté ci-dessous.

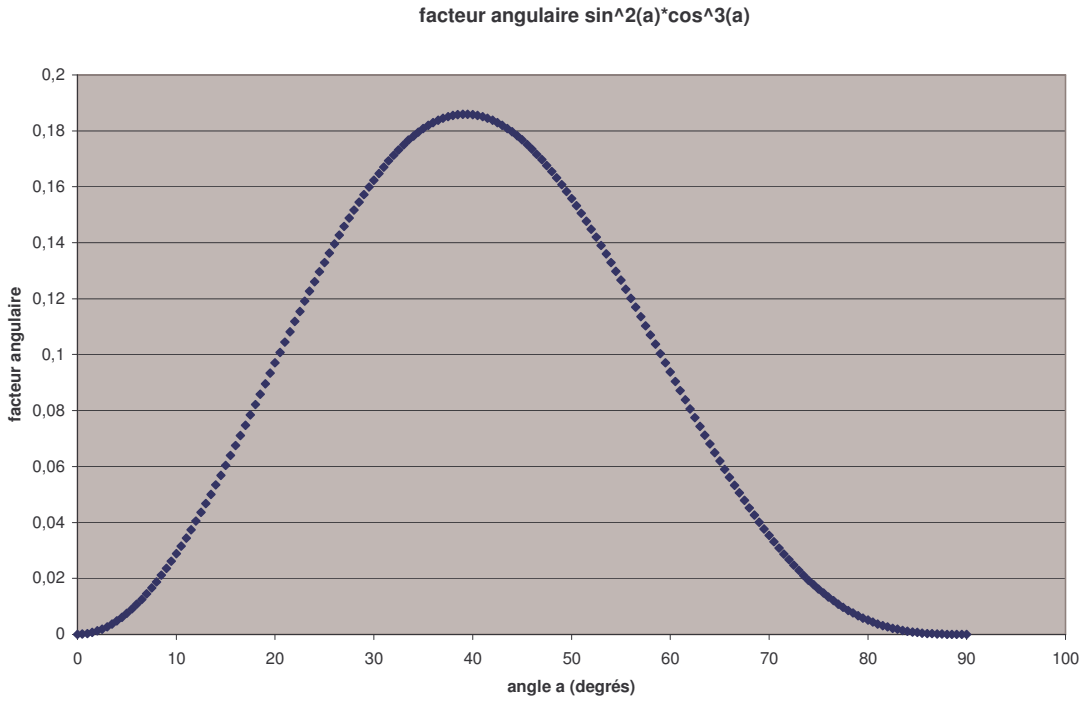

Fig. 26. Facteur angulaire prévu par le modèle présenté.

Nous avons travaillé avec un angle de 32° qui correspond, dans le cadre de ce modèle, à une vitesse de formation à l'origine égale à 90 % de la valeur maximale.
Les expériences effectuées pour un angle voisin de l'angle optimal 45° conduisent à une vitesse à l'origine comprise dans la même gamme. Etant donnée l'incertitude sur les vitesses à l'origine, il serait illusoire de les comparer aux mesures effectuées à 32° où l'écart n'est que de 10%.

Influence de la nature de la molécule.

Nous avons remarqué au paragraphe III.3.e.que, dans les mêmes conditions, les couches de G2MO se caractérisent par une vitesse de formation du réseau près de l'origine au moins deux fois plus grande que pour les couches de PMMA DR1 d'épaisseur initiale h_0 = 275 nm.
Or, la formule de la vitesse à l'origine qui dérive du modèle prévoit que celle-ci est proportionnelle à la fraction A de lumière absorbée :

$$dh_1(0)/dt = - K^2 D\, v\, A$$

Les conditions d'éclairement étant identiques pour les PMMA DR1 et les azodendrimères, K et v ont la même valeur dans les deux cas.
De plus, la fraction de lumière absorbée dans les deux cas est presque la même : l'absorption $A = 1\text{-}e^{-\beta h0}$ est égale à 0,9 (en lumière non polarisée) pour la couches de PMMA DR1 d'épaisseur initiale h_0 = 275 nm et nous mesurons A = 0,97 (en lumière non polarisée) pour la couche de G2MO.
Aussi, la vitesse deux fois plus grande que nous avons observé pour les G2MO ne peut s'expliquer par un facteur d'absorption deux fois plus grand.

Nous attribuons donc la différence observée, dans le cadre du modèle présenté, à **un facteur *D* plus élevé dans le cas des G2MO**. Or :

$$D = l^2 \phi \frac{\lambda}{hc} . I_0 . V$$

Le comportement des G2MO et G4MO diffèrerait de celui des PMMA DR1 par une efficacité quantique Φ plus élevée, un volume entraîné plus grand ou encore un pas de déplacement plus grand. Cette dernière interprétation permet d'envisager un déplacement des dendrimères plus efficace que celui des polymères qui présentent des enchevêtrements.
Pour comprendre ce résultat, nous pouvons comparer la fraction de masse « efficace », c'est-à-dire la proportion d'azobenzène, qui participe au mouvement : nous estimons que la masse « efficace » représente la moitié pour le PMMA DR1 alors qu'elle est plus de deux tiers pour les dendrimères de méthyl orange de différentes générations.
Une gêne stérique plus grande pourrait également induire une efficacité quantique plus faible dans les azo-polymères.

IV.3.3. La perte d'activité optique, origine de la saturation ?

Plusieurs indices suggèrent que la perte d'activité optique préside à la saturation du réseau que rapportent tous les travaux antérieurs sur le sujet, et que nous avons observée.
Certes, le temps caractéristique d'activité optique est plus grand (une quarantaine de minutes) que le temps de formation du réseau. Néanmoins, nous pensons qu'il se combine efficacement à l'effet modérateur mais insuffisant mentionné au paragraphe IV.2.b.β. où les zones les moins éclairées qui sont les plus peuplées s'opposent au mouvement de matière issu de zones plus éclairées mais davantage dépeuplées.
De plus, nous soulignerons à la fin du chapitre V. que l'hypothèse simplificatrice d'un temps caractéristique d'activité optique τ uniforme revient à sous-estimer l'effet du « bleachng » sur la saturation.
Un autre indice est apporté par les travaux de Tripathy et al. qui rapportent une amplitude maximale à saturation pour un angle voisin de 40° entre faisceaux interférents. Cette dépendance en fonction des conditions d'inscription du réseau nous conduisent à penser que « le temps est compté » : si la durée d'activité des chromophores est limitée dans le temps, alors la valeur à saturation sera d'autant plus grande que le processus est rapide. L'angle optimal de 40 ° est proche des 45 ° que nous prévoyions au paragraphe IV.3.2.

IV.4. Elargissements du modèle.

IV.4.1. Cas du réseau de polarisation.

Nous avons montré expérimentalement qu'une intensité lumineuse uniforme mais de polarisation modulée périodiquement donnait lieu à un réseau de surface semblable à ceux obtenus avec une intensité modulée.
Le modèle proposé permet de rendre compte de cette observation expérimentale. Cette fois, l'intensité lumineuse étant uniforme, la probabilité d'isomérisation, donc de déplacement, est la même en tout point. En revanche, le déplacement du chromophore étant supposé se produire selon la direction du champ, son déplacement « efficace » suivant l'axe (Ox) (pour construire le réseau de surface) varie dans l'espace. On peut donc définir un libre parcours moyen efficace suivant la direction (Ox) :

$$l(x) = l \cos \theta(x)$$

où l'angle $\theta(x)$ varie périodiquement selon $\theta(x)=\frac{Kx}{2}$ avec $4\pi/K$ la période spatiale à laquelle tourne la direction de polarisation.
En revanche, les réseaux de polarisation devraient se distinguer par leur dynamique : le modèle prévoit une vitesse de formation du réseau nulle à l'origine.

IV.4.2. Tentatives d'effacement.

Dans le cas des tentatives d'effacement par exposition à un faisceau unique, l'équation d'évolution de la surface libre $h(x,t)$ devient :

$$\frac{\partial h}{\partial t} = D\frac{\partial^2}{\partial x^2}(1-e^{-\beta h(x,t)})$$

On peut comprendre la difficulté à effacer un réseau préalablement inscrit en considérant une couche d'épaisseur initiale h_0 à la surface de laquelle on a inscrit un réseau de surface libre $h_0+h_1(x,t)$ en l'exposant pendant une durée T à un motif de franges d'interférence. En début d'effacement, le facteur d'absorption vaut $\beta_0 e^{-T/\tau}$. Si l'on suppose T suffisamment grand, le facteur d'absorption β est alors suffisamment petit pour développer $exp(-\beta(h_0+h_1(x,t))$ en $e^{-\beta 0}(1-\beta h_1(x,t))$.
L'équation d'évolution de $h_1(x,t)$ s'écrit alors :

$$\frac{\partial h_1}{\partial t} = D\beta_0 . e^{-T/\tau} . e^{-\beta h 0}\frac{\partial^2 h_1}{\partial x^2}$$

Il s'agit d'une équation de diffusion qui prévoit que h_1 tend vers 0.
Néanmoins, le coefficient de diffusion associé $D\,\beta_0\,e^{-T/\tau}$ est petit si le temps d'exposition T préalable a été grand et a conduit au photo-blanchiment d'une grande fraction des chromophores. On comprend ainsi que pour des réseaux exposés à trop grande intensité, comme le rapportent Barret et al., il soit impossible en pratique d'observer l'effacement du réseau.

IV.4. Justifications du modèle développé.

Une théorie des moteurs moléculaires de type « thermal ratchet » a été développée par Prost et al. [20], à la suite des travaux de Magnasco, pour rendre compte du mouvement d'une molécule alternant entre deux états. Sa mise en mouvement suppose l'existence d'une asymétrie spatiale (potentiel périodique asymétrique subi pour chaque forme) et temporelle (introduite par un pompage qui déséquilibre la probabilité d'occupation des deux états et qui conduit à une alternance entre les deux potentiels). Dans ce cadre, les fluctuations thermiques sont transformées en travail. Ce modèle ne permet pas de décrire le mouvement photo-induit des azobenzène étudiés. En effet, le potentiel d'interaction dipôle-champ ne présente pas d'asymétrie spatiale et, même si tel était le cas, sa périodicité, de l'ordre du micromètre, conduirait à un pas *l* micronique.
Néanmoins, nous retenons des modèles de mouvement moléculaire développés la nécessité d'une brisure de symétrie dans l'espace et dans le temps. L'existence d'un pas *l* à chaque cycle d'isomérisation pourrait être attribué aux cycles trans-cis-trans effectués de façon asymétrique : isomérisation de la forme trans à la forme cis par excitation photonique et

[20] Prost, J. ; Chauwin, J. F. ; Peliti, L. ; Adjari, A. *Phys. Rev. Lett.* **1994**, *72*, 2652.

retour de la forme cis à la forme stable trans par une voie optique différente. En effet, la molécule peut passer en forme cis suivant deux chemins réactionnels distincts. Nous pensons également que le retour à la forme trans par voie thermique, qui s'effectue en moins d'une seconde pour les chromophores de type pseudostilbènes, participe également au mécanisme de diffusion. Nous nous figurons difficilement comment une molécule revenant à la forme trans par une voie photonique, symétrique à l'excitation, pourrait subir un déplacement.
Le déplacement exige également une interaction avec un substrat, ou son environnement, qui sous-tend un processus de dissipation qui brise la symétrie dans le temps.

V. Les conséquences du modèle et ses limites à rendre compte des phénomènes observés.

V.1. Peut-on envisager observer le déplacement photo-induit d'une molécule unique ?

Comme nous l'avons souligné au paragraphe II.2., l'observation du déplacement photo-induit de molécules isolées est rendu délicat par la nécessité de maîtriser l'interaction substrat / molécule. De plus, l'ordre de grandeur de l, la fréquence à laquelle une molécule est déplacée d'un pas ainsi que sa durée de vie sont des paramètres cruciaux.
Aussi, nous proposons **un calcul d'ordre de grandeur pour évaluer le déplacement d'un chromophore au cours de sa durée de vie optique.**
A cet effet, nous considérons un laser d'intensité incidente 15 mW/10 mm^2 polarisé linéairement dans le plan de la surface.

Déplacement du chromophore en fonction du temps.

- Dans le cadre du modèle proposé, et à la lueur du résultat du paragraphe IV.3.1., chaque pas *l* effectué par un chromophore est de l'ordre de quelques nanomètres.
- La fréquence à laquelle une molécule effectue un pas l est déterminée en effectuant le rapport du nombre de molécules sollicitées par unité de volume et de temps n_d sur la densité de molécules.

Nous calculons un ordre de grandeur de $n_d = (\Phi \beta \lambda / hc) I$ avec les valeurs explicitées au chapitre IV :

n_d est de l'ordre de 5.10^{17} molécules mises en mouvement par mm^3 et par seconde.

D'autre part, un calcul partant de la densité du PMMA, conduit à une densité également voisine de 1 pour le PMMA DR1. Avec la masse molaire, on en déduit :

10^{18} mm^{-1} pour la densité des chromophores d'azobenzène.

Dans le cadre de ces ordres de grandeur :

un chromophore effectue un mouvement toutes les 2 secondes.

Donc :

après t secondes le chromophore a effectué t/2 translations.

Dans l'hypothèse où, sous l'effet d'une lumière polarisée rectilignement, le déplacement d'un chromophore est une marche aléatoire, de pas *l* à une dimension (suivant la direction de polarisation), après *N* translations, donc après *t* secondes, il se sera déplacé de : $\sqrt{\frac{t}{2}}l$

Distance parcourue par le chromophore au cours de la durée d'activité optique.

Pour une intensité de 15 mW / 10 mm^2, la durée d'activité optique a été estimée à **40 minutes**, soit 2400 secondes au paragraphe III.1.c.

D'après ce qui précède, le modèle de marche aléatoire à une dimension prévoit un déplacement du chromophore de **quelques centaines de nanomètres au cours de cette durée d'activité optique donc dynamique.**

VI.2. Les limites du modèle.

VI.1.a. Comportement en champ proche.

On crée un champ évanescent dans une couche de PMMA DR1 par réflexion totale du faisceau laser sur la lame de verre située face arrière. Exaltant ce champ, une pointe d'AFM de platine donne naissance à un champ polarisé perpendiculairement à la surface de l'échantillon et dont l'intensité, maximale au niveau de la pointe, peut atteindre 10^5 fois l'amplitude initiale.
Une pointe de platine d'ouverture angulaire 20°, située à une vingtaine de nanomètres de la couche, conduit à une accumulation de matière d'amplitude 80 nm et d'extension latérale 100 nm X 100 nm.

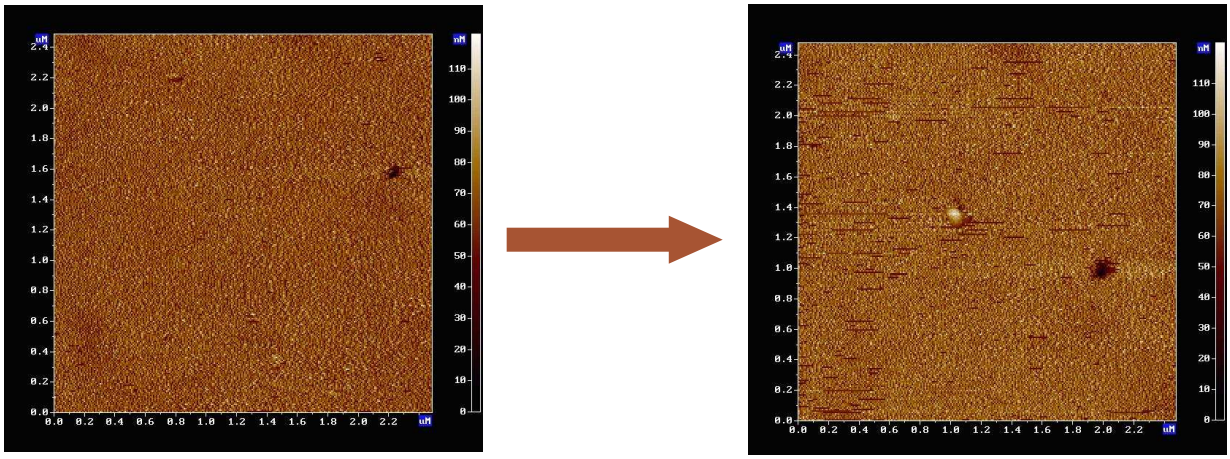

Fig. 27. Image AFM d'une accumulation de matière d'amplitude 80 nm à l'endroit de la pointe. Il convient de noter que la seconde image a subi un décalage par rapport à la première. On peut prendre comme point de repère le trou qui se trouve à droite.

Le déplacement de matière que nous avons observé est différent de celui obtenu à faible intensité avec un dispositif interférentiel. **Il se produit des zones périphériques les moins éclairées pour conduire à une accumulation de matière sous la pointe où l'intensité est très grande**. Peretti et al. montrent qu'avec un champ exalté plus faible, une configuration identique conduit à une fuite de matière vers les zones périphériques sombres.
Ce résultat suggère que le mouvement de matière diffère à faible et à forte intensité.
Il convient également de noter que la couche de PMMA DR1 est exposée dans le cas présenté ci-dessus à un champ proche, contrairement au cas des réseaux des paragraphes précédents. **Peut-être le mouvement photo-induit diffère-t-il en champ proche et en champ lointain**.

VI.1.b. Inversion de phase du réseau de surface.

Ce changement de comportement vis-à-vis du profil d'intensité lumineuse semble également évoluer au cours du temps.
La plupart des réseaux de surface que nous avons réalisés en in situ ou « temps réel » se brouillent après quelques minutes. **En revanche, plusieurs séries d'images mettent en**

évidence un comportement différent : le réseau de matière se translate d'un demi interfrange au cours de sa formation.

Les quatre images qui suivent montrent l'évolution d'un réseau de surface sur PMMA DR1 que nous avons enregistré par la méthode in situ ou « temps réel ». Au cours du temps, le balayage par la pointe AFM de la surface révèle une fréquence double (Fig. 28 et 29) puis une inversion des maxima et minima de la hauteur *h(x,t)* de la surface libre.

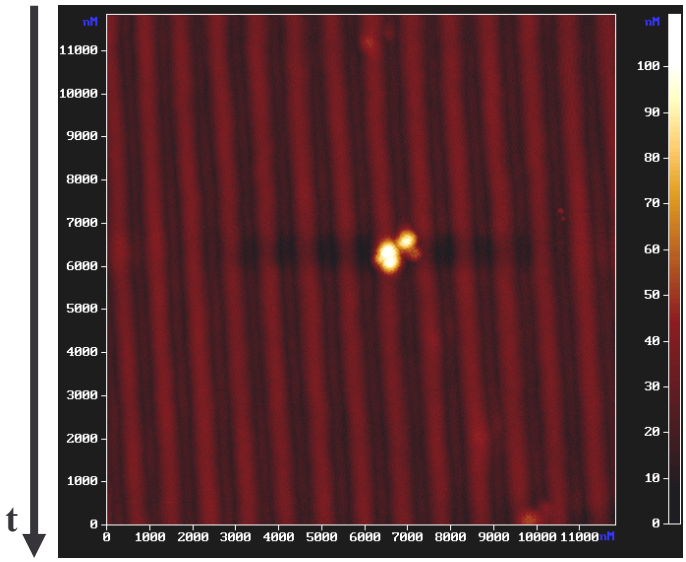

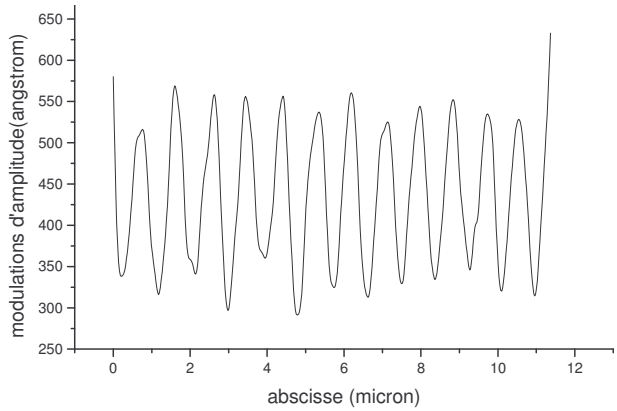

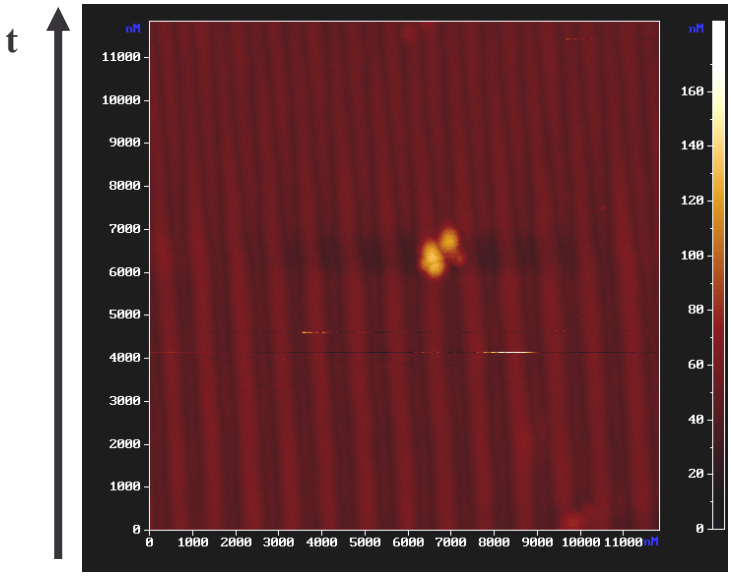

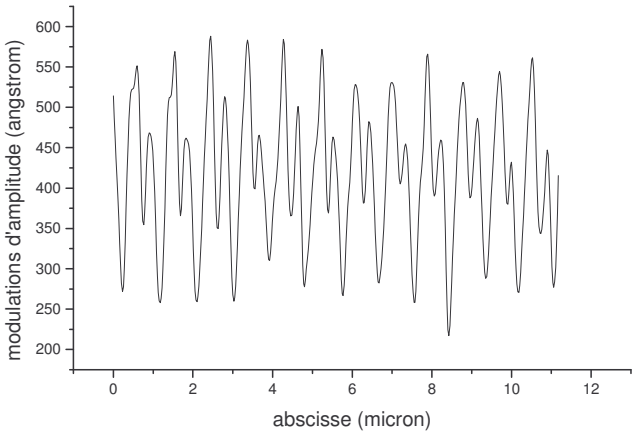

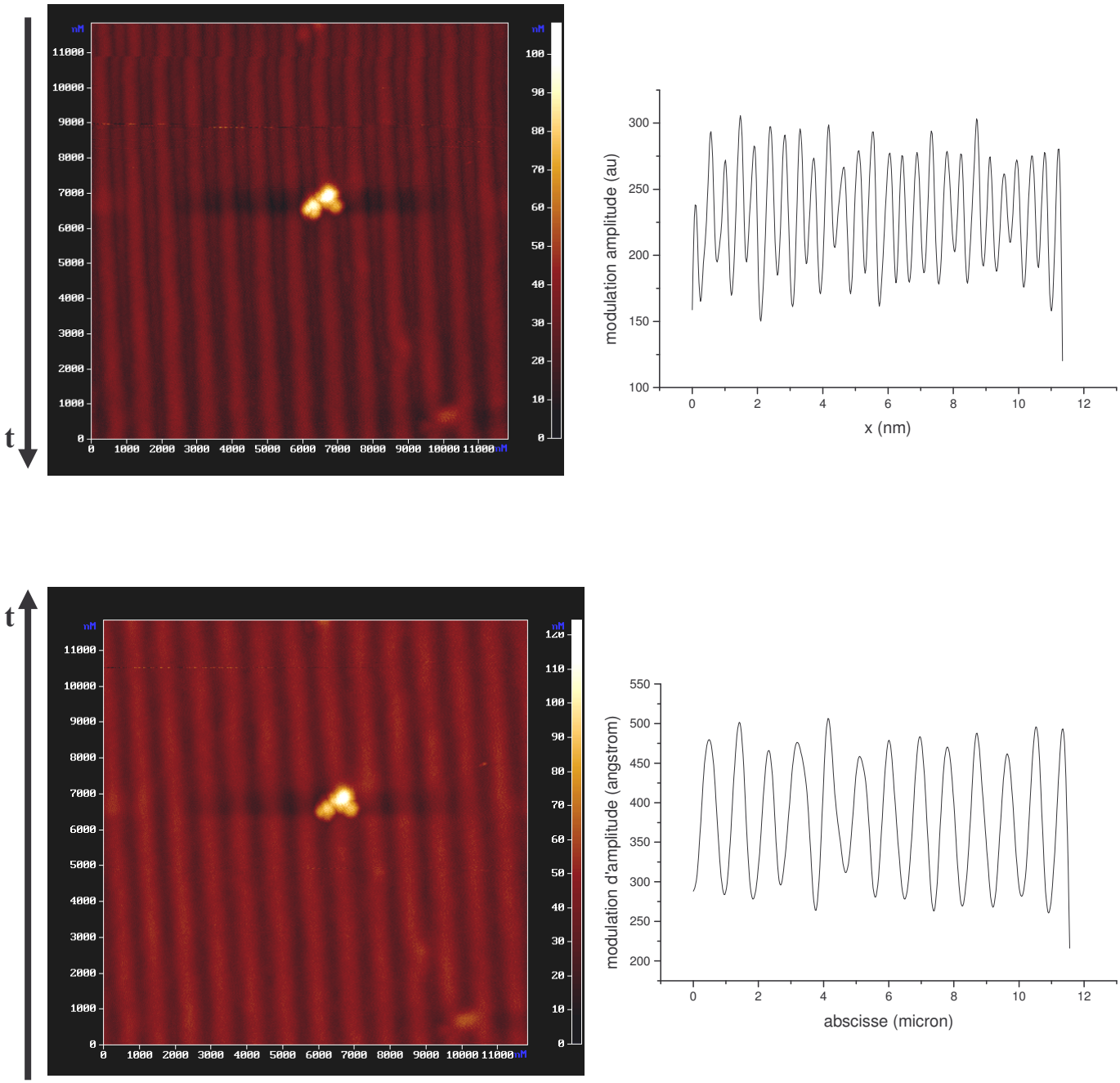

Fig. 28. Images AFM successives : A,B,C et D alternativement balayées de haut en bas et de bas en haut montrent l'apparition d'un réseau de fréquence double qui conduit ensuite à un déphasage de π. Le défaut sert de point de repère.
Les *coupes associées aux images AFM successives font apparaître le doublement de fréquence momentané puis sa disparition. En revanche, le déphasage n'apparaît pas ici.*

Cette observation n'est pas marginale : le déphasage de π au cours du temps, entre le réseau de surface et le profil d'intensité lumineuse, a été mis en évidence par les travaux de l'équipe de J. Perretti par une acquisition simultanée du profil d'intensité et du réseau de surface.
Ce résultat suggère que **le mécanisme proposé** d'une marche au hasard pilotée par la lumière ne **peut-être le seul phénomène à l'œuvre**. Il semble être en compétition avec un processus de type « interaction champ-dipôle » où les dipôles s'accumulent là où le champ est le plus intense. Le mécanisme proposé par Pedersen et al [6], présenté au chapitre I.1., pourrait également rendre compte de ce mouvement vers les zones les plus éclairées.
On peut également penser que le champ électrique à l'intérieur de la couche, auquel sont sensibles les chromophores, ne se réduit pas au champ transmis. Il faudrait tenir compte du

champ diffracté par le réseau qui se forme, et pour lequel l'approximation en champ lointain ne peut être faite ici. De plus, comme le montrent les travaux récents de Lagugné Labarthet et al., l'état de polarisation de l'onde à l'intérieur de la couche est délicat à déterminer.
Ainsi, l'évolution du profil observée dans certains cas doit-elle peut-être attribuée à **l'évolution du champ électrique dans la couche**.

Nous concluons ce mémoire en soulignant l'existence de mouvements de masse photo-induits pour des familles de molécules différant de celles contenant une fonction azobenzène.
Il convient également de noter que l'intérêt du mouvement de matière contrôlé par la lumière repose sur la possibilité d'aller au-delà des limites de la lithographie. En particulier, cela suppose de parvenir à focaliser la lumière au-delà de la limite imposée par la diffraction.
L'exaltation d'un champ électromagnétique, champ évanescent exalté par une pointe métallique par exemple, semble être la voie à suivre pour donner au contrôle photo-induit un rôle de « réglage fin » sur une extension de quelques nanomètres, là où la lithographie classique ne peut accéder.

INTRODUCTION

The light-induced motion of some azobenzene-containing molecules in an environment of polymers, liquid crystals or sol-gel matrices has been evidenced ten years ago[21,22]. Upon low intensity illumination at an appropriate wavelength, thin films of such materials undergo significant topographical changes: the corrugation can reach more than half of the initial thickness of the layer.

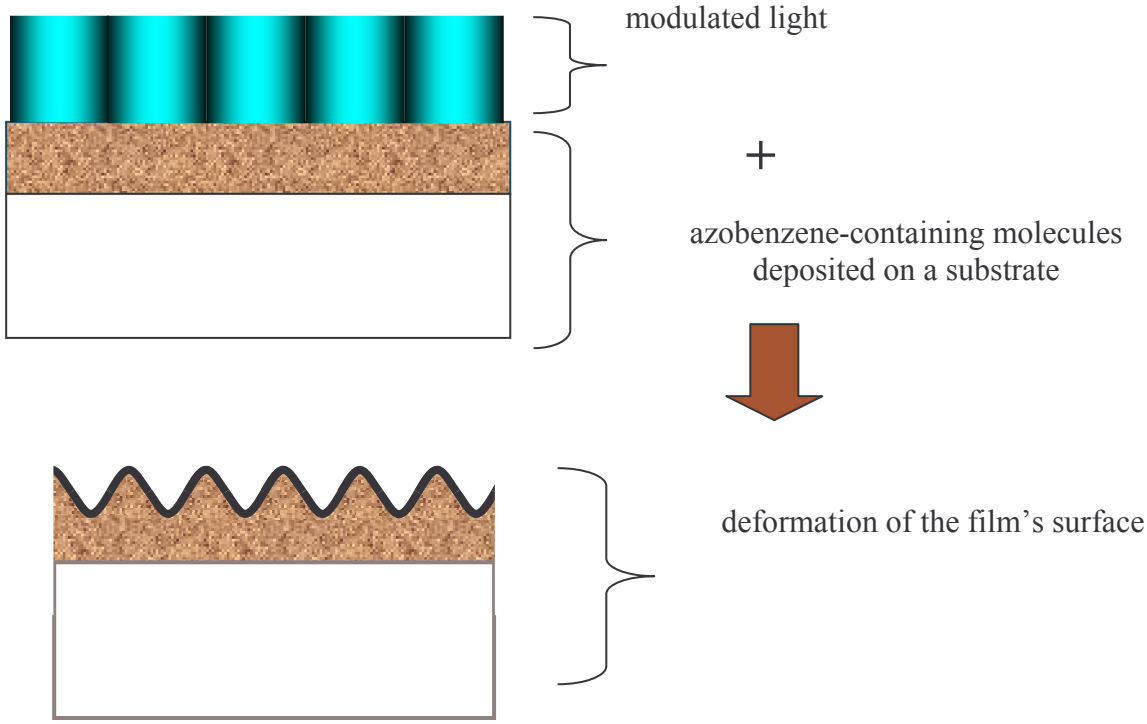

Fig. 1. Schematic representation of the effect of a light modulated pattern on an azobenzene-containing film. Surface deformations can reach several hundreds of nanometers for a one micron thick film. They evidence that a light-induced massive motion takes place in the layer.

[21] Rochon, P. ; Mao, J. ; Natansohn, A. ; Batalla E. *Polymer. Prepr.* **1994**, *35*, 154.
[22] Rochon, P. ; Batalla E.; Natansohn, A. *Appl. Phys. Lett.* **1995**, *66*, 136.

Ten years later, the mechanism that accounts for this light-induced mass motion remains a tangled and divisive question. This phenomenon occurs for intensities too low to perform ablation or to increase the temperature of the film. Several diverging models have been developed but none accounts for all observations. The only consensual view over this process is that the isomerisation of the azobenzene dye plays a major role. However, an essential question is still to be answered: **do the molecules move collectively or is it an individual molecular motion?**

The answer to this question is far from being of purely theoretical interest. Indeed, an individual light-induced molecular motion would open great perspectives in the development of nanotechnologies. For instance, in the context of molecular electronics, molecular architecture could benefit from a way to control its nano-components beyond the diffraction limit. Moreover, storing information at a molecular scale upon light exposure conjures up attractive perspectives of miniaturization.

In this memoir, we present an AFM study and a model of this light-induced surface deformation induced on thin layers of azobenzene-containing polymers and dendrimers by a low intensity laser (473 nm line). Azobenzene containing polymers have already been extensively studied, which a priori lends itself to a comparison with previous studies. As for azobenzene containing dendrimers, they have been scarcely studied so far and they may lead, in the long run, to a better understanding of the phenomenon since, as opposed to polymers, they do not have a main chain that introduces an additional anisotropy.

Using these experimental results, we propose and discuss an interpretation of this phenomenon. This interpretation lies on the assumption of an individual molecular motion where each step is triggered by the absorption of a photon.

The debate over the mechanism of the motion remaining unsolved, we shall dedicate a first chapter to the various diverging models that have been developed. We shall highlight what they describe adequately and what they cannot account for.

Following this state of the art, we present the experimental set-ups and the different molecules which we have used to evidence the light-induced process: molecules containing azobenzene functions were spin cast on glass. We got layers that we exposed to a light pattern. Simultaneously or following this exposition, we observed the induced morphological changes with an AFM study of the layer. In this second chapter, we also comment our choices: why studying layers of molecules when we uphold an individual motion view on the phenomenon? Why use an AFM to follow the surface changes when optical methods could be resorted to?

In the third chapter, we set out our experimental results: the isomerization of the azobenzene function being widely acknowledged to play a role in the process, we first tackle

to the absorption of light in our azobenzene-containing materials. Its time evolution is of particular interest to our purpose of understanding the dynamics of the light-activated motion. Then, results on the evolution of morphological changes allow us to evidence factors which come into play in the mechanism. They also highlight two characteristic values of the dynamics: a growth time at initial time and a saturation value, quite precious for the building of our model.

In a fourth chapter, we develop a model of light-driven random-walk following the work of Nunzi and al. We draw its mathematical implications when applied to the description of the evolution of an azo-layer. Confronting these consequences to our experimental results leads us to discuss the possibility of an individual motion.

Although the fifth chapter leaves hope to experimentally observe the motion of a single molecule in the framework of a diffusion process, it also underlines that this mechanism does not account for all observations: competing processes may be at work.

I completed my doctorate in the context of a European collaboration on Light Induced Molecular Motion: LIMM, which involved chemists and physicists.

This work was undertaken with the aim of gathering quantitative results on the time evolution of light-induced deformations, following what had been done by others since 1995 and further investigating other materials such as dendrimers and other experimental set-ups. However, our experimental observations progressively called into question our understanding of the phenomena at work.

CHAPTER I

The mechanism of light-induced mass motion.

Light-induced mass motion in azobenzene-containing materials at room temperature was reported for the first time in 1995[23]. But light-induced orientation of azobenzenes has been known for much longer.

After a brief historical review of the study of the extensively dealt with orientation phenomenon, we shall show to which extent the light-induced mass motion mechanism remains a tangled and divisive issue. Some view it as a collective process resulting from interactions between azobenzenes. Other groups give an interpretation in terms of individual motions of azobenzene functions.

I.1 Preliminary study of the light-induced orientation of azo-compounds.

As underlined by Natansohn and Rochon[24] in a 2002 review dedicated to *Photoinduced Motions in Azo-Containing Polymers*, the first mention in the literature of a change in a physical property under illumination with polarized light involving an azo aromatic compound (Congo Red) dates back to 1957: Teitel[25] observed that a viscous solution became dichroic when subjected to polarized light and that the effect lasted for about a week.

---

[23] Rochon, P. ; Batalla E.; Natansohn, A. *Appl. Phys. Lett.* **1995**, *66*, 136.
[24] Natansohn, A.; Rochon, P. *Chem. Rev.* **2002**, *102*, 4139.
[25] Teitel, A. *Naturwissenschaften*, **1957**, *44*, 370.

A few years later, Neporent et al.[26,27] explained the phenomenon by rotations of the photo-absorbing molecules to a preferred direction.

But it was only in 1971 that Makushenko et al.[28,29] ascribed this rotation to the photo-induced isomerization of azobenzene.

Then, the subject of light-induced effects on azobenzene materials was altogether overlooked until 1984, when Todorov et al.[30] reported the first optical application in holography by photo-inducing anisotropy in a solution of methyl orange in poly(vinyl alcohol).

They explained the observed anisotropy as a consequence of the orientation of the azobenzenes perpendicularly to the laser polarization direction.

The absorption probability of an azobenzene function is proportional to the square of the cosine of the angle between the polarization direction and the induced dipole in the azobenzene function (the direction of which is almost that of the main axis of the azobenzene). The absorption goes along with a random reorientation of the chromophore. Thus, for those functions whose dipole direction happens to be orthogonal to the polarization direction, there is no more interaction with the laser. They end up oriented perpendicularly to the polarization direction.

In 1987, Eich et al.[31,32] discovered the same light-induced orientation in liquid crystalline polymers containing azobenzene groups.

From 1991 to 2002, the research around light-induced orientation of azobenzene containing compounds “practically exploded with hundreds of publications each year” as Natansohn and Rochon[1] put it in their 2002 review.

However, the fact that upon illumination something more was going on that just an orientation of the azobenzene function was reported for the first time only in 1995[1].

I.2 Light-induced motion: a tangled and divisive issue.

I.2.a. « Collective motion » models.

Barret and al, who have been among the first[1] to observe light-induced mass motion in azobenzene-containing polymers, proposed a model based on the change in free volume

[26] Neporent, B. S.; Stolbova, O. V. *Opt. Spectrosc.* **1961**, *10*, 146.
[27] Neporent, B. S.; Stolbova, O. V. *Opt. Spectrosc.* **1963**, *14*, 331.
[28] Makushenko, A. M.; Neporent , B. S.; Stolbova, O. V. *Opt. Spectrosc.* **1971**, *31*, 295.
[29] Makushenko, A. M.; Neporent , B. S.; Stolbova, O. V. *Opt. Spectrosc.* **1971**, *31*, 397.
[30] Todorov, T.; Nikolova, L.; Tomova, N. *Appl. Opt.* **1984**, *23*, 4309.
[31] Eich, M.; Wendorff, J. *Makromol. Chem.* **1987**, *8*, 467.
[32] Eich, M.; Wendorff, J.; Reck, B.; Ringsdorf, H. *Makromol. Chem.* **1987**, *8*, 467.

requirement in areas where light leads to the isomerisation of azobenzene moieties[33]. The trans to cis change in configuration goes along with an increase in the free volume required around the chromophore. This leads to a local pressure increase in areas where free volume is lacking up to the yield pressure value. Thus, the polymer layer is described as a viscous fluid where matter flows under a pressure gradient.

In such a mechanism, the motion is triggered by the isomerization but it actually occurs only because there is a bunch of molecules and a modulation in the mesoscopic properties of the layer. Then, Barret[34] and al developed a more quantitative approach by resorting to the equations of hydrodynamics. This computation describes properly the effects of most of the parameters involved in the motion induction. Nevertheless, it does not account for the effects of light polarisation which happens to be remarkable: as we shall expose in paragraph III.2.b., the polarisation state of the incident light is essential in the possibility to induce a mass motion.

Pedersen and al explain this mass motion in the context of a mean field theory[35.] In their view, the light-induced orientation of the azobenzene dyes perpendicular to the electric field, as described above, leads to a local order. The mean-field that they generate will tend to align other chromophores in the same local direction, and also causes an attractive force between side-by-side chromophores oriented in the same direction. Overall, this results in a net force on chromophores in illuminated areas, causing them to order and aggregate.

In this model, mass motion is driven by the local order gradient: molecules tend to converge towards most ordered areas, where pressure is lesser.

This model takes into account the effects of light polarisation, but it leads to an accumulation of matter in bright areas. However, at low intensity, it was shown that matter flows away from light, except for those polymers which happen to be liquid crystals[36]. This description also suits cases of high intensity exposures where matter converges towards highly illuminated areas. Nevertheless, these are not the conditions of most out our experiments which are presented in the following chapter. Nevertheless, we refer to this model in chapter V where we report our unexpected experimental observations.

Others describe this phenomenon as a structuring of the film under the light-induced orientation of the azobenzene dyes. Indeed, assuming a certain rigidity between the main chain of the polymer and the azobenzene moieties of the side chains, they contend that the

---

[33] Barrett, C. J.; Natansohn, A. L.; Rochon, P.L. *J. Phys. Chem.* **1996**, *100*, 8836.
[34] Barrett, C. J. ; Rochon, P. L. ; Natansohn, A. *J. Chem. Phys.* **1998**, *109*, 1505.
[35] Pedersen, T. G. ; Johansen, P.M. ; Holme, N.C.R. ; Ramanujam, P.S. *Phys.Rev.Lett.* **1998**, *80*, 89.
[36] Bublitz, D.; Helgert, M. ; Fleck, B. ; Wenke, L. ; Hvilsted, S. ; Ramanujam,P.S. *Appl. Phys. B* **2000**, *70*, 863.

orientation of the azobenzene functions perpendicular to the electric field leads to an orientation of the backbones parallel to the field. Then, the film is described as an elastic medium which stretches in the diresction of the electric field.

This description describes fairly well the behaviour of azobenzene-containing materials, including the effects of the polarization of light. But it does not suit azo-dendrimers which, unlike polymers, do not have a main axis.

Another model of the « collective » kind has been presented by Baldus and Zilker[37] in 2001. It involves spatial variations of the permittivity $\varepsilon(\vec{r})$ of the azobenzene-containing layer. The mechanism assumes that a spatial modulation of the refractive index is generated by the ordering of the azobenzene dyes under modulated irradiation. The modulation of the index leads to a modulation of the permittivity $\varepsilon(\vec{r})$. A force is then exerted between the film and the optical electric field. The driving force is found to be proportional to the square of the electric field in the intensity gradient direction and to the gradient of permittivity at any point: $\vec{f} = -\frac{\varepsilon_0}{2}\vec{E}^2\vec{\nabla}\varepsilon$. In this framework, matter is moved from areas of high permittivity that is to say out of areas of illumination. But such a mechanism is not restricted to azobenzene containing compounds. Any system in which a modulated ordering can be achieved, leading to a modulation of the refractive index, should display such properties. So why should azobenzenes – as well as acrylate-rich hybrid glass materials and fluorozirconate of chalcogenide glasses as we shall underline in the conclusion of this memoir – be the only compound to undergo light-induced mass motion?

I.2.b. «Individual motion» models.

Kumar et al.[38,39] describe the light-induced mass motion they observe in films as the result of an interaction between the inhomogeneous electric field $\vec{E}$ and the induced dipole $\vec{p} = \overline{\overline{\alpha}}\vec{E}$ associated to an azobenzene chromophore, $\overline{\overline{\alpha}}$ being its polarizability matrix. The interaction potential is $U_p = -\vec{p}\cdot\vec{E}$ and the time-averaged force resulting from the field variations is $\vec{f} = \left\langle \left(\vec{p}\cdot\vec{\nabla}\right)\vec{E} \right\rangle$.

[37] Baldus, O.; Zilker, S.; *Appl Phys B* **2001** *72* 425.
[38] Kumar, J. ; Li, L. ; Liang, X. L. ; Kim, D.Y. ; Lee, T.S. ; Tripathy, S.K., *Appl. Phys. Lett.* **1998**, *72*, 2096.
[39] Viswanathan, N.K. ; Balasubramanian, S. ; Li, L. ; Kumar, J. ; Tripathy, S.K. *J. Phys. Chem. B.* **1998**, *72*, 2096.

They justify the fact that, among all materials containing polarizable groups, light-induced mass motion is only observed in azobenzene-containing compounds, by contending that the repeated isomerization of the azobenzenes leads to a plasticization of the film's surface permitting material mobility well below the glass temperature.

This model accounts for the effects of light polarization reported in the literature[1,40] and that we shall experimentally evidence in chapter IV. The force exerted on the azobenzene dipoles being proportional to $\left(\overline{\overline{\alpha}}\vec{E}\cdot\vec{\nabla}\right)\vec{E}$, it makes sense that, given the field modulation (expressed through the gradient operator) some polarization states will not allow to put the azobenzene in motion.

Nevertheless, since the interaction potential is $U_p = -\vec{p}\cdot\vec{E}$, it is minimized in areas where the field amplitude reaches a maximal value. So, this mechanism leads to a piling up of the molecules in the brightest areas and to depletion in the darkest ones.

The mechanism proposed by Nunzi et al.[41,42] consists in a one dimensional random walk motion of the azobenzenes along the polarization direction. The motion of the azo dye is referred to as a "caterpillar-like" molecular motion. In their view, an isomerized azobenzene function is shifted by a given distance along the polarization direction of the electric field.

This is the description that we shall start from in chapter IV to describe the behaviour that we expect from our experiments on azobenzene containing films.

According to Delaire et al.[16], this model accounts for some effects of light polarization but fails to describe the mass motion observed when the intensity is uniform and only the polarization is modulated. However, we show in section IV.4.a. that even the effects of purely polarized patterns can be accounted for by such a "caterpillar-like" motion model.

[40]Delaire, J. A. ; Nakatani, K. *Chem. Rev.* **2000**, *100*, 1817.
[41] Lefin, P. ; Fiorini, C. ; Nunzi, J. M. *Pure Appl. Opt.* **1998**, *7*, 71.
[42] Lefin P.; Fiorini, C.; Nunzi, J. M. *Opt. Mater.* **1998**, *9*, 323.

CHAPTER II

Materials and methods.

II. 1.Which molecules to evidence the mass motion?

We carried out the experimental study of light-induced motion on two families of azobenzene-containing molecules deposited by spin coating on glass. The process and its parameters are described in the following paragraph.

First and foremost, we used PMMA DR1. It is a polymer whose statistical molar composition is 70% of PMMA and 30 % of DR1 functions. The latter has an azobenzene functionalized side chain. PMMA DR1 has already been extensively studied and lots of data are available[43,44]. Moreover, PMAA DR1 is easily purchasable.

Nevertheless, we extended our study of light-induced molecular motion to generation 2, 3 and 4 POPAM dendrimers which have methly-orange functions (azobenzene derivatives).

Unlike polymers such as PMMA DR1, POPAM dendrimers do not have a main chain imposing a symmetry breaking along its direction that may introduce spurious effects.

Moreover, to our knowledge the study of their mass motion has been scarcely studied.

We also studied dendritic molecules referred to as Fréchet's molecules.

[43] Delaire, J. A. ; Nakatani, K. *Chem. Rev.* **2000**, *100*, 1817.
[44] Natansohn, A. ; Rochon, P. *Chem. Rev.* **2002**, *102*, 4139.

These dendrimers which are not purchasable have been synthesized by the group of Professor Vögtle from the Kekulé-Institut für Organische Chemie und Biochemie in Bonn, with whom we collaborated in the context of the LIMM European project.

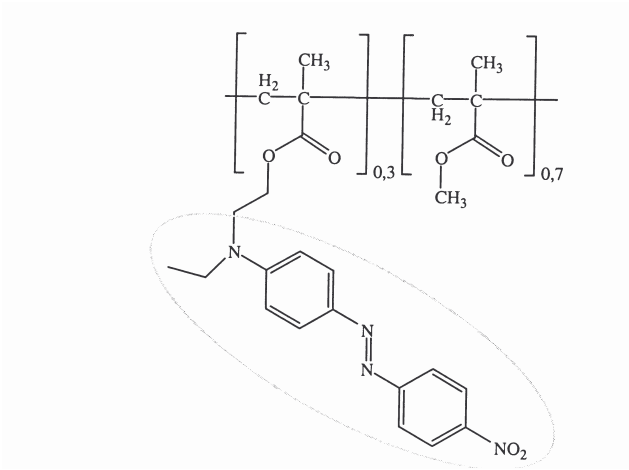

Fig. 2. PMMA DR1 statistical unit.

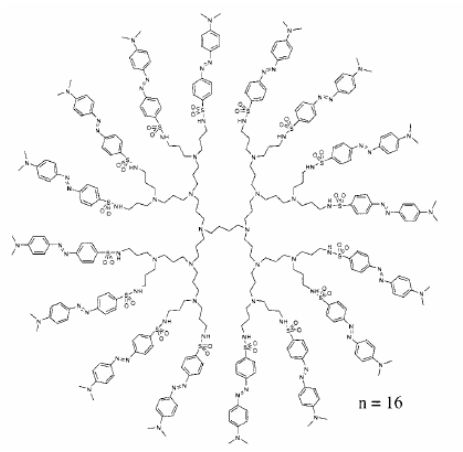

Fig. 3. POPAM methyl orange G3 dendrimer.

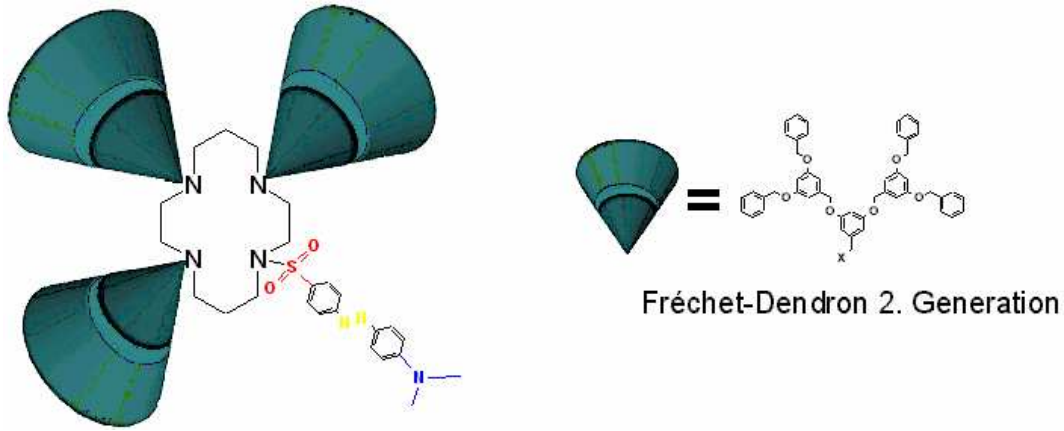

Fig.4. Frechet's azo-molecule : méthyl orange and Frechet dendrons

II. 2. Which environment for the azobenzene-containing molecules?

We dissolved azobenzene-containing molecules in chloroform. Then, we deposited them by spin-coating on a glass substrate. The parameters used for the spin-coating were a speed of 20000 rpm for 10 seconds. Then, the films were annealed at 80°C for 30 minutes.
This way, we get thin films whose thickness ranges from 0,1 µm to 1 µm. We shall see in section III.1.b. that, for a given azobenzene-containing molecule / chloroform composition,

the thickness of the layers that we get is controlled by 10%, except for a few samples for which the uncertainty can reach 30 %.

These layers are environments dense in azobenzene chromophores: we estimate the density to be around 10^{21} molecules per cubic millimetre.

The choice of layers as an environment to evidence the light-induced molecular motion may strike as paradoxical in a work which presents an interpretation of this phenomenon in terms of an individual motion.

However, the study of isolated molecules is quite tricky to achieve.

Indeed, preparing samples of isolated azobenzene-containing molecules, referred to as "sub-monolayers" deposited on a substrate is a difficult task

Indeed, if one wants to observe the motion of single molecules, it is mandatory to find the appropriate substrate which interacts enough with the molecules to allow a friction generated motion which requires a coupling (we shall expose our assumptions for the motion in section IV.4.) . But the interaction should not be too strong for the molecule not to remain stuck to the substrate and to move.

The search for a preparation procedure of "sub-monolayers" and the attempt at observing an individual molecular motion were undertaken in our research team as I was working on thin layers.

Isolated GMO dendrimers were obtained as it is shown on the AFM image below. However, no single molecule motion was observed. This does not invalidate the possibility of observing the motion of a unique molecule. We shall underline in the last chapter that the duration of the experiment and the lifetime of the chromophores (which will be discussed in section III.1.c.) are critical parameters that may explain why no light-induced motion was observed.

Or maybe the molecule / substrate interaction was too strong to allow the molecular motion. This is why we resorted to the study of thin films instead. What will be necessary is to link the experimental results obtained for these films with their expected behaviour in the context of an individual motion.

II.3. How to induce the mass motion?

To evidence the mass motion, the layers must be subjected to a light pattern modulated in space at a micrometer scale. Indeed, we are expecting to observe the motion of molecules so the intensity gradient, being known to play an essential role, should be large enough at the mesoscopic scale.

We resorted most of all to interference patterns obtained by the division of a blue laser wave front. This choice was made for several reasons.

First, for an angle between interfering beams around 30 degrees, the pattern is a sinusoidal modulated intensity of micrometric period. This way, we get a modulation at the scale for which we want to observe a molecular motion.

Furthermore, the periodicity of the pattern which spans over hundreds of micrometers makes it much easier to spot than a pattern of identical periodicity which does not repeat itself.

But this configuration we also opted for since it lends itself to a comparison with works of other groups.

The laser should be coherent enough, at least a few centimetres. Otherwise, the equality of the path of the interfering beams would be a critical condition which otherwise would make the optical set-up quite tricky. A good coherence also gives enough interference fringes for the pattern to be easily spotted. We worked most of the time with a solid laser which gives a 473 nm line. Its coherence length is several tens of centimetres.

We also carried out a few experiments with the 488 nm line of an Argon laser which is also of great coherence.

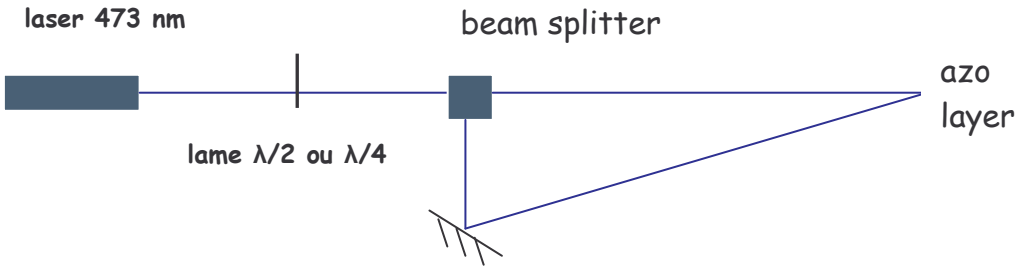

Fig.5. Illumination of an azo-layer with an interference pattern.

We used mainly three interference configurations. The calculations which lead to the expressions given below are detailed in annex II.

Linearly polarized interfering beams.

The solid laser, as well as the Argon laser, is linearly polarized. Its polarization direction is vertical that is to say perpendicular to the plane defined by the two interfering beams resulting from the split-up (that is to say perpendicular to the optical table).

In what follows, we shall refer to the direction perpendicular to the interfering beams as the Y axis. The Z axis is defined by the direction perpendicular to the layer exposed to the beams.

As for the X axis, which completes the orthogonal set of axes, it is located in the plane of the sample.

- *For two interfering beams whose linear polarization direction is along the Y axis*: the pattern consists in interference fringes parallel to the Y axis. The light intensity distribution is modulated along the X axis: $I(x) = 2I_0(1+\cos Kx)$.
This configuration is referred to as the *s polarization state*.

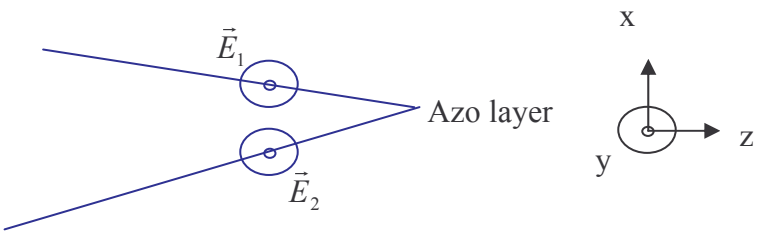

Fig. 6. Interference of s polarized beams

- *For two interfering beams whose linear polarization is located in the plane defined by the beams:* the pattern consists in interference fringes parallel to the Y axis. The light intensity distribution is modulated along the X axis: $I(x) = 2I_0(1+ v\cos Kx)$ where $v = \cos^2\alpha$ is the visibility factor which depends on the angle between the two polarization directions which is equal to the angle between the two interfering beams.
This configuration is referred to as the *p polarization state.*

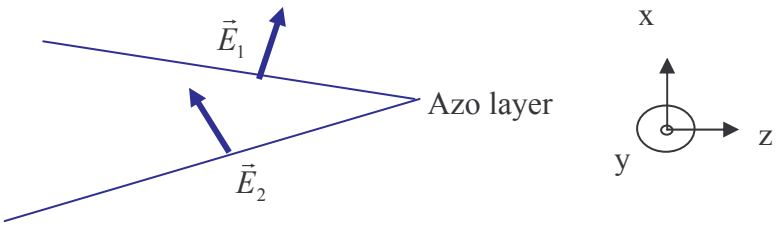

Fig. 7. Interference of p polarized beams

Circularly polarized interfering beams.

- *If both beams are either both left or both right circularly polarized:* the resulting pattern is circularly polarized and the intensity modulation is $I(x) = 2I_0(1+\cos^2\alpha/2.\cos Kx)$.

- *If one of the beams is left circularly polarized and the other is right circularly polarized:* as the calculation presented in annex II shows the intensity is almost uniform. It is the linear polarization direction which is modulated: it rotates periodically in space.

In the experiments presented in the following chapter, we have widely used the interference pattern of two linearly p polarized beams. The other three configurations have mainly be resorted to for qualitative observations.

II. 4. Observation of the mass motion: the atomic force microscope (AFM).

Subjected to various light patterns, the azobenzene-containing layers display surface deformations.

We observe and measure these deformations through the medium of an atomic force microscope (AFM) used in semi-contact mode. We worked with a Stand Alone© from NT-MDT™. The AFM tips used to scan the surface are chosen as supple (thus as long) as possible in order to minimize its interaction with the surface.

The AFM sweeping amplitude is 60 µm × 60 µm, which is large enough to allow the observation of the layer surface deformation induced by a light pattern modulated at the micrometer scale as referred to above.

We shine a PMMA DR1 layer for ten minutes with an interference pattern whose light modulation follows:

$$I(x) = 2I_0 (1 + v \cos Kx)$$ where the step $2\pi / K$ is equal to 0,85 µm.

After illumination, the exposed area is spotted by a mark on the glass side, which allows us to put the AFM tip at the right place.

The AFM image that we get displays a periodic surface deformation as shown on Fig. 5. The deformation period is equal to the one of the light interference pattern and its shape is quite similar to a sine form.

Thus, upon exposure to a light interference pattern, we observe a surface relief grating such as those described in the literature.

The order of magnitude for the value of the maximum deformation amplitude observed is tens of nanometres. We shall describe in the following paragraph how to find this maximum.

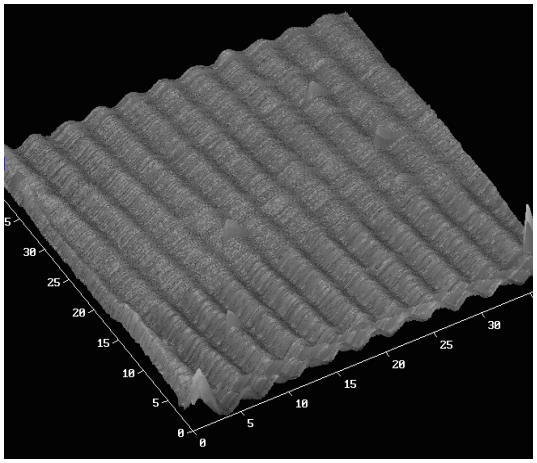

Fig. 8 AFM image of a surface relief grating recorded on a PMMA DR1 film after having been exposed for a few minutes to an interference pattern.

One could object that there is a widely used optical method to study such a surface relief grating, especially as it is quickly carried out an as it allows to follow the amplitude evolution of the grating. This method consists in shining a red laser beam on the sample, at the same place where the surface relief grating is being recorded. The light-induced motion leading to a sine shape grating, the red laser light cast on it is diffracted[1,2]. The diffraction pattern obtained by transmission or by reflection consists in a set of periodic spots along the X axis (defined in section). The brightest spot being the central one corresponding to the zero order of diffraction and the increasing n orders on both sides of it being less and less intense as n increases.

In order to follow the evolution of the grating's amplitude, the teams who use this method assume that the first order's intensity should be proportional to the amplitude of the surface relief grating.

However, in the context of a work which intends to account for an individual motion mechanism, the choice of the AFM makes more sense. Indeed, it allows a direct observation of the surface whereas the optical method described above is based on the global properties of the film.

Besides, annex III shows that a calculation, even under its most simplified form, leads to a non linear relation between the amplitude of the sine form grating and the intensity of the first order peak. This result calls into question the use of such an optical method in the context of a quantitative study quantitative of the amplitude's time evolution.

Furthermore, in highly exposed areas the chromophores are progressively oriented in a plane orthogonal to the polarization direction. The resulting modulation of the chromophores'

orientation leads to a modulation of the refraction index of the film whose periodicity is similar to that of the deformation amplitude[45].

Finally, the direct observation of the free surface with an AFM ended up being very learning. Indeed, as we shall realize in chapter V, this method displays still not well understood phenomena that we were not expecting as we started to tackle this matter.

We have also contemplated resorting to methods inspired from the nanolithography technique to observe the light-induced motion.

Using an optical microscope, it is possible to project a mask of a few hundreds micrometers on a film. Scanning this surface with an AFM tip, it could be possible to check if the molecules have left the illuminated area.

II.5. Experimental procedures: ex-situ and real-time AFM observations.

The experiments that we carried out can be divided into two types:

- Ex situ experiments which consist in two steps.

First, the sample is exposed to a light pattern in order to record a surface deformation.

Then, the area of the sample that has been exposed is scanned with an AFM in order to determine the effects of light on the free surface.

- In situ experiments for which the surface deformation is recorded and AFM scanned at the very same time. This method enables us to perform a real-time study of the induced surface deformation of the films.

II.5.a. Ex situ experiments.

As a first step, the free surface of the film is exposed to the interference pattern as depicted below.

In what follows, we shall refer to this as a "front side" exposure, as opposed to a "back side" exposure for which the sample is illuminated through the glass substrate.

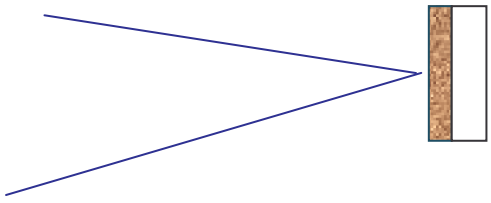

[45] Labarthet, F. ; Buffeteau, T. ; Sourisseau C. *J. Phys. Chem. B.* **1998**, *102*, 2654.

Fig. 9. The film is front side exposed prior to the ex situ study.

Once the [illegible] the 10 mm^2 area on which the pattern was shone. This is done on the back side of the sample by marking the illuminated area with a pen before switching off the laser.

Then, the pinpointed area can easily be placed under the AFM tip.

However, the intensity profile of both interfering beams is not uniform. It consists in a Gaussian distribution of energy whose major part is concentrated on a 200 µm × 200 µm surface. The pattern resulting from the superimposition of the two beams, the intensity maximum is located in a restricted area. Given that light is triggering the phenomenon and that the effects on the free surface should be all the more noticeable as the intensity is high, we are expecting the noticeable surface deformations to be restricted to an area much smaller than a square millimetre.

Thus, it is crucial to find out this restricted area.

This is why, following the rough pinpointing with a marker, the sample is placed on a translatable X-Y stage which enables us to displace the sample by steps of 10 µm. Then, by placing the AFM's head over the sample, we can successively slightly move the sample with the X-Y stage and image the surface with the AFM, repeating this procedure until the maximal deformation has been found.

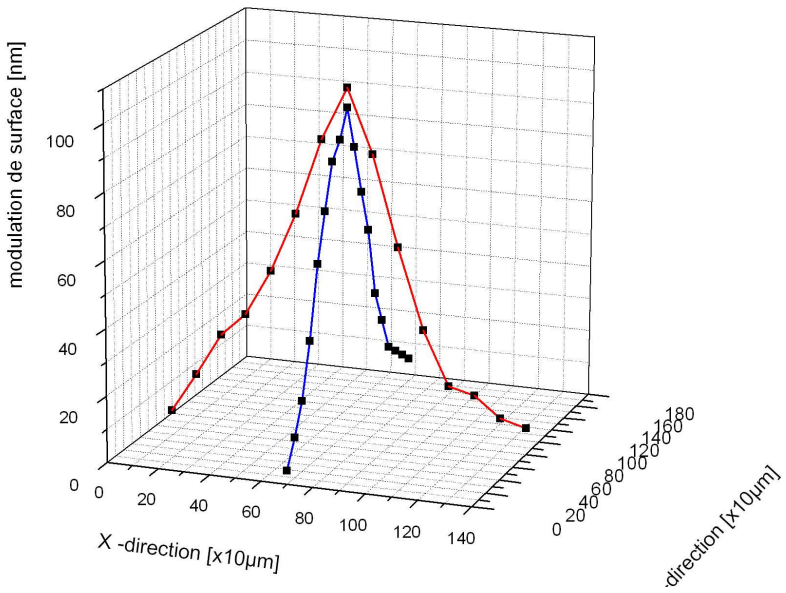

Fig. 10. The 10 mm^2 exposed surface is then scanned with an AFM. An X-Y stage is used to find the maximal amplitude corresponding to the area where the intensity was maximal. This figure shows that the maximum is to be found in a 100 μm by 100 μm area.

However laborious and time-consuming it may seem, looking for the maximum is an essential step to a quantitative approach.
Nevertheless, AFM studies reported in the literature do not mention it.

Most of them consist in drawing point by point the evolution of the surface relief grating amplitude versus the time of the exposure to an interference pattern. In this case, each point on the curve corresponds to the maximal value actually obtained with an AFM as described above, for a given exposure time.
This process is quite time-consuming since each time on a curve requires several experiments to assess the error bar. And each experiment takes the corresponding recording time (from a few seconds up to several hours) plus the determination of the maximum deformation with the X-Y stage as described above.

II.5.b. In situ or "real-time" experiments.

In situ experiments consist in simultaneously recording the surface grating and measuring its amplitude with an AFM.
This process was undertaken in order to save time since it does not require minutes or hours to determine just one point on a curve.
The free surface of the film being sterically occupied by the AFM imaging device, it is necessary to expose the sample to the light pattern through the glass substrate, that is to say from its back side.
We built a support in order to hold the AFM scanning head in a vertical position so that its tip can scan the free surface of a film which is simultaneously exposed to the laser beam.

We also equipped the support with a motor which allows the approach of the tip towards the surface.

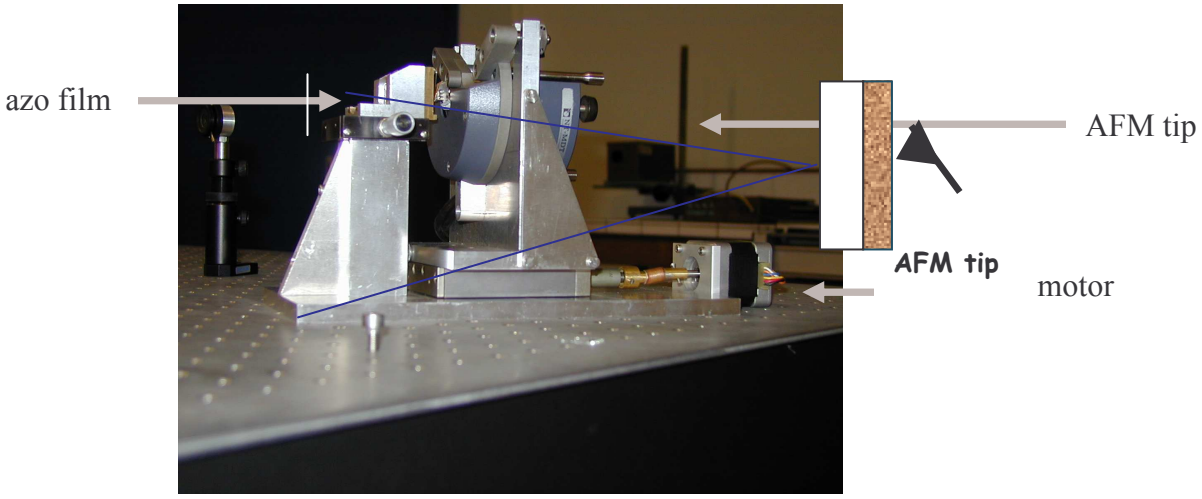

Fig. 11. AFM support for real-time study.

Fig. 12. In situ or « real-time » device: the film is exposed through its back side while its free surface is scanned by the tip of an AFM.

As the film is being exposed through its back side, the AFM tip which is simultaneously scanning the surface displays the evolution of the grating which is being inscribed. The amplitude of the grating increases progressively under the tip as revealed by the progressively appearing grating on the AFM image.

Once the simultaneous recording / imaging process is over, the AFM images which bear the information about the growth of the amplitude needs to be extracted from them.

This is achieved through a Labview 5.1™ program that we wrote in order to extract from each line the corresponding amplitude.

In order for this procedure to be valid, the sweeping conditions must be such that the time it takes the AFM tip to sweep one line should be small compared to the characteristic evolution time of the amplitude. Actually, a 1 Hz sweeping frequency proved satisfying.

The Labview 5.1™ program consists in taking the Fourier transform from each line of the AFM images and retaining from it the amplitude at the appropriate spatial frequency which is the frequency K common to the interference pattern and to the surface relief grating.

Once normalized, the values obtained for each time are plotted on an amplitude-versus-time graph which describes the evolution of the surface grating as rendered by the AFM.

This method is much less time-consuming than the ex-situ method. Nevertheless, because it involves a back side exposure, it happened to display spurious phenomena that prevented a full use of most of the curves that we get as we shall show in section III.3.a. But it also proved

quite enriching since it allowed us to evidence processes that would have been altogether overlooked with the ex situ method. These will be exposed in chapter V.

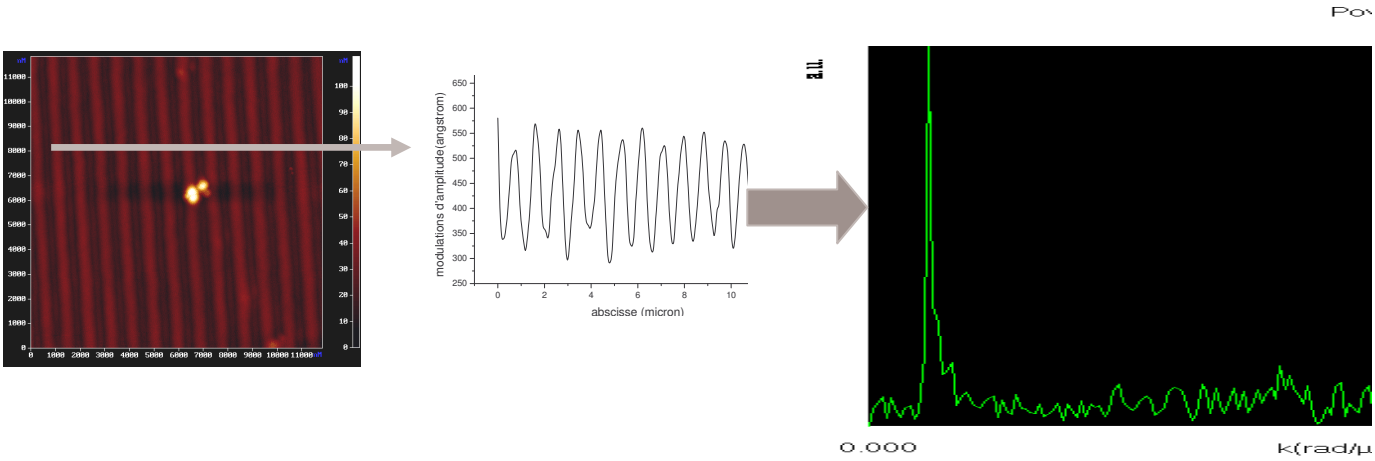

Fig. 13. Analysis of an AFM image recorded during a real-time experiment. Each line of the image corresponds to a sampling time t_i to which is associated the amplitude of the grating h_i through a program that we wrote in Labview. It consists in taking the Fourier Transform of the i^{th} cut and retaining the area under the peak corresponding to the periodicity of the grating.

Chapter III
Experimental results.

The experimental results presented in this chapter aim at finding out the essential characteristics and parameters of the light-induced motion.

The isomerization process being acknowledged to play a major role in the molecular motion, we start this chapter with a study of the absorption properties of the azobenzene-containing materials.

Then, we draw the main characteristics of the light-induced motion: does matter flow away from or towards illuminated areas in our experimental conditions? Is it more than just a thermal effect? Are polymers the only azobenzene-containing materials which move under illumination? Do single non-substituted azobenzenes undergo light-induced motion?

Once these questions have been addressed, we present the time evolution of a light-induced surface deformation and the way parameters such as the intensity of light, the thickness of the film, the way of illuminating the sample, the nature of the molecule influence this evolution.

III.1. Absorption properties of PMMA DR1.

However tangled the mechanism of the light-induced molecular motion may be, it is unanimously acknowledged that it is triggered by the trans / cis isomerization of the azobenzene functions.

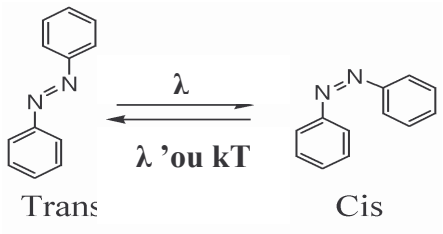

Fig. 14. Isomerzation of the azobenzene function.

The isomerization of the azobenzene function can occur following two mechanistically differing paths, either with an inversion or with a rotation of the azobenzene function.
Thus, the understanding of light-induced mass motion requires sticking first and foremost to the absorption properties of azobenzene-containing materials and their evolution with time.

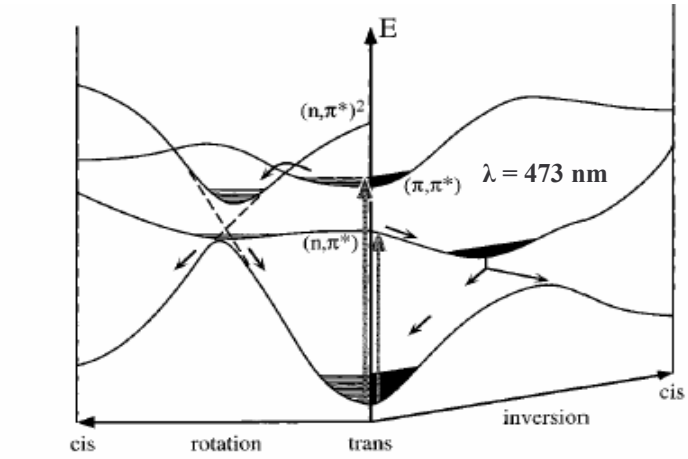

Fig. 15. Potential energy diagram of unsubstituted azobenzene according to Rau[1]. The arrows indicate possible reaction paths after excitation of the chromophore in the trans configuration.

III.1.a. Absorption spectrum of PMMA DR1 layers.

We started with a visible spectroscopy study of PMMA DR1 and GMO films.

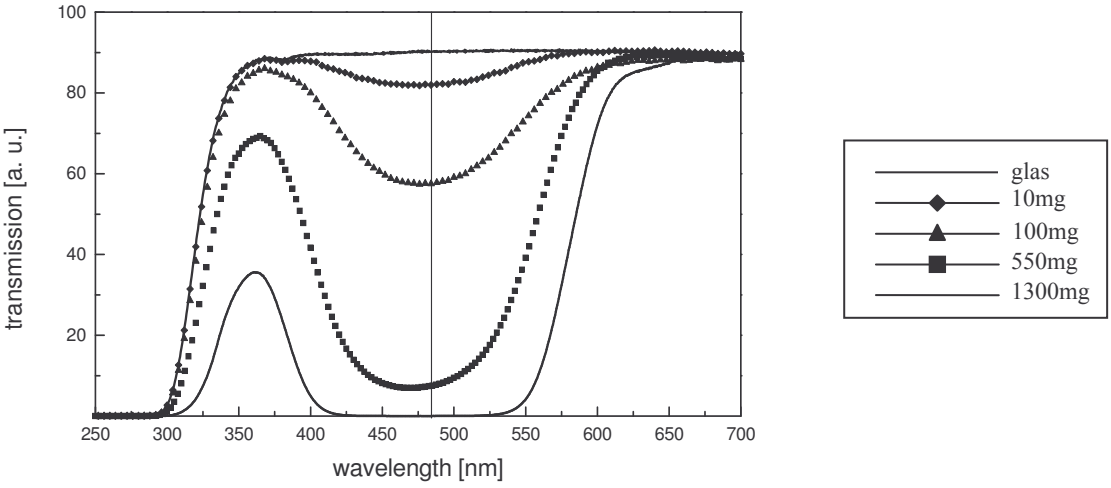

Fig. 16. Transmission spectra for PMMA DR1films of various thicknesses.

The absorption band in the blue-green range of the azobenzene-containing polymers that appear above is quite wide. The value of the wavelength used to induce the mass motion is not critical in the sense that, though most experiments reported in the literature were carried out with the 488 nm line of an Argon laser, the 473 nm of the solid laser that we used is still right in the middle of the absorption band.

For PMMA DR1 – as well as for the other azo-molecules used – the azobenzene function is substituted with both an electro-donor and an electron-acceptor group. . According to the classification of azobenzenes achieved by Rau[46], such bi-substituted functions – which are referred to as "pseudostilbenes" – have π-π* and n-π* bands which are practically superimposed. As a consequence, the light around 400-500 nm that activates the trans-cis isomerization also activates the back cis-trans isomerization. The resulting absorption spectrum that we observe displays a large band between 400 and 550 nm.

The thermal back isomerization is also much faster for pseudostilbenes.

Thus, photo-activated pseudostilbenes perform successive trans-cis-trans isomerization cycles.

[46] Rau, H. *Photochemestry of azobenzenes*. In: Rebek, J. editor, *Photochemestry and photopjysics*, vol. 2, Boca Raton, FL: CRC Press, **1990**, p. 119.

The substitution of azobenzenes seems to play a major role in the mass motion process as reported in the literature[47]. We shall evidence its role in section III.3.d.
At high light intensity, the back isomerization to the trans form is ensured by the photonic mechanism. Nevertheless, at low intensity, we figure that the thermal process may prevail.

III.1.b. Measure of the absorption coefficient β at λ=473 nm for PMMA DR1 films.

As a first step, we want to link the composition of the solutions used for the spin-coating to the thickness of the films that we get.
In order to measure precisely the thickness of the layers, we use a scanning electron microscope.

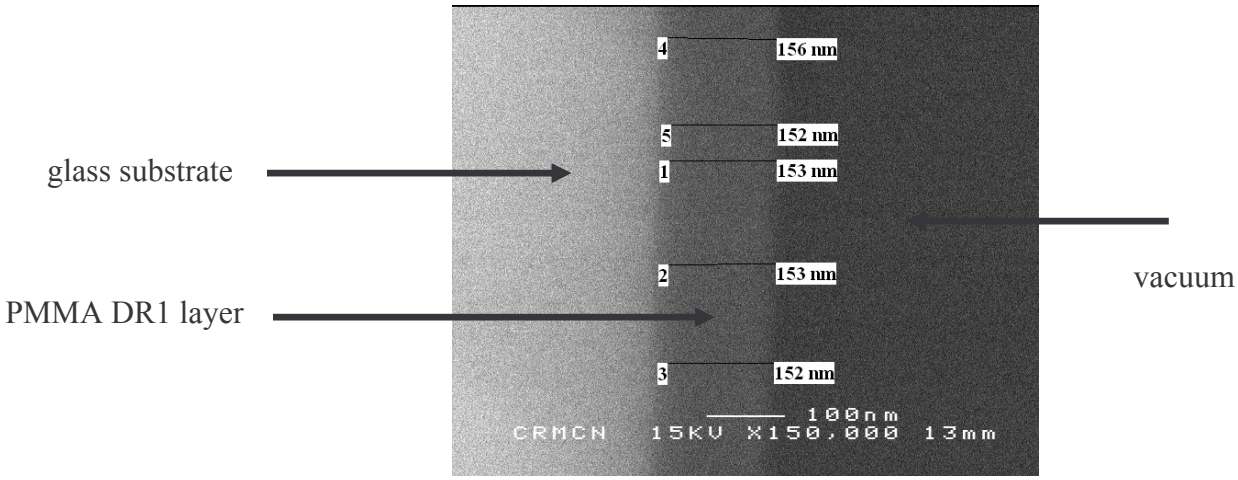

Fig. 17. Scanning Electron Microscope image of a PMMA DR1 film prepared by spin-coating of a solution whose concentration is 250 mg/10 mL.

This way, it is possible to relate the PMMA DR1 / chloroform composition to the thickness of the film that we get by spin-coating.

[47] Almeria, N.; Rochon, P. *Chem. Rev.* **2002**, *102*, 4139.

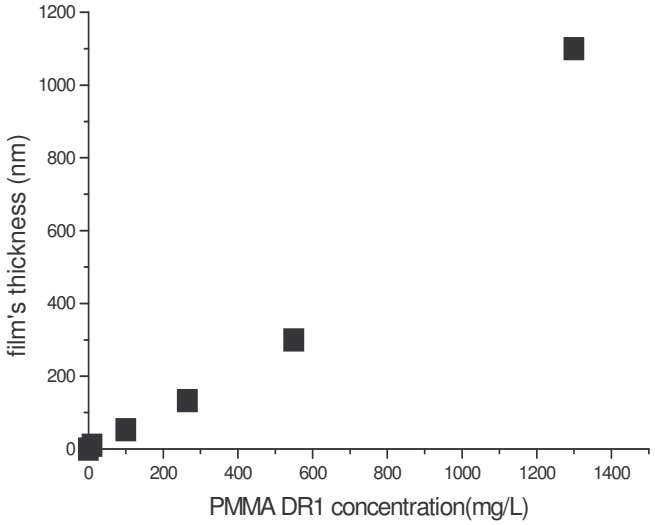

Fig. 18. Relation between the concentration of PMMA DR1 in chloroform and the thickness of the film that we get by spin-coating. Points are deliberately big to show that the relation is roughly linear.

The transmission of the layers at λ = 473 nm is given by the spectrogram of the layer as presented in section III.1.a.

Assuming that the absorption process in the film is linear in intensity, we can apply Beer-Lambert's law $I_t = I(0)\, e^{-\beta h0}$ which links the thickness of the layer h_0 to the intensity I_t that it transmits. Thus, the determination of the thickness and the transmission for two points give the value of the absorption coefficient: β = 8 μm^{-1}. This means that the intensity of the laser beam is attenuated by a factor e when it goes through 120 nm.

It is interesting to compare this value of the penetration depth to the range of the thicknesses that we get by spin-coating. The values of the thickness estimated in section III.1.a. are definitely not negligible compared to the penetration depth which is around 120 nm. Thus, in what follows we shall not assume that the films are thin, especially when it comes to calculations in chapter IV.

Knowing the value of the absorption β, we can determine the variations of a film's thickness at the scale of one centimetre through an absorption method.

Indeed, from Beer Lambert's law $I_t = I(0)\, e^{-\beta h0}$, we can link the relative variation of the film's thickness δz to the relative variation of the transmitted intensity δI:

$$\frac{\delta I}{I} = \beta . \delta z$$

The following graph displays the variations of the locally transmitted intensity at the scale a few millimetres for five films prepared in the same way: spin-casting of a solution of PMMA DR1 in chloroform whose concentration is 250 mg / 10 mL.

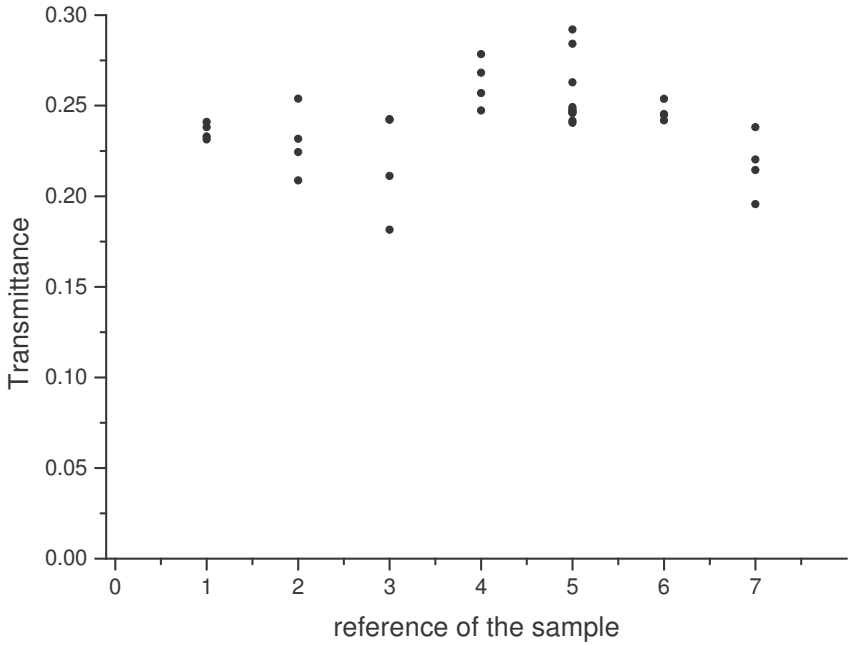

Fig. 19. Transmitted intensity at λ = 473 nm obtained at several points of seven different samples originating from a similar composition (250 mg of PMMA DR1 in 10 mL of chloroform). The values result from an UV-visible spectrum achieved with non-polarized light.

Scanning electron microscope observations of these films show that the distribution of the thickness is comprised between 110 nm and 150 nm. The median of the distribution is 130 nm but the average is much closer to 140 nm.

If we stick to the intensity transmitted by such films, we realize that most samples display a +/- 6 % uncertainty in the transmitted intensity which means that the variations δz of the thickness at the lateral scale of a few millimetres is +/- 7,5 nm for a 150 nm thick film which corresponds to a +/- 5 % corrugation of the film. A few films display a +/- 12 % variation in the locally transmitted intensity which means a +/- 15 % roughness for these layers.

This preliminary study of the initial topography of the spin-coated films is mandatory since thickness is one of the parameters that come into play in the model presented in the following chapter.

III.1.c. Estimation of the loss of optical activity of the chromophores: evidencing the bleaching process.

III.1.c.α.Two different absorption decay rates, two different processes.

In order to follow the evolution of the absorption properties of an exposed PMMA DR1 film, we studied the evolution of the intensity transmitted by such a film on which is cast a laser beam at λ = 473 nm. The incident intensity is 15 mW / 10 mm^2 which is a value similar to that used to record the surface gratings. The polarization is linear. The incident laser's fluctuations were checked to be negligible enough.

The value of the transmission is that of the film only. The influence of the glass substrate – mainly through the few percent of reflected light depending on the incident angle – have been subtracted for each experiment.

The experiment shows that the transmitted intensity increases with time, as the layer is being subjected to the laser beam. In other words, the film absorbs less and less: the absorption coefficient $\beta(t)$ decreases with time.

This means that the azobenzene chromophores become optically inactive during the exposure. Since the molecular motion is associated to the absorption process, this suggests that the inactive chromophore can not take part in the mass motion. An area exposed to a laser beam of modest intensity (a few mW / 10 mm^2) becomes transparent to the naked eye. We shall refer to it as a "bleaching process".

In order to assess the decrease of the optical activity, we studied the evolution of transmission versus time. The evolution below was obtained for a 150 nm thick PMMA DR1 film exposed to a linearly polarized laser spot at λ = 473 nm and whose intensity is around 10 mW / 10 mm^2.

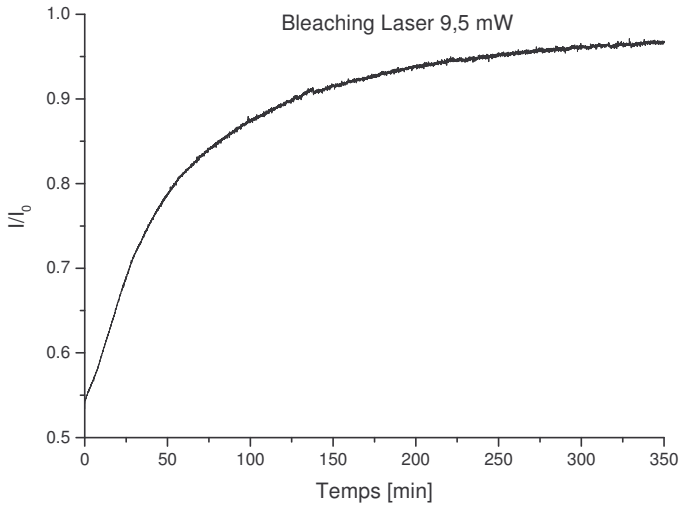

Fig. 20. Evolution of the transmission at λ=473 nm for a 150 nm thick PMMADR1 film.

If we have a closer look at the transmission evolution close to the origin, we see that it evolves must faster during the first seconds.

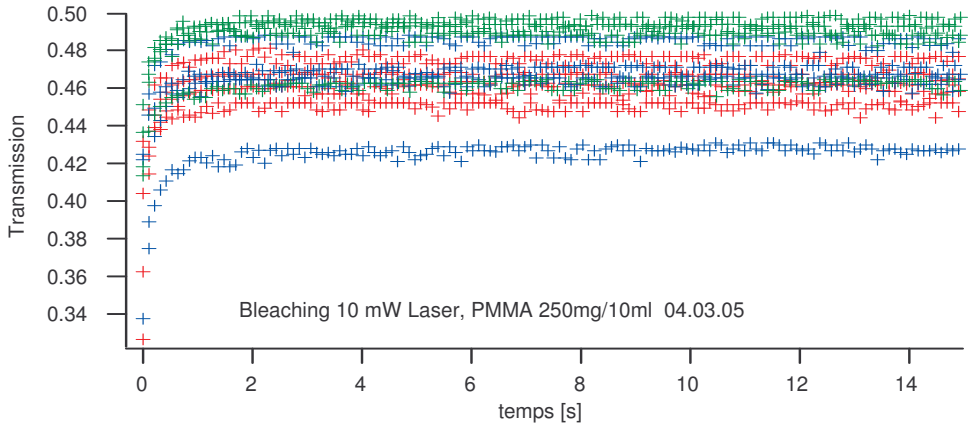

Fig. 21. Fast increase of the transmission of a 150 nm thick PMMA DR1 layer exposed to a beam of intensity equal to 15 mW / 10 mm^2.

We note that the increase of the film's transmission displays two rates.
First, as shown on Fig. 21., it increases quite quickly from 30 % to 50 % of the incident signal in a matter of 2 seconds.
Then, it increases at a much lower rate up to more than 95 %.

The value of the transmission that we measured for similar films with the non-linearly polarized light of a spectroscope is around 25 % up to 30 %. This shows that the orientation comes into play so fast that even the first points on Fig. 20 are already affected by it.

For intensity I of 10 mW / 10 mm^2, the characteristic raise time of the transmission, which can be regarded as the lifetime of the azobenzene's activity, is around 55 minutes.
At I = 15 mW / 10 mm^2, it takes around 40 minutes for a large part of the azobenzenes to lose their photo-activity.
Several experiments carried out at different intensities show that this lifetime is inversely proportional to the intensity of the incident laser beam.
This is evidenced by the graph below where the transmission curves obtained for different intensities cast on a 150 nm thick film have been normalized by expressing the abscissa as the product of the intensity times the exposure time.

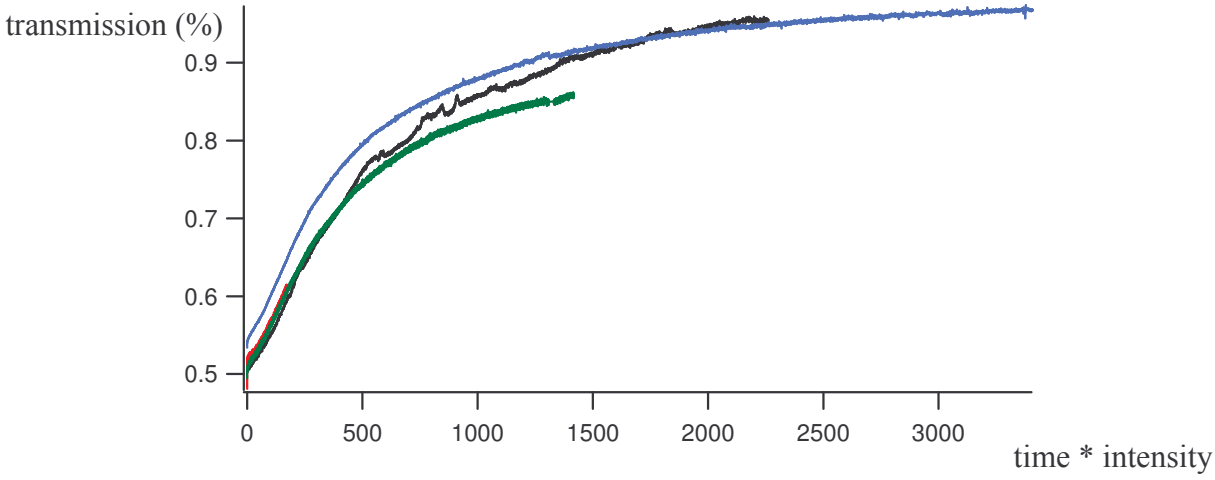

Fig. 22. The bleaching curves obtained at different intensities coincide when expressed versus the product time by intensity. This suggests that only the total dose of energy received matters for the bleaching process.

This normalization evidences that the characteristic lifetime (no matter the criterion chosen to define it) times the incident intensity is a constant.
From these data we can draw:

$$I\,\tau_{B.} = \gamma \text{ where } \gamma \text{ is a constant that we evaluate to be } \gamma = 35 \text{ J} / 10 \text{ mm}^2.$$

One could contend that this drastic change in transmission is due to the matter that was moved away by the bright spot.
Actually, though it plays a role, it does not account for what we observe here.
The first reason is that an infra-red study shows that there is still matter where the film was exposed.
A second argument is that surface relief gratings also appear bleached to the naked eye. Yet, a simplistic calculation of the transmission of a sine shape grating where troughs have been dug down to the glass substrate leads to a transmission factor much lower than the 95 % observed here after a one hour exposure.
A third evidence of the chemical alterations caused by the laser is brought by the comparison of absorption spectra preceding and following a forty minutes exposure. As shown on Fig. 23., a forty minutes exposure the 473 nm line of a laser results in a drastic decrease of the absorption at 473 nm but not so much in the rest of the spectrum. This decrease – which is specifically in the range of the azobenzene function's absorption – leads to think that matter is not altogether pushed away. It rather suggests that part of the azobenzenes were bleached.

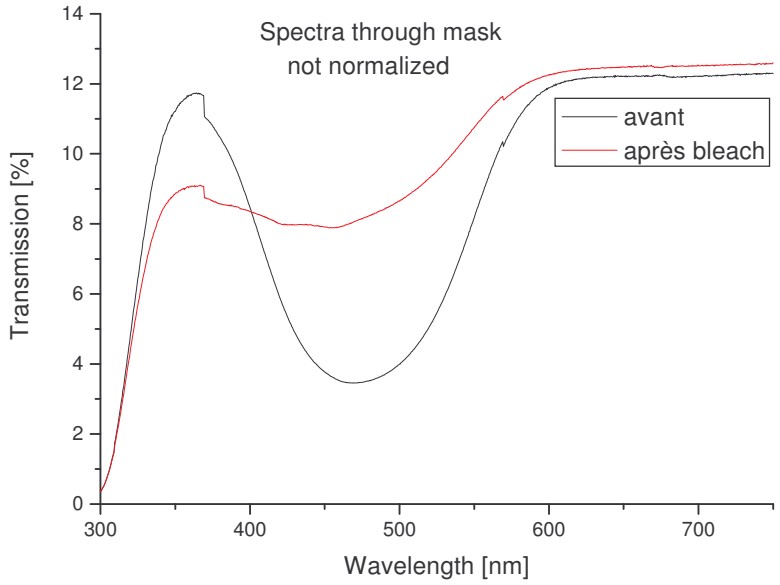

Fig. 23. Transmission spectrum (before normalization) of a 150 nm thick PMMA DR1 layer prior and following exposure to a blue laser beam. The noteworthy increase of the transmission is restricted to the 450-550 nm band. There is still absorption at other wavelengths, which indicates that there is still matter at the exposed point.

We propose two mechanisms to account for the two steps decrease of the optical activity reported above.

- We consider the slow decrease of the optical activity during the hour following the beginning of the exposure to be an irreversible damaging of the azobenzene chromophores due to an oxidation process.
This slow decrease of the transmission follows an exponential law that we evidenced with a curve fitting. This is exposed in section III.1.c.

- As for the fast decrease of the optical activity which occurs during the first seconds, it is a reversible phenomenon.
Indeed, a film that has been exposed only for a few seconds to the laser beam recovers its initial transmission value.
Furthermore, rotating the laser's polarization direction by 90 degrees after having exposed the film to the laser beam for a few seconds, we note that the transmission comes back to the minimal value it had at the beginning and then increase again.
These observations suggest that the early evolution of the transmission is linked to an orientation of the principal azobenzenes in the plane perpendicular to the laser's polarization

direction. The orientation of azobenzenes in an amorphous polymer (methyl orange/polyvinyl alcohol) was described as early as 1984 by Todorov et al[48]. The absorption probability of an azobenzene function is proportional to the square of the cosine of the angle between the polarization direction and the induced dipole in the azobenzene function (whose direction is almost that of the main axis of the azobenzene). The absorption goes along with a random reorientation of the chromophore. Thus, for those functions whose dipole direction happens to be orthogonal to the polarization direction, there is no more interaction with the laser. They become optically inactive through a statistical orientation process.
This way, we can explain the reversibility observed above.
The recovery of the initial absorption after a few seconds may be due to a random thermal back isomerization.
As for the recovery of the absorption under a 90 degrees polarization direction change, it can be understood by the fact that the azobenzene which are oriented perpendicularly to the field and which are inactive end up being parallel to the laser polarization when the laser is rotated, and thus optically active.

For the model that we shall develop in section IV., we will have to take into account that, for a film subjected to a linearly polarized light, the actual absorption coefficient β is not equal to the value calculated in section III.1.a. (8 μm^{-1}) and that it is much smaller. Indeed, in a matter of two seconds under exposure to a linearly polarized light, the absorption of a 150 nm thick PMMA DR1 layer decreases from A = 70 % to A = 50 % as shown above on picture 21. In this case, the actual absorption coefficient of the film is not equal to β = 8 μm^{-1} but to 4,5 μm^{-1}. This actual coefficient renders the fact that a fraction – almost 50 % – of the molecules is optically inactive as early as the very beginning of the experiment.
We carried out the same calculation on 630 nm thick films, which led to a similar fraction of "deactivated molecules" as soon as the experiment starts.

III.1.c.β. Time evolution of the absorption coefficient $\beta(t)$ caused by the bleaching process.

As mentioned above, β decreases quickly in the first two seconds, from 8 μm^{-1} to 4,5 μm^{-1}.
Then, under the effect of what we assume to be a bleaching process, it follows a law that we can draw from the evolution of the transmission of the 275 nm thick film exposed to a beam of given intensity presented in section III.1.c.α.

[48] Todorov, T. ; Nikolova, L. ; Tomova, N. *Appl. Opt.* **1984**, *23*, 4309.

Since we can write the transmission as $e^{-\beta h_0}$, plotting the data resulting from the operation $-\frac{1}{h_0}\times$ experimental values of the transmission versus time gives us the time evolution of the absorption coefficient β.

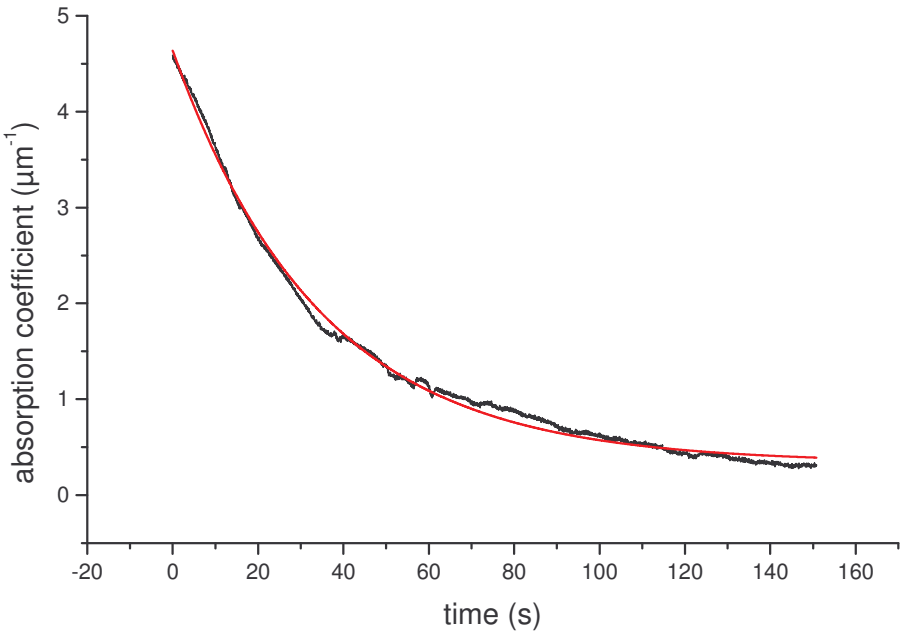

Fig. 24. Time evolution of the absorption coefficient β. We view this evolution as a result of the bleaching of the azobenzene chromophores.

The curve fitting which appears in red on the graph above shows that the expression of the time evolution absorption coefficient β is:

$$\beta(t) = 0{,}35 + 4{,}3\exp\left(-\frac{t}{35}\right)$$

The corresponding characteristic decay time is 35 minutes.

III.2.Key parameters of the light-induced mass motion.

III.2.a. Influence of the light intensity gradient on the motion direction.

As a first step, it is mandatory to check that in our experimental conditions matter is flowing from bright areas to darker ones.

For that purpose, a PMMA DR1 layer is backside subjected for 5 minutes to a 15 mW/ 10 mm^2 intensity laser spot, which is more than what we worked with but remains reasonable in terms of likely temperature increase as we will see in the following paragraph.

The AFM image below shows that matter has moved from the centre of the laser spot, where light intensity is maximal, to the less exposed peripheral areas.

The matter accumulation on the right and left of the hole as well as the concentric rings that appear on the picture will be discussed in the following paragraph.

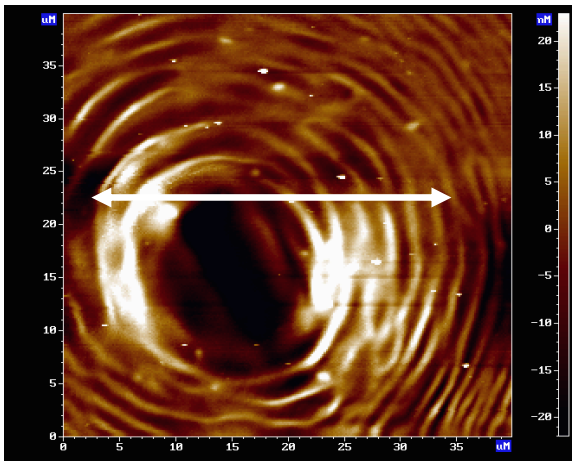

Fig. 25. AFM image of a 275 nm thick PMMA DR1 film after a 10 minutes backside exposure to a 15 mW / 10 mm^2 laser beam linearly polarized along the direction indicated by the white arrow above.

III.2.b. Influence of the polarization direction of the light: an evidence that the mass motion can not be reduced to a purely thermal phenomenon.

Before going further into the study of light-induced molecular motions, it is compulsory to check that we are not just focusing on an ablation process or a local increase of the polymer layer temperature beyond the glass transition temperature.

A first point that rules out this assumption is brought by the role of light polarization in the mass motion process.

The first evidence that we have of the role of light polarization is given by the experiment presented in the previous paragraph.

As mentioned above, the laser spot which is shone on the PMMA DR1 layer is linearly polarized along the horizontal direction of the picture. Besides, the AFM image displays an

accumulation of matter along that direction on both sides of the hole. This suggests that matter was pushed away from bright areas along the polarisation direction.
This is not the only observation of the kind. Kumar and al exposed a PMMA DR1 layer to laser spots of similar Gaussian intensity profiles but of various polarization directions.
As a result, a circularly polarized spot leads to a hole with matter equally set all around it; as opposed to a linearly polarized light which leads to an accumulation of matter in the polarization direction.

In order to further investigate the influence of light polarization on light-induced motion, we expose PMMA DR1 layers to a common intensity modulated interference pattern as mentioned in paragraph II.3 $I(x) = 2I_0(1 + v \cos Kx)$ but for different polarization states.
If the laser polarization is parallel to the interference fringes then the light modulation is maximal since the visibility factor is $v = 1$ in that case.
However, after a one hour exposure, AFM images display a negligible periodical surface corrugation of less than 3 nm of amplitude.
In the same conditions but with a polarization direction along the x axis, that is to say along the intensity gradient direction and for which $v < 1$, we get AFM images of large amplitude surface gratings.
The polarization state was controlled through a polarizer which leaves less than 1 % of the unsuitable component of the field. This small fraction left may explain that a slight surface relief grating can be noticed in the case of a polarization perpendicular to the x axis.
This experiment was carried out for several layer thicknesses, for various angles between the interfering beams and at varied intensities which all led to the same result: when the electric field does not have a component along the intensity gradient direction, the mass motion is negligible.
One can picture the mass motion as occurring along the polarization direction in both above mentioned cases. However, in the first case there is no intensity modulation along the motion direction. Thus, it seems that both an intensity modulation and a non-zero component of the electric field along the intensity gradient are necessary for the motion to occur.

Even more striking, intensity modulation is not a sine qua non requirement for mass motion. Polarization in itself can lead to a significant surface relief grating.
Indeed, we exposed PMMA DR1 layers to a modulated polarization pattern as described in section II.3, where light intensity is uniform and the linear polarization direction rotates periodically as the abscissa x changes.

In this configuration, AFM images reveal surface relief gratings of significant amplitude and the period of which is equal to that of the gratings obtained in the intensity modulation configuration for the same angle between the interfering beams.

The dynamics of such surface relief gratings will be commented on in section III.4.

We have to point out that the polarization gratings we worked with were not obtained with perfectly circular waves. Indeed, for these experiments we used a semi-reflecting mirror device instead of a cubic beam splitter, which led to a not altogether controlled state of the reflected left-circular circularly polarized wave. This latter is reflected into an elliptically polarized wave instead of the ideal right-circular one.

Nevertheless, even in a not ideal case of two counter-propagating circularly polarized waves, the intensity modulation remains negligible and periodic polarization modulation prevails.

These three evidences of the influence of the direction of light overrule the hypothesis that the phenomenon tackled here is just about thermal effects or changes in the free volume as first contended by Barrett et al[4]. Paragraph III.2.e. will provide an additional point against a purely thermal theory.

Yet, the temperature increase may play a competing role with other processes that have been mentioned in chapter I and that we shall investigate in what follows.

Thus, we shall conclude this paragraph with a simplistic assessment of the temperature increase in the case of a layer regarded as a semi-infinite plane of equation $z > 0$ of initial temperature T_0 exposed to a constant light intensity I_0.

The evolution of the temperature $T(z,t)$ in the layer is governed by the diffusive heat equation: $\frac{\partial T}{\partial t} = \frac{\kappa}{\rho.c}\frac{\partial^2 T}{\partial z^2}$ where ρ is the mass per unit volume of PMMA DR1, c its heat capacity and κ its thermal conductibility.

The solution for a semi-finite plane $z > 0$ is:

$$T(z,t) = T_0 + \frac{2I_0}{\kappa}\sqrt{\frac{\kappa}{\rho.c}t}\left(\frac{1}{\sqrt{\pi}}\exp\left(-\frac{\rho c.z^2}{4\kappa.t}\right) - \sqrt{\frac{\rho.c}{\kappa}}\frac{z}{2\sqrt{t}}\left(1 - \frac{2}{\sqrt{\pi}}\int_0^{\sqrt{\frac{\rho.c}{\kappa}}\frac{z}{2\sqrt{t}}}\exp(-u^2)du\right)\right)$$

At the very surface of the layer $z = 0$, the temperature increase is maximal:

$$T(0,t) - T_0 = \frac{2I_0}{\kappa}\sqrt{\frac{\kappa}{\pi\rho.c}.t}$$

Thus, we can assess the temperature increase at the surface of the film for an intensity of I_0 = 15 mW / 10 mm^2.

Thermal characteristics for PMMA[49] and PDR1[50] being close, we take for PMMA DR1:

$$\rho = 1{,}19.10^3 \text{ kg / m}^3;\ c = 1{,}46.10^3 \text{ J / kg};\ \kappa = 200 \text{ W / K}.$$

Thus:

$$T(0,t) - T_0 = 0{,}10.\sqrt{t}$$

This means that, for the duration of the grating's formation, the temperature increase is negligible compared to what it should be to reach the glass transition temperature which is around 373 K.

Indeed, it takes just from a few minutes to a few tens of minutes for the surface relief grating to be recorded.

Yet, after a one hour exposure to a 15 mW / 10 mm^2 intensity, the temperature reached by the free surface of the film is:

$$T(0,3600) - T_0 = 6K$$

This calculation shows that the glass temperature of the polymer is far from being reached.

III.2.c. Are azobenzene-containing polymers the only azo-molecules to undergo light-driven motion?

Various light-induced motion experiments have been carried out on azobenzene containing polymers. In most cases, the azobenzene function is grafted to the backbone as a side chain. But several groups also studied chemical compounds where azobenzene chromophores are part of the main chain or diluted as dyes in a polymer matrix.

In all cases, a mass motion is reported after exposure to a laser pattern.

However, to our knowledge few experiments have been carried out on non polymeric azobenzene containing material. Four years ago, Votgle et al published an article evidencing the formation of a surface relief grating upon illumination of azobenzene-containing dendrimer film.

But the literature is scarce on the subject though there is much to learn about it.

---

[49] MatWeb website :http://www.matweb.com

[50] Yager, K.G.; Barrett, C.J. *J. Chem. Phys.* **2004**, *120*, 1092.

Indeed, one could contend that the main chain of the polymer plays an essential role in the process. As mentioned in chapter I, some describe the surface relief grating as a consequence of the orientation of the polymer main chains along the direction of the electric field.

In order to overrule this assumption, we used POPAM where no main chain may introduce a spurious effect.

We expose layers of generation 2, 3 and 4 POPAM MO dendrimers to a modulated intensity pattern similar to the one shone on PMMA DR1. As a result, we get surface relief gratings similar to those observed for PMMA layers.

Figures 26 and 27 below present the surface corrugation observed on the AFM image of a G2MO layer exposed for 5 minutes to an interference pattern. The intensity is equal to 15 mW/10 mm^2.

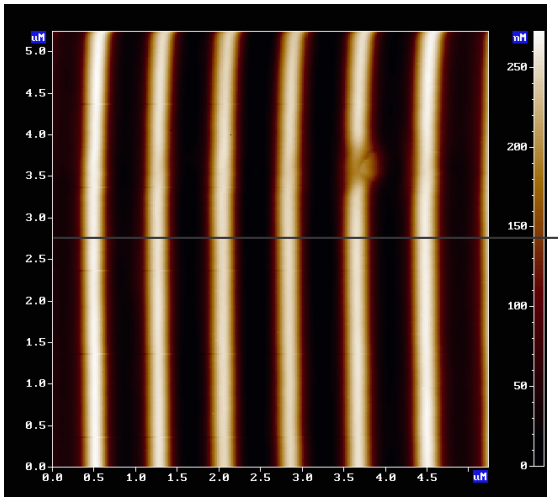

Fig. 26. Surface grating obtained on a G2MO layer after a 5 minute exposure to a 15 mW / 10 mm2 intensity pattern.

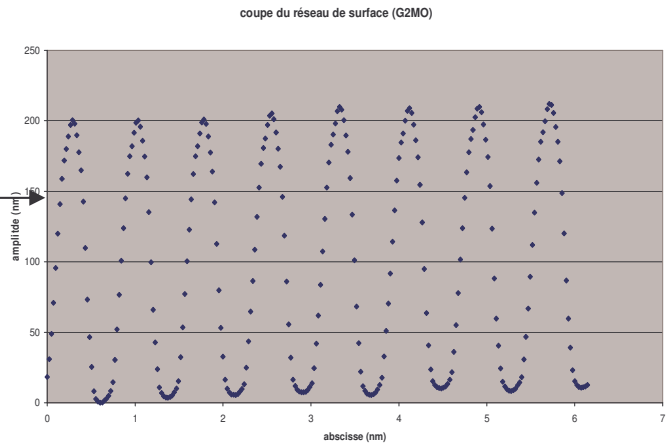

Fig. 27. Section evidencing a noteworthy mass motion in G2MO layers. The peak-to-peak amplitude reaches 200 nm.

III.2.d. Importance of the substitution of the azobenzene functions.

We evidenced in the previous paragraph that the main chain of the polymer is not required for the motion to occur.

But do non-substituted azobenzenes by themselves display such a mass motion?

To answer this question, we deposited by spin casting layers of azobenzene molecules.

These layers were exposed to intensity modulation patterns in conditions similar to those used for PMMA DR1 and GMO dendrimers. We also tried s linearly polarized configurations, various angles and even the 488 nm line of an Argon laser, though the azobenzene absorption

bandwidth is large enough – 100 nm from 430 nm to 530 nm as evidenced in section III.1.a. – to include 473 nm as well.

In all cases, AFM images show no sign of surface alteration. The surface remains the same.

First, this can be regarded as an additional point against a purely thermal theory. Indeed, azobenzene fusion point is 341 K whereas PMMA DR1 glass transition temperature is around 373 K. Thus, if an azobenzene layer is not altered after a few minutes long exposure, there is no reason why it should prevail for PMMA DR1 layers.

Another conclusion that can be drawn from these unsuccessful trials at inducing molecular motion in azobenzene layers is that the azobenzene's environment comes into play.

The previous paragraph allows us to overrule the assumption that there is no motion due to the lack of main chain. But another difference between non-substituted azobenzenes and those azobenzene containing molecules that move is that the latter are substituted with both an electro-donor and an electro-acceptor group. They belong to what we referred to in paragraph III.1.a. as the pseudostilbene category for which a quick back isomerization to the trans form is allowed through both a fast thermal back isomerisation and a photonic excitation which occurs at the same wavelength. Thus, such substituted azobenzene can perform trans-cis-trans isomerization cycles.

This property seems to play an essential role in the light-induced mass motion.

Some groups[13] view the photonic back isomerization as the trigger of the motion.

We propose another analysis in paragraph IV.4.

III.2.e. Life time of the light-induced deformation of the free surface.

The evolution of a surface relief grating after light is switched off is a precious piece of information to discuss the mechanism at work.

Surface relief gratings as those presented above have a life time superior to two years. Indeed, AFM images of two years old gratings show that the surface deformation remains the same.

It is interesting to note that the only care that was taken was to cover them in order to protect them from dust. Otherwise, no thermal caution or isolation from light was given to the samples.

This result evidences the fact that surface tension which tends to flatten the surface plays a minor role in the process.

We shall take into account this result in section IV.1. where we formulate the hypotheses of the model. This way, we shall not add a surface tension term to the equation that we will write.

III.3. Mass motion dynamics.

III.3.a. Structure of the curves describing the evolution of the deformation's amplitude.

Now that these main characteristics have been checked, we shall tackle the dynamics of the mass motion.

To do so, we study the evolution of the amplitude of the surface relief grating obtained when layers are exposed to a p linearly polarized intensity modulation pattern as described in paragraph II.3 : $I(x) = 2I_0(1 + v \cos Kx)$.

As described in paragraph II.5., we shall either use the ex-situ or the real-time method

We stated in paragraph II.4. that AFM images display a surface modulation of the same periodicity as the interference pattern used to inscribe it.

In order to follow the light-induced deformation, we shall stick to the evolution of the grating's amplitude which is equal to half of the peak-to-peak amplitude.

For the first thirty minutes of the grating's building, its shape is a sine form. For larger times, we have observed that the profile diverges from an ideal sine form but remains periodic.

So, at the beginning, the amplitude of the grating can be regarded as $h_1(t)$ where the local height $h(x,t)$ is expressed as $h(x,t) = h_0 + h_1(t).\cos(Kx)$, h_0 being the initial thickness of the film.

The following two figures show the time evolution of this amplitude obtained for all ex situ dynamics and – as we underline below – for only some of the in situ dynamics.

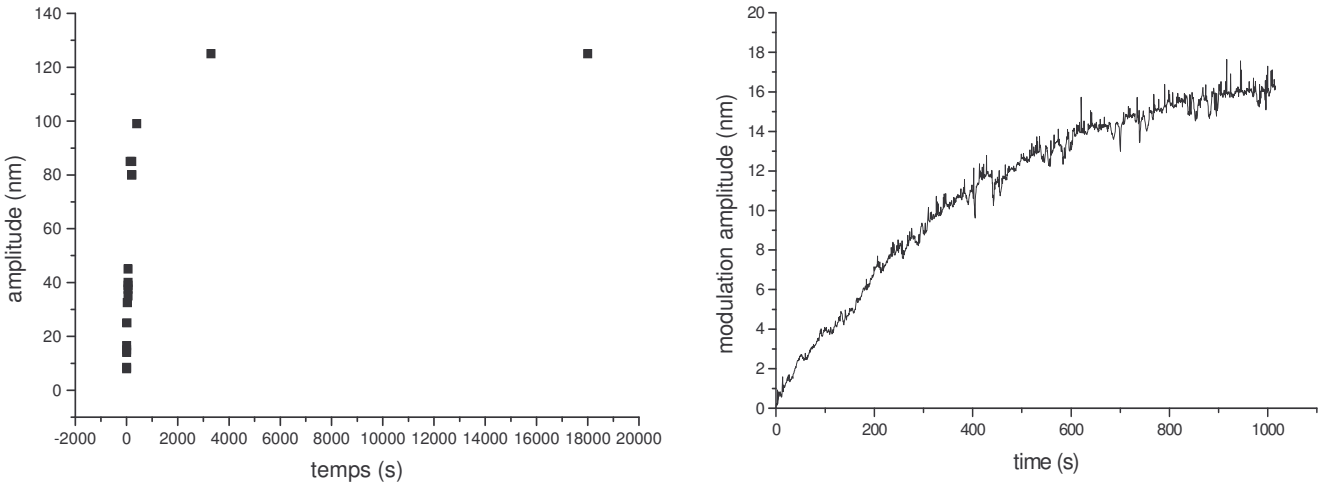

Fig. 28. Time evolution curves of the amplitude of surface relief gratings recorded in different conditions. The graph on the left was obtained with the ex situ method where each

point requires a time-consuming experiment as described in section II.5.a. as opposed to the graph on the right obtained with the real-time device presented in section II.5.b. Nevertheless, we expose in what follows the difficulties met as well as the information drawn from the real-time approach.

All the curves which describe this evolution and which we got through the ex-situ method have the same shape. They are concave and they show two characteristic parameters that we shall work with in the rest of this memoir.

- First, a saturation value for the amplitude: h_{sat}
- But also a raise time of the phenomenon. For reasons that will exposed below, we will retain the growth rate at the origin: $\frac{dh_1}{dt}(0)$ to the study the influence of various parameters. The curve being concave, this value at the origin is the maximal value of the growth rate.

Most evolution curves obtained with the in-situ or « real-time » method cannot be fully exploited. Indeed, the grating's initial growth rate is similar to that obtained with the ex-situ method (as we shall evidence numerically in section III.3.b.). Nevertheless, in most cases after having been exposed for a few minutes, the surface of the film is altered. The surface relief grating is progressively blurred. As for the curve giving the evolution of the modulation amplitude, it quite often displays puzzling behaviours. Some of the few gratings which are not altogether blurred and destroyed after a few minutes of exposure display a break point. These observations can be justified by a spurious phenomenon of deformation – strains which come into play in the layer. In the cases of films subjected to light through their back side, the most significant mass motion takes pace at the bottom of the film which neighbours the glass substrate. So, unlike front side exposed films where the main motion happens to be unbound at the free surface, they are subjected to strains from the glass substrate and from the entire layer which does not transmit the deformation in a linear way.

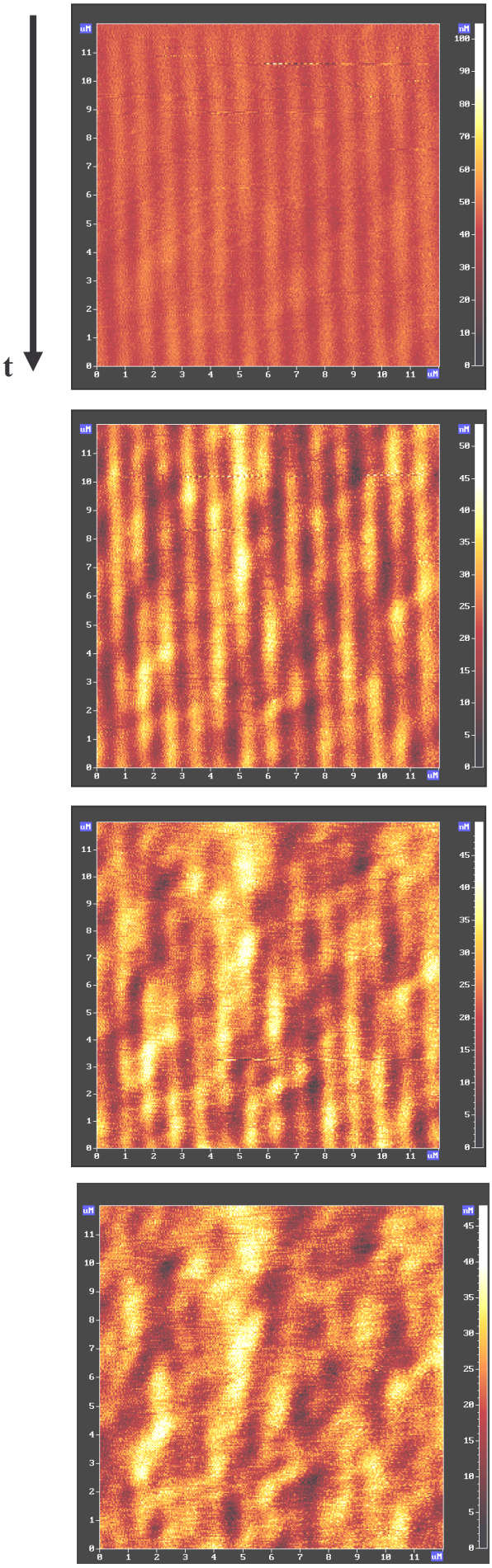

Fig.29. Real-time AFM images of the evolution of the surface relief grating inscribed with an interference pattern at the surface of a PMMA DR1 film. The first two images are scanned downwards, the third upwards, the fourth downwards. Starting from the third image, we can see a progressive degradation of the surface grating. This can occur after only five minutes of exposure to the pattern.

Nevertheless, the curves that we get with the « real-time » method remain valid for early times. Although most of them do not contain any information about the saturation value of the modulation amplitude h_{sat}, the information about the initial behaviour that they provide is similar to what we get in the same conditions with the ex-situ method where the layer is front side exposed. We shall bring experimental justifications of this assertion in section III.3.b.

The two characteristics drawn here are of great interest to comprehend better the mechanism.

-The initial growth rate lends itself to a quantitative analysis that will be carried out in the following chapter.

- The amplitude at saturation is somewhat tricky to analyze, as we shall see further. Nevertheless, the understanding of its origin is essential. Is the molecular motion occurring in the film self-limited? Is it caused by the loss of optical activity evidenced in section III.1.c.

In all the cases exposed below, we shall note that the saturation amplitude is always reached before the film is completely dug. For instance, it is equal to 30 nm for a 55 nm thick layer and to120 nm for a 275 nm thick layer.

In the following sections, we assess through ex-situ and in situ AFM studies, as described in section II.5., the influence of various parameters on the molecular motion. Given the uncertainties which mar the value of the initial growth rate, the results presented below aim less at computing a quantitative analysis than at providing us with trends that we shall use to assess the relevance of the model proposed in chapter IV.

III.3.b. Influence of the layer's thickness.

In this section, we show that the larger the thickness h_0 of the layer, the faster the mass motion. But this relation is sub-linear.

We also evidence that the light-induced mass motion is taking place in the entire bulk of the film and cannot be reduced to a purely free surface phenomenon. First because the thicker the layer, the larger the amplitude reached at saturation. But also because front side and back side exposure lead similar behaviours at early times.

III.3.b.α Influence of the layer's thickness on the grating's formation dynamics.

The influence of the initial thickness of the film h_0 endows us with a better understanding of the process.

We compare two PMMA DR1 films differing in initial thickness h_0. Both of them are exposed in identical conditions to a p linearly polarized interference pattern at an intensity equal to 15 mW/ 10 mm^2 and for an angle α between the interfering beams equal to 32°.

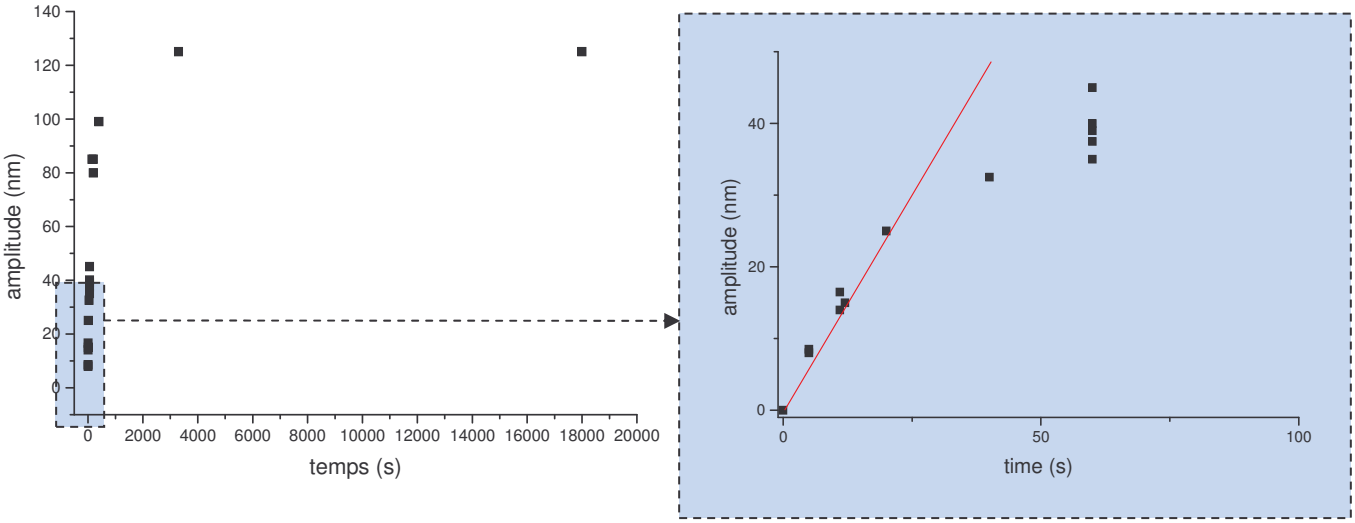

Fig. 30. Dynamics for h_0 = 275 nm

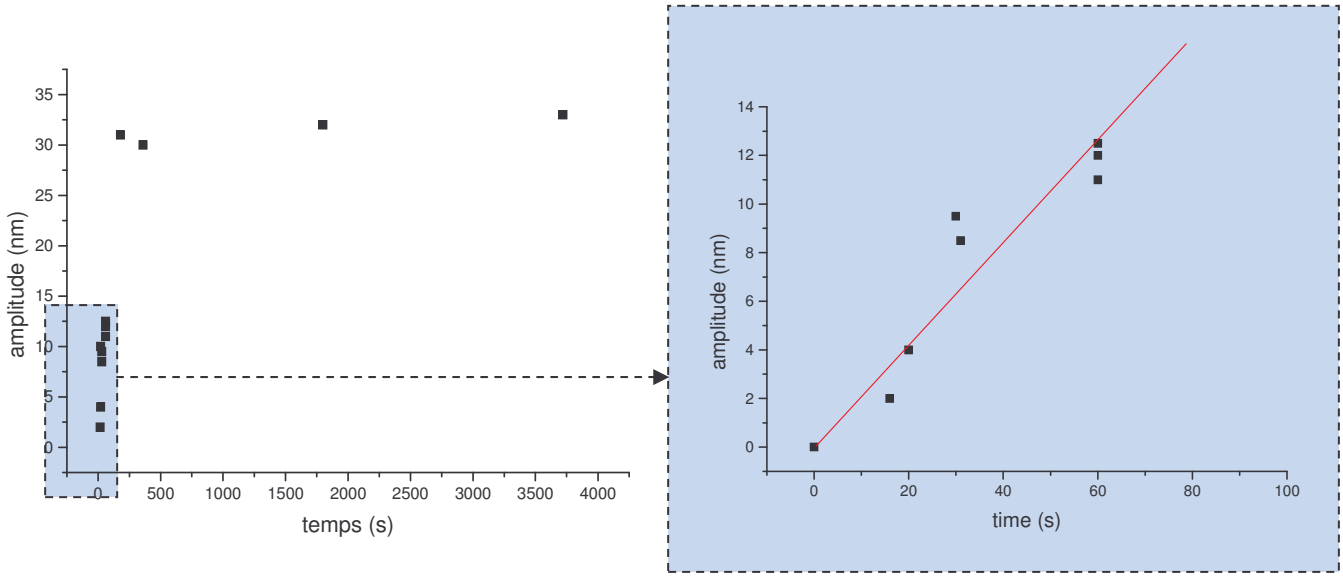

Fig. 31. Dynamics for h_0 = 55 nm

	h_0 = 275 nm	h_0 = 55 nm
initial growth rate	1 +/- 0,1 nm/s	0,3 +/-0,05 nm/s
saturation amplitude	120 +/- 7 nm	30 + / - 4 nm

It emerges that the two characteristic values retained to describe the evolution of the surface relief grating are all the bigger as the film is thicker.

This indicates that the entire bulk of the layer takes part in the mass motion and not only its surface. If it were a purely surface phenomenon, as the plasticization process proposed by Kumar et al., the grating's growth rate and its amplitude at saturation should be the same for two films of different thickness.
The following paragraph also evidences that the mass motion takes place in the entire bulk of the film.

III.3.b.β. An identical dynamics at early times for front side and back side illuminated films.

For a 55 nm thick PMMA DR1 film subjected through its back side to an intensity modulated pattern as described in the previous paragraph, the real-time device described in section III.5.b. gives an initial growth rate around 0,3 nm/s which is quite similar to the initial growth rate found for a front side exposed layer.

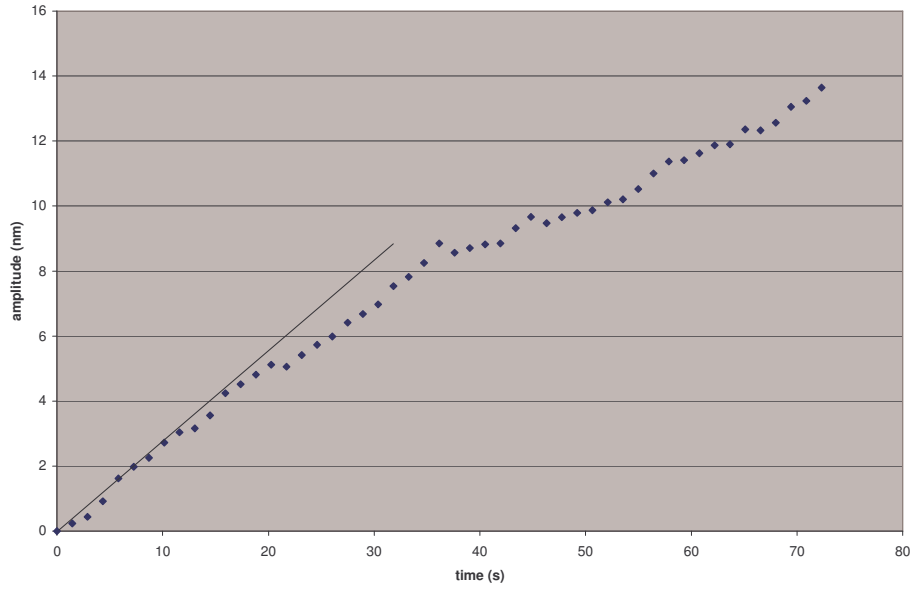

Fig. 32. Evolution of the amplitude of the surface grating at early times for a 55 nm thick PMMA DR1 film exposed through its back side.

Here again, a purely surface process would lead to a strong dependence on the way the film is illuminated. In this case, we would expect back side exposed layers to give a much more modest grating.

III.3.c. Effects of the intensity of light.

The effect of the intensity of light clearly manifests itself on the initial growth rate of the film.

For a 275 nm thick PMMA DR1 film on which is cast a p linearly polarized intensity modulated pattern, we find:

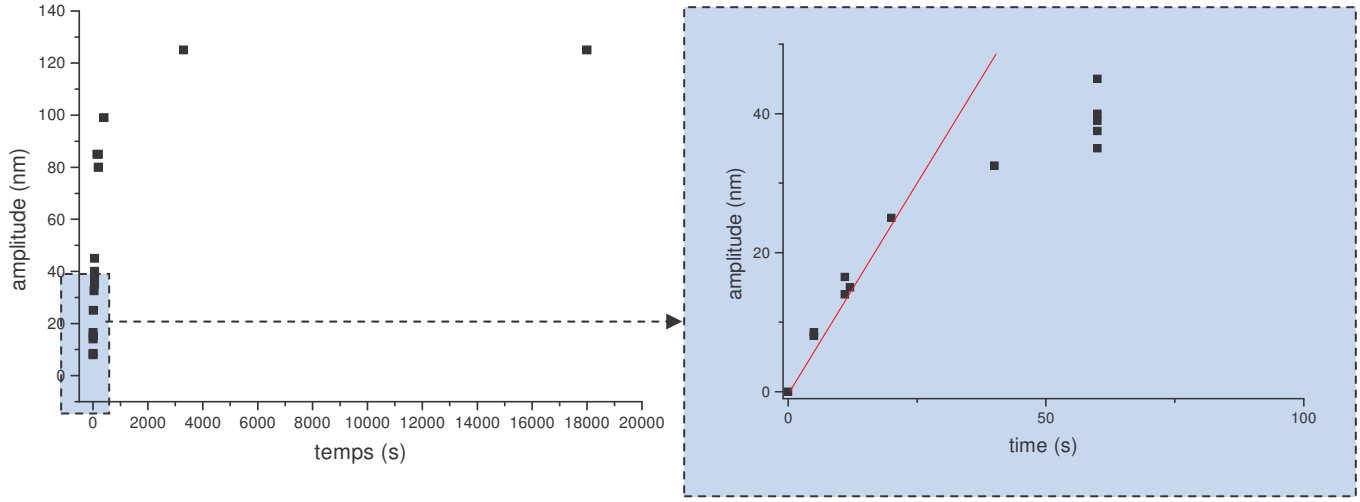

Fig. 33. Dynamics for 15 mW / 10 mm²

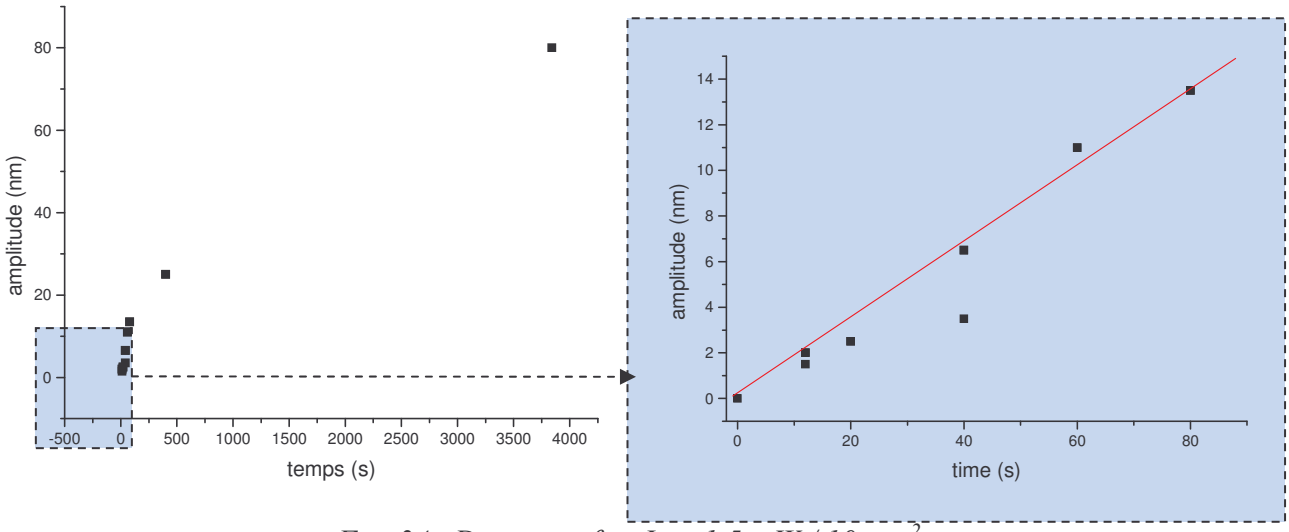

Fig. 34. Dynamics for I_0 = 1,5 mW / 10 mm²

	I_0 = 15 mW / 10 mm²	I_0 = 1,5 mW / 10 mm²
initial growth rate	1 +/- 0,1 nm/s	0,11 +/- 0,02 nm/s
saturation amplitude	120 nm à 15 % près	80 nm à 15 % près

The initial growth rate of the grating obtained with a I_0 = 15 mW / 10 mm² average intensity pattern is ten times faster than for I_0 = 1,5 mW / 10 mm².

Given that the intensity is ten times smaller in the second case and that the initial growth rate is ten times slower, we could expect the saturation amplitude to be reached ten times later but with a similar value as in the first case.

Nevertheless, repeated experiments show that the saturation amplitude that is reached for an intensity of 1,5 mW / 10 mm^2 is only around 80 nm as opposed to 120 nm for an intensity ten times bigger.
This suggests that time is counted and in a way that is quite complex to comprehend.
Indeed, the reasons that come to mind – and which we shall develop in the chapter to come – is that either the mass motion process in itself or the bleaching process described in section III.1.c. plays a limiting role in time. Nevertheless, in both cases we would not expect the saturation amplitude to be modified by the intensity. As far as the mass motion process is concerned, the intensity should only influence the rate at which the grating is growing. As for the bleaching process, its effects have been shown in section III.1.c. to be proportional to the intensity. Thus, the saturation amplitude should be reached much later but the value of the amplitude should remain unchanged.
In section IV.3.c. we propose an interpretation of the saturation that we observe as the result of a coupling between the mass motion and the bleaching process.

III.3.d. Nature of the azobenzene-containing compound.

III.3.d.α. Azobenzene-containing dendrimer films respond faster than PMMA DR1 ones but the saturation amplitude is similar.

The nature of the azobenzene-containing compound from which the film is made plays a major role on the characteristic growth time of the film.
It emerges that, for azobenzene-containing dendrimer films, the formation of the surface relief grating is much faster than for PMMA DR1 layers.
A G2MO film, whose absorption factor is superior to 95 %, and subjected to an interference pattern with I_0 = 15 mW / 10 mm^2 gives a surface relief grating which is built faster than for PMMA DR1 samples. The initial growth rate for G2MO films is 2,5 nm/s as opposed to the thickest PMMA DR1 layers which initially grow twice slower although they absorb a similar fraction of the incident intensity.

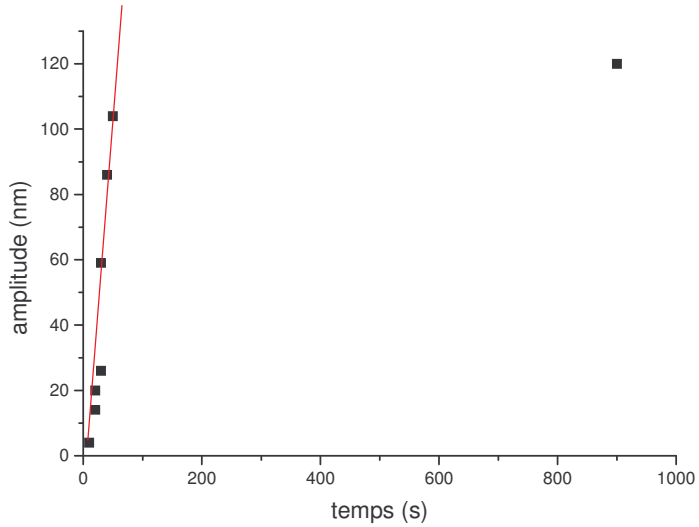

Fig. 35. Evolution of the amplitude of the surface grating inscribed on a G2MO film absorbing more than 90 % of a non-polarized light.

We also evidenced a much faster growth of the grating for G4MO films. Indeed, in conditions similar to those described in the previous paragraph, a G4MO film illuminated through its back side displays an initial growth of more than 4 nm/s.

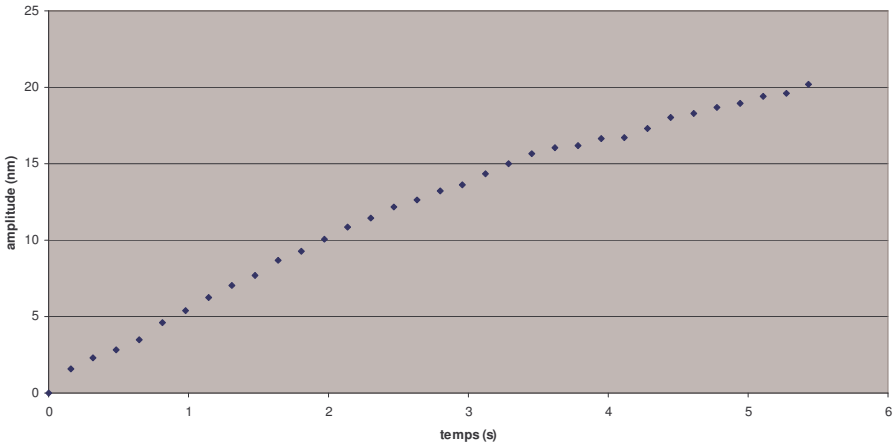

Fig.36. Time evolution of the amplitude of the grating at early times for a G4MO film exposed through its backside.

We did not carry out a series of ex situ experiments giving the time evolution of a surface relief grating on a G4MO film that would confirm this result. However, we do not think the value of the growth rate could have been over estimated in such a configuration. Indeed, in situ experiments require placing the AFM tip as close as it gets to the intensity maximum, otherwise a much slower dynamics of formation could be observed. But how could it be more?

As for the amplitude reached at saturation, it is similar to the one observed for PMMA DR1 films of similar thickness.

III.3.d.β. Asymmetrical azo-compounds do not respond faster.

As mentioned in section II.1., we also used Fréchet's molecules which are non-polymeric azobenzene-containing molecules. Unlike POPAM methyl orange, they do not have a circular symmetry.

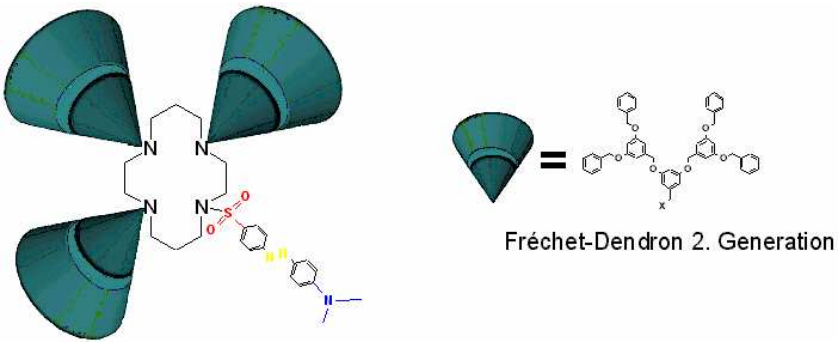

Fig. 37. Fréchet's molecule

The idea is that, should there be competing motions between azobenzene groups which are part of the same molecule, we would expect this asymmetrical Frechet's to give a more efficient mass motion.

Nevertheless, the initial growth rate that we observe for this Fréchet's molecule – whose absorbance is quite the same as GMO and thick PMMA DR1 films (at least $A = 0,7$) – is similar to the one that we get for PMMA DR1 films, that is to say around 1 nm.s^{-1}, in similar conditions (modulated intensity interference pattern, I_0 = 15 mW / 10 mm^2, angle between the interfering beams equal to 32°).

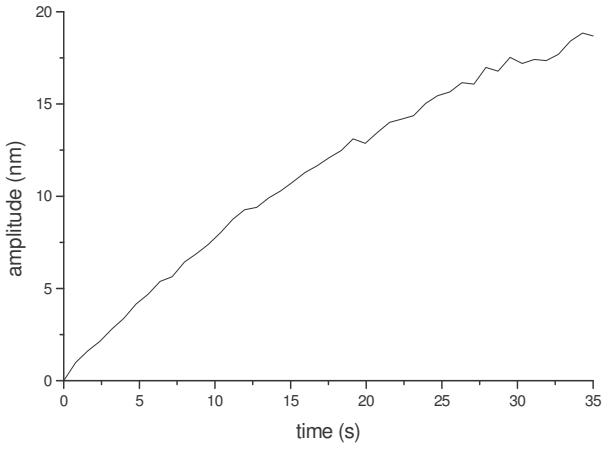

Fig. 38. Early time evolution of the amplitude of a Fréchet's molecule film exposed to an intensity modulated interference pattern.

III.4. Time evolution of a surface grating inscribed with a modulated polarization pattern.

Polarization plays a major role in light-induced molecular motion. In paragraph III.2.b. we referred to a surface relief grating obtained for a negligible intensity modulation combined with a large polarization modulation, however limited our mastery over the pattern may have been as we underlined in paragraph III.2.b.

Even if we do not pretend to have used an ideal polarization grating configuration as calculated in annex II, polarization modulation prevails over a negligible modulation of intensity and, as such, we find it interesting to present the formation dynamics of such a surface relief grating.

This dynamics was obtained for a 275 nm thick PMMA DR1 layer.

The recording conditions are similar to those used previously: the angle between the interfering beams, as well as the intensity, is about the same.

The only slight difference is that the 488 nm line of an Argon laser was used instead of the 473 nm line of the solid laser used for the experiments presented above. However, this should not affect the absorption process since the absorption bandwidth is way larger that the 15 nm difference between the two lasers, as we can see in section III.1.a.

What really differs is the light pattern shone on the PMMA DR1 layer. This time, the intensity of light is about the same all over the sample but, following section II.3., the linear polarization direction varies periodically along the X axis defined by the intersection of the sample with the plane generated by the two interfering beams.

The resulting grating amplitude evolution is presented below.

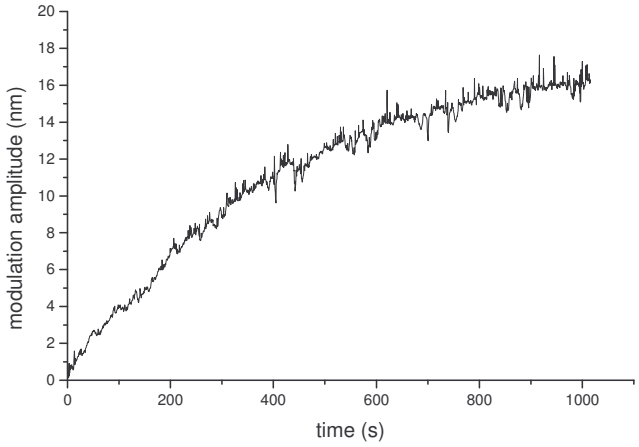

Fig. 39. Time evolution of the amplitude of a surface relief grating inscribed with a light pattern uniform in intensity and whose polarization state is modulated as calculated in annex II.

The initial growth rate is inferior to 0,1 nm/s for this 275 nm thick PMMA DR1 film subjected to a 5 mW/cm^2 polarization pattern. If a similar layer were exposed to a modulated intensity pattern as used in the previous sections, we would expect from it to grow at least three times faster, following the observations reported in section III.3.c.

We also observe that the saturation value is reached much later. After a one hour exposure, the grating is still growing, as opposed to exposures to intensity patterns for which the saturation is reached after a few minutes.

We will show in section IV.4.a. that the model presented in this memoir can provide a hint as to how to interpret these results on the initial growth rate and the saturation amplitude.

III.5. Erasing attempts.

We noted in section III.2.e. that surface relief gratings remain unaltered at least two years after having been recorded.

But we would like to know whether it is possible to erase a grating by subjecting it to a laser spot of locally uniform intensity and polarization at the scale of the grating.

We carried out these erasing attempts on layers of various thicknesses and we ended up with equivocal results.

In most cases, the grating's amplitude remains unaltered.

However, for layers of similar thickness, we have sometimes observed a decrease of the amplitude and on rare occasions (two noteworthy experiments) an increase of the grating's amplitude.

These puzzling results suggest that the intensity distribution in the layer's bulk is difficult to grasp. The incident uniform beam cast on the grating is diffracted by it. The resulting diffracted near-field in the bulk may depend on uncontrolled parameters such as the exact form of the grating or the angle between the surface and the laser beam. The resulting light distribution in the layer could, depending on its position compared to deformation profile, could then enhance or flatten the relief grating.

However puzzling this set of data, we can draw from it a trend which converges with what Barret et al. observe: a surface grating is all the more difficult to erase as the film is thick.

The increase of the modulation amplitude under illumination by a single beam aimed at erasing a grating is not a marginal observation. Kumar and Tripathy[51] report a noteworthy

[51] Jiang, X.L.; Li, L.; Kumar, J.; Kim, D. Y.; Tripathy, S. K. *Appl. Phys. Lett.* **1998**, *72*, 2502.

increase of the amplitude gratings inscribed with circular and linear polarizations when subjected to a beam whose linear polarization is perpendicular to the grooves.

We shall conclude this part by a presentation of a successful erasing attempt.

It was carried out on a 275 nm thick PMMA DR1 layer exposed to a beam of intensity equal to 30 mW / 10 mm^2. The time evolution of the amplitude was obtained with the real-time method.

The initial decrease rate is quite slow: a few thousandths of nanometres per second, as opposed to an initial growth rate hundreds of time faster, the order of magnitude being 1 nm/s. This slowness of the erasing process that we observe will be discussed in section IV.4.b.

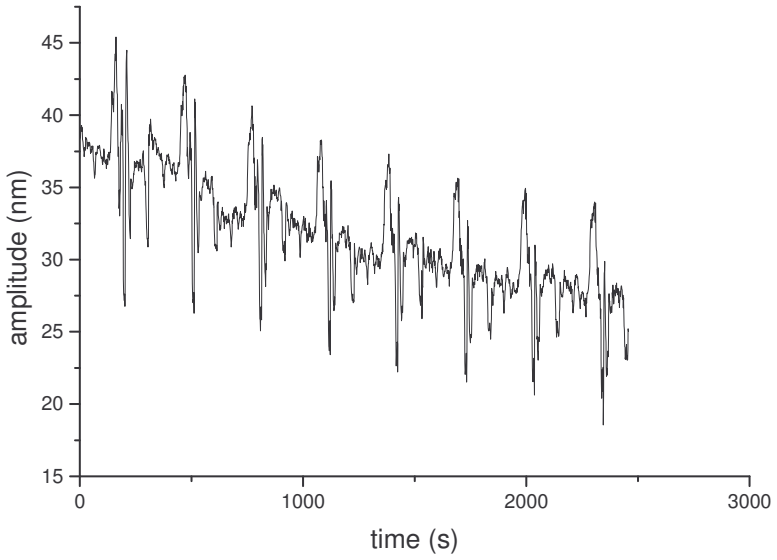

Fig. 40. Decrease of the amplitude of a surface relief grating exposed to a single laser beam of intensity 30 mW / 10 mm^2. The initial growth rate is around 7.10^{-3} $nm.s^{-1}$.

CHAPTER IV

Model, discussion and consequences.

IV.1.The assumptions: a light-driven random walk motion.

The model presented in this chapter and which aims at accounting for the light-induced motion of azobenzene-containing materials the mechanism described by Nunzi et al., as we mentioned in section I.2. It lies on the assumption of an individual phenomenon of a probabilistic kind.

We formulate five assumptions:

-When an azobenzene function absorbs a photon, it can undergo, given some quantum efficiency, an isomerization from the stable trans form to the cis excited form. In a pseudostilbene environment, as it is the case for the materials that we studied, the back isomerzation from the cis to the trans state is activated by the same wavelength and takes only a millisecond[52]so that the azobenzene functions perform trans-cis-trans cycles. The back thermal isomerization is also quite fast (less than one second). Each isomerization cycle goes along with a motion of the azobenzene of a distance *l.* **(*A1*)**

[52] Lagugné Labarthet, F.; Sourisseau, C. *New. J. Chem.* **1997**, *21*, 879.

- This motion of the chromophore tends to drag the molecule to which it is grafted (polymer chain or dendrimer). We consider in the calculation which follows that the volume V dragged by an azobenzene function corresponds to the PMMA DR1 statistical unit to which it belongs or to the fraction of dendrimer to which it is grafted.
For PMMA DR1, we roughly calculate: $V = 1\ \text{nm}^3$. **(*A2*)**

- The chromophore's shift of l occurs along the polarization direction. It can go either way with the same probability which means that it undergoes a one-dimensional radom-walk. **(*A3*)**

- In section III.1.c., we evidenced a decay of the azobenzene's optical activity when subjected to light. The decreasing amount of molecules taking part in the motion is rendered by a decreasing absorption coefficient. ***(A4)***
-Finally, we assume that the azobenzene functions grafted to a given azo-molecule – a polymer chain or a dendrimer – are not simultaneously optically activated. Otherwise, simultaneous activations would lead to competing motions since each chromophore is assumed to be equally likely to go one way or other along the polarization direction. The resulting motion would be nil. **(A5)**

Assumption **(*A1*)** enables us to express the number of molecules n_d, per unit volume and per unit time, that are shifted by l. It is a fraction Φ of the molecules that absorb a photon. This fraction includes the quantum efficiency of the trans to cis isomerization process and the probability of a thermal back isomerization since we defined this latter as the efficient path for the motion to occur.
The expression of the amount of azobenzene n_d put in motion per unit volume and unit time can be found as in annex I by writing the light intensity decrease undergone by a beam going through a layer of infinitesimal thickness dz and whose absorption coefficient is β.

$$n_d = \phi\beta\frac{\lambda}{hc}I$$

λ is the wavelength of the incident light, h is Planck's constant and c stands for the speed of light.
This means that the amount of molecules n_d which are put in motion is proportional to the local intensity.

The quantum efficiency of the process Φ takes into account the quantum yields of trans to cis and cis to trans isomerizations. Following Rau, we take $\Phi_{trans-cis}$ = 0,1 and $\Phi_{cis-trans}$=0,5 for PMMA DR1 which belongs to the pseudostilbene category.

Assuming that all molecules performing trans-cis-trans cycles undergo diffusion motion, the resulting quantum efficiency is roughly Φ = 0,05

So, molecular motions are more likely to occur in areas exposed to high intensities. As a consequence, these highly exposed areas are depleted as matter is piling up in darker areas where the probability of moving is much smaller.

One could contend that such a model leads to a defeating "tug-of-war" with the main chain since the numerous azobenzene functions grafted to the main chain are equally likely to move one way or another along the polarization direction.

Nevertheless, we believe that all the azobenzene chromophores grafted to a given chain do not perform an isomerization trans-cis-trans cycle at the same time, and thus their motions, which are not simultaneous, are not competing. Indeed, as we shall estimate in section IV. an azobenzene dye is activated every second, which is quite a long time compared to the duration of an isomerization trans-cis-trans cycle.

IV.2. Application of the model: time evolution of the free surface of a film exposed to a linearly polarized interference pattern.

IV.2.a. Evolution equation of the free surface h(x,t).

As underlined in chapter II, it is necessary to bridge the gap between our model which is of the « individual motion » type and our experimental results which we got for layers, that is to say for environments with a large number of molecules. To do so, we apply assumptions ***(A1)*** and ***(A2)*** to an azobenzene-containing material layer deposited on a glass substrate which we fix at $z = 0$. The initial thickness is assumed to be uniform all over the layer. It is equal to h_0 along the z direction.

This layer is subjected to a light pattern the intensity of which is modulated along the x axis and is exponentially attenuated as light is passing through the layer.

- For a layer that is exposed front side to the light pattern, that is to say directly exposed and for which the maximum intensity is located at is free surface $z = h$, the light intensity profile writes:

$$I(x,z) = I(x)e^{-\beta(h-z)}$$

- For a layer that is exposed back side to the light pattern, that is to say indirectly exposed through the glass substrate and for which the maximum intensity is located at the bottom of the layer $z = 0$, the intensity profile writes:

$$I(x,z) = I(x)e^{-\beta z}$$

As shown in annex II, the intensity profile for a p linear polarisation is:

$$I(x) = I_0 (1 + v \cos Kx).$$

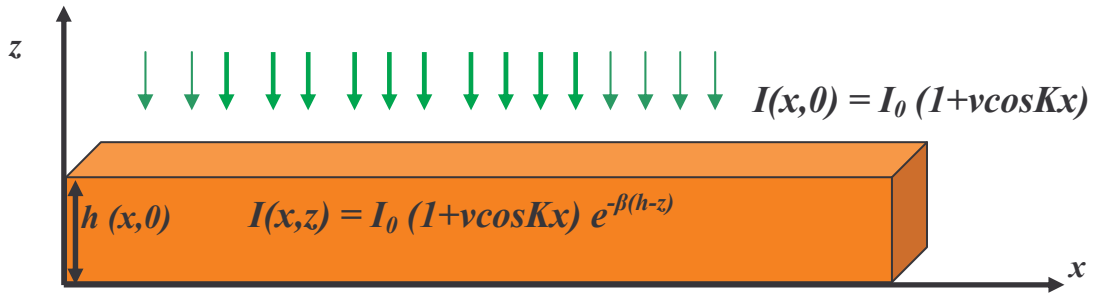

Fig. 41. Configuration for a front side exposed layer.

We establish the evolution equation followed by the local thickness $h(x,t)$ along the z axis by writing two relationships:

- Firstly, we determine an expression for the algebraic flux of molecules $J(x,t)$ from left to right, along the x direction, that crosses the surface of matter located at x.
- Secondly, we write the conservation of matter for a slice of arbitrary thickness dx.

Moreover, we shall assume in what follows that the characteristic optical activity lifetime τ is uniform in order to simplify the calculations to come. However, it is important to keep in mind that the characteristic optical activity lifetime τ is inversely proportional to the local light intensity as highlighted in paragraph III.1.c.

The calculation presented above is computed in the case of a front side exposed layer. Nevertheless, carrying out the calculation for a back side exposed layer would lead to the same expression. We shall justify this allegation once we get to the evolution equation of $h(x,t)$.

- The flux, noted *J(x,t)*, is equal to half of the molecules activated in the portion of the layer comprised between (*x-l*) and *x*, located on the left of the surface minus half of the molecules activated in the portion of the layer between *x* et (*x+l*), on the right. The molecules which under a shift beyond these slices do not reach the surface located at x, given that *l* is the step of the shift.

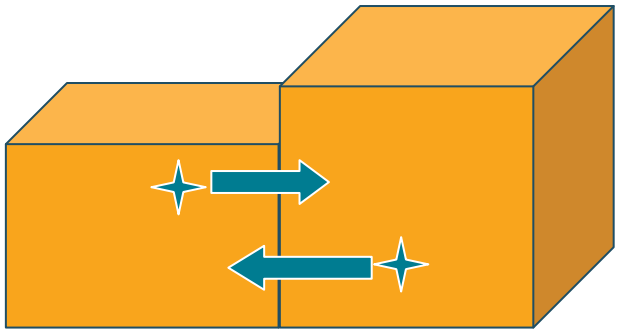

Fig. 42. Determination of the molecular flux J(x,t) through the surface located at x. J(x,t) is equal to half of the molecules activated in the volume comprised between (x-l) and x minus of the molecules activated in the volume comprised between (x-l) and x.

Thus, the flux *J(x,t)* through the surface of matter located at x, the length and the width of which are respectively equal to *h(x,t)* along the *z* axis and unitary along the *y* axis.

J(x,t) = 1/2 molec. activated between (x-l) and x- 1/2 molec. activated between x and (x+l)

$$J(x,t) = \frac{1}{2}\int_0^1 dy \int_{x-l}^{x} dX \int_0^{h(X,t)} dz \cdot n_v(X,z,t) - \frac{1}{2}\int_0^1 dy \int_{x}^{x+l} dX \int_0^{h(X,t)} dz \cdot n_v(X,z,t)$$

Integrating over y gives:

$$J(x,t) = \frac{1}{2}\int_{x-l}^{x} dX \int_0^{h(X,t)} dz \cdot \phi\beta \frac{\lambda}{hc} I(X,z) - \frac{1}{2}\int_{x-l}^{x} dX \int_0^{h(X,t)} dz \cdot \phi\beta \frac{\lambda}{hc} I(X,z)$$

Let us assume that the shift *l* of the molecules is small compared to the characteristic distance of the variations of intensity along the *x* axis, the integral along that direction can be written:

$$J(x,t) = \frac{1}{2} l \int_0^{h(x-l,t)} dz \cdot \phi\beta \frac{\lambda}{hc} I(x-l,z) - \frac{1}{2} l \int_0^{h(x+l,t)} dz \cdot \phi\beta \frac{\lambda}{hc} I(x+l,z)$$

This assumption also allows us to carry out a first order limited development:

$$J(x,t) = \frac{1}{2} l.(-2l).\frac{\partial}{\partial x}\left(\int_0^{h(x,t)} dz \cdot \phi\beta \frac{\lambda}{hc} I(x,z)\right)$$

Replacing *I(x,z)* by its expression mentioned above, which is valid for p linearly polarized states $= I_0 (1 + \nu \cos Kx).e^{-\beta(h-z)}$, the molecular flux at x changes into the form:

$$J(x,t) = -l^2 \phi\beta \frac{\lambda}{hc}.I_0 \frac{\partial}{\partial x}[(1+\nu\cos(Kx)) \int_0^{h(x,t)} dz \cdot e^{-\beta(h-z)}]$$

Integrating along Z and simplifying by β leads to:

$$J(x,t) = -l^2 \phi \frac{\lambda}{hc}.I_0 \frac{\partial}{\partial x}[(1+\nu\cos(Kx)).(1-e^{-\beta h(x,t)})]$$

- At this point, we can write the law of conservation of matter for a slice of arbitrary thickness *dx*, whose height and width are respectively equal to *h(x,t)* along *z* and unitary along (*Oy*). Assuming the density of polymer to remain constant as the morphological changes occur, we can write the volume conservation between time *t* and time *t+dt*:

$$1.dx.[h(x,t+dt) - h(x,t)] = V.J(x,t).dt - V.J(x+dx,t).dt$$

J(x,t) being the flux of chromophores, we need to multiply by the volume *V* dragged by each chromophore. Following assumption ***(A2)***, the volume dragged by the chromophore is the PMMADR1 statistical unit.

$$\frac{\partial h}{\partial t}.dt.dx = -V.\frac{\partial J}{\partial x}.dx.dt$$

Using the expression of *J(x,t)* that we got above, we can write:

$$\frac{\partial h}{\partial t} = l^2 \phi \frac{\lambda}{hc}.I_0.V.\frac{\partial^2}{\partial x^2}.[(1+\nu\cos(Kx)).(1-e^{-\beta h(x,t)})]$$

which can be put under the terse form:

$$\frac{\partial h}{\partial t} = D.\frac{\partial^2}{\partial x^2}[(1+\nu\cos(Kx)).(1-e^{-\beta h(x,t)})]$$

where $D = l^2 \phi \frac{\lambda}{hc} . I_0 . V$

Here, despite similarities with a classical diffusion equation, here D is not a diffusion coefficient since it is not expressed in $m^2.s^{-1}$ but in $m^3.s^{-1}$.

As for the absorption factor $\beta(t)$, it is a decreasing function of time: $\beta(t) = \beta_0 e^{-t/\tau} + \beta_\varepsilon$.

IV.2.b. Solution to the evolution equation.

In order to fully solve the evolution equation above, one needs to resort to a numerical method. Yet, we can analytically compute the expression of $h(x,t)$ for t close to the origin. This way, we obtain an expression of the grating formation rate at $t=0$. We also analytically draw consequences for the saturation amplitude.

IV.2.b.α.Analytical solution at early times: initial grating growth rate of the surface grating.

As displayed by AFM images, at the beginning of its formation the grating has a sinusoidal shape. Besides, the periodicity of the grating is equal to the periodicity of the interference pattern.

So, in these conditions, we can write $h(x,t)$ during the first seconds as :

$$h(x,t) = h_0 + h_1(t).\cos(Kx) + \varepsilon(x,t)$$

where $\varepsilon(x,t) << h_1(t).\cos(Kx)$ as well as for their partial derivatives.

We can introduce this expression of $h(x,t)$ in the evolution equation.

$$\frac{dh_1}{dt}\cos(Kx) + \frac{\partial \varepsilon}{\partial t} = D\frac{\partial^2}{\partial x^2}((1+\nu\cos(Kx))(1-e^{-\beta(h0+h1(t)\cos(Kx)+\varepsilon)}))$$

AFM images also show that the grating amplitude in the first seconds is small compared to the penetration depth $\frac{1}{\beta}$.

Thus, we can linearize $e^{-\beta h_1(t)}$ as $1-\beta h_1(t)$. This leads to:

$$\frac{dh_1}{dt}\cos(Kx) + \frac{\partial \varepsilon}{\partial t} = D\frac{\partial^2}{\partial x^2}((1+\nu\cos(Kx))(1-e^{-\beta h0}(1-\beta h_1(t)\cos(Kx)+\varepsilon))$$

An identification of the terms associated to *cos(Kx)* gives:

$$\frac{dh_1}{dt}(t) = -K^2 D\left(e^{-\beta h_0}\beta.h_1(t) + \nu\left(1 - e^{-\beta h_0}\right)\right)$$

The solution to this differential equation is similar to that of the charging of a capacitance:

$$h_1(t) = -\nu\frac{e^{\beta h_0 - 1}}{\beta}\left(1 - \exp\left(-\frac{t}{K^2 D\beta.e^{-\beta h_0}}\right)\right)$$

It leads to a saturation value whose expression is: $\nu\frac{e^{\beta h_0} - 1}{\beta}$ reached in a characteristic time $K^2 D\beta.e^{-\beta h_0}$.

It is somewhat tempting to relate the saturation that we experimentally observed to this expression. However, we must keep in mind that working on the saturation value we are dealing with big values of time t for which the linearization, which led to the differential equation, is not valid anymore. Furthermore, for later times, AFM images show that the surface deformation cannot always be regarded as a sine form.

So, we shall deal with the saturation value further in this section.

Nevertheless, we are going to use in what follows this differential equation at the origin of time *t = 0*.

Indeed, it gives the expression of the grating's formation rate at *t = 0*:

$$\frac{dh_1}{dt}(0) = -K^2 D\nu\left(1 - e^{-\beta h_0}\right)$$

where: $D = l^2\phi\frac{\lambda}{hc}I_0 V$

We note that: $\frac{dh_1}{dt}(0) < 0.$

This is in accordance with the fact that the layer is depleted in areas where the intensity of light is maximal. Indeed, maximal intensities are obtained for values of *x* such as:

$$cos(Kx) > 0$$

Thus, for such values of x, $\frac{\partial h}{\partial t}(0,x) = \frac{dh_1}{dt}(0).\cos(Kx)$ is negative that is to say the level of the free surface is inferior to the initial value h_0.

And for the values of x where $cos(Kx) < 0$, they give: $\frac{\partial h}{\partial t}(0,x) > 0$.

This expression of the growth rate at $t = 0$ can be written using the absorption factor of the initially flat film whose thickness is equal to h_0:

$$A = (1 - e^{-\beta h0})$$

$$\frac{dh_1}{dt}(0) = - K^2 D \nu A$$

This expression enables us to compare the initial growth rate of two films differing in the nature of the azobenzene containing molecule without the need of knowing the absorption coefficient β and the thickness h_0 of the films. One just need to know the fraction A of the light intensity that is absorbed by a film at $\lambda = 473$ nm.

IV.2.b.β.Origin of the saturation amplitude.

Role of the bleaching process in the saturation amplitude.

Apart from the bleaching process, the light-driven diffusion model presented in this memoir could in itself lead to a saturation of the surface relief grating growth. Indeed, one can figure out a situation such that motions in dark and highly populated areas are exactly compensated by motions in depleted zones where a higher light intensity induces more excitations of the chromophores.

However, if we do not take the bleaching process into account, that is if we set β as a constant β_0, the evolution equation of the free surface $h(x,t)$ does not admit a saturation value for our experimental conditions($\nu = 0,85$ and thickness such that $h_0 > 55$ nm).

Indeed, let us assume that the grating amplitude reaches a saturation value.

This would mean that:

$$\frac{\partial h}{\partial t} = 0$$

The evolution equation gives:

$$\frac{\partial^2}{\partial x^2}[(1 + \nu \cos(Kx)).(1 - e^{-\beta h sat(x)})] = 0$$

Thus:

$$[(1+\nu\cos(Kx)).(1-e^{-\beta hsat(x)})] = px + C$$

where p and C are two constants.
Given the periodic boundaries conditions, a linear dependence on x does not make any sense.

So:

$$(1+\nu\cos(Kx)).(1-e^{-\beta hsat(x)}) = C$$

This means that no matter the abscissa x, the amount of activated chromophores in the column of matter located at x is the same.
Thus, if the saturation were reached, the free surface profile should be $h_{SAT}(x)$, it should be written:

$$h_{SAT}(x) = \frac{1}{\beta}\ln\left(\frac{1+\nu\cos Kx}{(1-C)+\nu\cos Kx}\right)$$

For the values of *x* were the intensity is maximal, the free surface is located at:

$$h_{SAT}^{MIN}(x) = \frac{1}{\beta}\ln\left(\frac{1+\nu}{(1-C)+\nu}\right)$$

As for the values of *x* were the intensity is minimal, the free surface is located at:

$$h_{SAT}^{MAX} = \frac{1}{\beta}\ln\left(\frac{1-\nu}{(1-C)-\nu}\right)$$

This expression is valid provided that $1-C-\nu > 0$.
In our experimental conditions $\upsilon = 0{,}85$. This means that C should be inferior to 0,15.
Besides, for a given thickness h_0, the value of C is imposed by the conservation of matter, hence by the conservation of volume if, once again, we assume incompressibility. Indeed, for a spatial period of span $\frac{2\pi}{K}$, the total volume should be equal to:

$$\int_{-\pi/K}^{\pi/K} h_{SAT}(x)dx = \frac{2\pi}{K} h_0$$

In other words, the average amplitude over a period should be equal to h_0:

$$\frac{K}{2\pi} \int_{-\pi/K}^{\pi/K} h_{SAT}(x)dx = h_0$$

We calculate the value of the integral $\frac{K}{2\pi}\int_{-\pi/K}^{\pi/K} \frac{1}{\beta} \ln\left(\frac{1+\nu\cos Kx}{(1-C)+\nu\cos Kx}\right)dx$ in the [0;0,15[range of allowed values for C using Mathematica™.

As shown below, $\frac{K}{2\pi}\int_{-\pi/K}^{\pi/K} h_{SAT}(x)dx$ varies from 0 to 70 nm in that range.

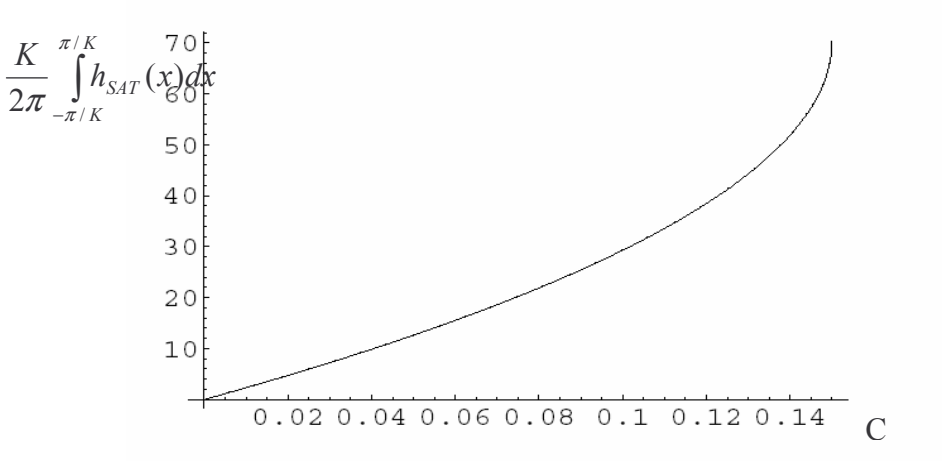

Fig. 43. Possible values for $\frac{K}{2\pi}\int_{-\frac{\pi}{K}}^{\frac{\pi}{K}} h_{SAT}(x)dx$ *in the range of allowed values for C.*

This means that for layers thicker than 70 nm, there is no possible allowed value for C. Thus, the relationship which defines the saturation value, $(1+\nu\cos(Kx))(1-e^{-\beta hsat(x)}) = C$, is not valid. There is no mathematical solution for $h_{SAT}(x)$.

Now, most of our experiments were carried out on layers much thicker than 70 nm and saturation was observed for all of them, which was also broadly reported by other groups.

The diffusion model in itself, without any bleaching process or another phenomenon coming into play, cannot account for the saturation that is observed.
Besides, as we noted in paragraph III.2.a., the saturation amplitude is smaller than the layer's thickness, which means that saturation is reached before the grating troughs get to the glass substrate.
Thus, at this point it is tempting to consider saturation as a consequence of the bleaching process.
We shall call into question this viewpoint in the following chapter. But let us before stick for a while to the bleaching process.
However, solving an evolution equation for $h(x,t)$ which takes into account the time dependence of the absorption coefficient $\beta = \beta_0 e^{-t/\tau} + \beta_\varepsilon$ is not straightforward.
Furthermore, one should take into account that the absorption coefficient is space dependent. Indeed, as stated in paragraph III.1.c., the characteristic optical activity lifetime is inversely proportional to the local light intensity.

IV.3. Confronting the model to our experiments.

Confronting the model to our experiments follows a twofold purpose. Firstly, we want to know if the model accounts for the phenomenon, at least in a qualitative manner. Secondly, beyond the qualitative aspect, equating the theoretical initial grating growth rate $dh_1(0)/dt$ that we obtained in section IV.2 to the experimental value leads to an order of magnitude for the step l of the assumed random-walk. This latter result is of major import in the context of our model: is the value of l obviously nonsensical so that it overrules the model? If not, does this order of magnitude leave hope of observing a single molecule motion?

IV.3.a. Order of magnitude for the step l.

Let us consider a 275 nm thick PMMA DR1 layer, subjected to a p linearly polarized interference pattern of 0,85 μm fringe spacing.
In theses experimental conditions, the grating growth evolution versus time obtained in the ex situ configuration, which we have presented in paragraph III.3.b., displays an initial grating growth rate $\frac{dh_1}{dt}(0)$ around 1 nm/s.

In paragraph IV.2.b.α., we computed the following expression for the initial grating growth :

$$\frac{dh_1}{dt}(0) = -K^2 D \nu A$$

In the experimental conditions mentioned above, we can estimate the value of v, K and A.

- The Λ = 0,85 µm fringe spacing is obtained for a 32° angle between the interfering beams.
- In a p polarisation configuration, it leads to a visibility factor $v = cos(32)$ = 0,85

- Concerning the wave number $K = 2\pi / \Lambda$, we get:

$$K = 7{,}5.10^6 \text{ m}^{-1}$$

-As for the absorption coefficient $A = 1\text{-}e^{-\beta h0}$, β = 8 µm-1 and h_0 = 0,275 µm give:

$$1\text{-}e^{-\beta h0} = 0{,}9$$

However, the actual value of the absorption is inferior to 0,9 after the film has been exposed for a few seconds to a linearly polarized pattern. As reported in section III.1.c., the fast orientation of the azobenzenes leads to a decrease of at least one third of the absorption in a matter of a few seconds. In the case of a 275 nm thick layer, a more realistic value of the initial absorption resulting from the fast orientation is: A = 0,75.

- The experimental initial growth rate $\frac{dh_1}{dt}(0)$ being around 1 nm/s, its expression – where ν, K and A have been replaced by their value in our conditions – leads to :

$$D \approx 2{,}5.10^{-23} \text{ U.S.I.}$$

As defined in paragraph *IV.2.a.*:

$$D = l^2 \phi \frac{\lambda}{hc} I_0 V$$

Where: λ = 473 nm, $hc \approx 2.10^{-25}$ kg.m^3.s^{-2}, I_0 = 1500 W.m^{-2}.

Following the second assumption **(A2)**, the volume V which the chromophore drags is the PMMA DR1 elementary statistical unit to which an azobenzene is grafted.
We assess the volume V of this elementary unit to be around 1 nm^3.

As for the quantum efficiency we take the value $\Phi = 0{,}05$ given by Rau et al.

With these values, we can deduce for the random-walk step:

$l \approx$ a few nanometres

At first sight, such a value for the mean free path in polymers may seem unrealistically big. One is expecting much more modest displacements when it comes to polymers.
However, the motion of polymers drastically differs when the solicitation is small compared to the typical intricacy distance.

The order of magnitude found for l is small compared to the light pattern modulation which is around one micrometer. This justifies the first order development done above.

In section V.1., we shall use this value of l to discuss the possibility of experimentally observing the motion of an isolated molecule or a group of isolated molecules.

IV.3.b. Relating the model to the parameters influencing the dynamics of the grating's growth.

IV.3.b.α. Influence of the intensity of light.

If we follow the model presented above, the initial growth rate is:

$$\frac{dh_1}{dt} = -K^2 D \nu A$$

It is proportional to the incident intensity I_0 through the factor D.

Experimentally, we evidenced in section III.3.c. the effect of the intensity of light on the growth rate.

	$I_0 = 15\ mW / 10\ mm^2$	$I_0 = 1{,}5\ mW / 10\ mm^2$
initial growth rate	1 +/- 0,1 nm/s	0,11 +/- 0,02 nm/s
saturation amplitude	120 nm à 15 % près	80 nm à 15 % près

Although we do not pretend to a quantitative approach, we noted that for two PMMA DR1 films of initial thickness h_0 = 275 nm and subjected to par 15 mW et 1,5 mW, the ratio of the initial growth rates gives approximately 10, which is in accordance with the model.

IV.3.b.β Influence of the thickness of the film.

Through the medium of the factor $A = (1-e^{-\beta h0})$, the expression of the initial growth rate leads to a faster building of the grating at $t=0$ for thicker films. This makes sense since in this case there are more molecules taking part in the mass motion process.
However, as we noted in section III.1.b., the characteristic penetration depth $1/\beta$ is smaller – or at least of the same order of magnitude – than the thickness of the layers we prepared.
This means that the films we worked with can be regarded as thick enough compared to the penetration depth. As a consequence, the effect of the absorption process is sub-linear.
We have evidenced experimentally that the thickness of the film plays a role on the grating's initial formation growth, in a sub-linear way, as reported in section III.3.c. Once again, although we do not pretend to a purely quantitative approach, we have noticed that, for two PMMA DR1 films which are respectively 275 nm and 55 nm thick, both of them subjected to a 15 mW / 10 mm^2 intensity, the ratio of their initial growth rate is somewhere around 3 as we reported on the table below.

	h_0 = 275 nm	h_0 = 55 nm
initial growth rate	1 +/- 0,1 nm/s	0,3 +/-0,05 nm/s
saturation amplitude	120 nm à 15 % près	30 nm à 15 % près

In the framework of our model, this difference in behaviour can be explained by the difference in the absorption properties of the two films since $\frac{dh_1}{dt}(0)$ is proportional to $A = 1-e^{-\beta h0}$.
In section III.1.b. we found β = 8 μm^{-1} for the absorption coefficient. But we noted in section III.1.c. that under exposure to a linearly polarized light the azobenzenes are partly oriented and the resulting absorption of the films is lower than expected. The actual absorption coefficient β is close to 5 μm^{-1} and the corresponding absorption are A = 0,25 for h_0 = 55 nm and A = 0,75.
So, sticking to the model developed in this chapter, we are expecting the ratio between the growth rates to be equal to 3.

We experimentally evidenced that the dependence of the growth rate on the thickness is indeed sub-linear, and the ratio for the films mentioned above is between 3 and 4.

As for the saturation amplitude, we have noted that it is four times bigger for the 275 nm thick film than for the 55 nm thick layer.

IV.3.b.γ Influence of the angle α between the two interfering beams.

The angle α between the two interfering beams play a role in the expression of the grating's initial growth rate $\frac{dh_1}{dt}(0)$ through the medium of the wave number K – which is proportional to $sin^2(\alpha/2)$ –, of the factor D where l^2 is proportional to $cos^2(\alpha/2)$) and of the visibility factor v – which is proportional to cos α. The resulting evolution of the angular factor $sin^2\alpha . cos^2\alpha$ is depicted below.

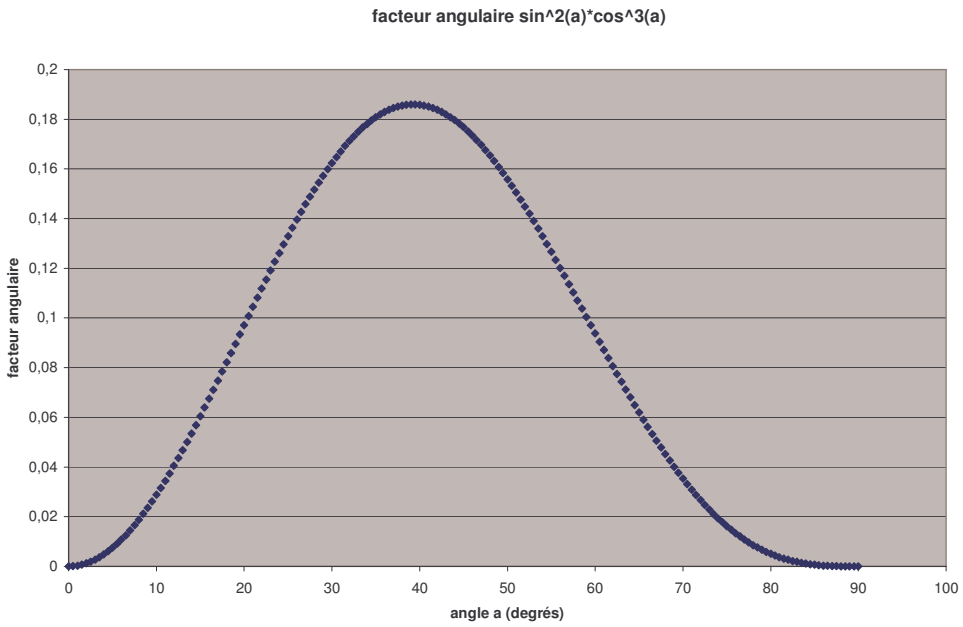

Fig. 44. Expected angular factor.

We carried out most of the experiments with an angle of 32° between the two interfering beams. At this value, we are expecting the initial growth rate to be 90 % of the maximal value.

IV.3.b.δ. Influence de la nature de la molécule.

We noticed in section III.3.e. that in similar conditions, G2MO films display a significantly faster growth rate at the origin of time. It is at least twice faster than for PMMA DR1 films of initial thickness h_0 = 275 nm.

We underlined in section IV.2.b.α. that the initial growth rate $\frac{dh_1}{dt}(0)$ that appears in our model is proportional to the fraction of light absorbed by the film, written A:

$$\frac{dh_1}{dt}(0) = -K^2 D v A$$

This allows us to compare PMMA DR1 and azodendrimer films without having measured the absorption factor and the thickness of the latter.

The illumination conditions being similar for PMMA DR1 and azodendrimer films, the spatial frequency K of the interference pattern and the visibility factor v have the same value in both cases.

Furthermore, the fraction of light which is absorbed by the PMMA DR1 film and by the azodendrimer film is almost the same: the absorption $A = 1 - e^{-\beta h_0}$ is equal to 0,9 (before orientation) for the 275 nm thick PMMA DR1 layer and we measured A = 0,97 (before orientation) for the G2MO film.

This means that the twice faster initial growth rate observed for G2MO is not caused by a much bigger absorption.

Thus, in the framework of the model presented in this memoir, only a bigger factor D can explain the behaviour of GMO. The expression of D is :

$$D = l^2 \phi \frac{\lambda}{hc} . I_0 . V$$

If we stick to the expression of D, the greater efficiency of G2MO et G4MO films compared to PMMA DR1 ones may be explained by a greater quantum efficiency Φ, a larger volume V dragged by each chromophore or a bigger step l.

A greater value of the step l in azo-dendrimers makes sense. Indeed, entanglements of the chains in polymers should make the motion much harder in PMMA DR1 than in azo-dendrimers. A greater hindrance in azo-polymers could also lead to smaller quantum efficiency than in azo-dendrimers.

It is also tempting to explain the bigger value of the step l for the dendrimers by comparing in both cases the fraction of « efficient matter », that is to say the proportion in mass of azobenzenes which are the active part of the molecule.

For PMMA DR1, the mass of one statistical mole of PMMA DR1 is equal to 178 g. The mass of the azobenzene function that it contains is 82 g. This means that the fraction of active mass is approximately 50 %.

As for the GXMO, no matter the generation X, the fraction of efficient matter is around 70 %.

IV.3.c. Saturation as a result of a coupling between the bleaching process and the diffusion mechanism?

Several experimental evidences suggest that the loss of optical activity plays a major role in the saturation of the grating's amplitude that we observed and that has been extensively reported by several groups.

One could contend that the characteristic optical activity lifetime – which is around 35 minutes for an intensity of 15 mW / 10 mm^2 – is slightly longer than the characteristic grating's formation time.

Nevertheless, we believe that combined with the moderating – yet insufficient – effect discussed in section IV.2.b.β. – for which darker and more populated areas oppose the massive motion from brighter and depleted areas – its role is enhanced.

As a first approach, this can be seen by reconsidering the discussion over the possibility of a saturation value undertaken in section IV.2.b.β. In that section, we have shown that the diffusion process in itself cannot lead to saturation: it appeared that if there were a saturation value it would guarantee the conservation of matter – described by the equation: $h_0 = \frac{K}{2\pi}\int_{-\pi/K}^{\pi/K}\frac{1}{\beta}\ln\left(\frac{1+\nu\cos Kx}{(1-C)+\nu\cos Kx}\right)dx$ – only for films of initial thickness $h_0 < 70$ nm.

Nevertheless, as we can see on the equation above, if the absorption coefficient β were much smaller, the conservation of matter would be guaranteed for much bigger values of h_0. In other words, the partial loss of optical activity of the layer favours the balance of the diffusion process and indirectly leads to saturation.

Of course, the expression of the saturation value drawn in section IV.2.b.β. and used here is not valid anymore for an absorption coefficient β that varies in time but it gives a hint as to how the coupling may work.

Moreover, the simplistic assumption that the characteristic optical activity lifetime τ is uniform all over the sample's free surface amounts to underestimating the effect of the bleaching process in time and its coupling to the self-limitation of the diffusion process. Indeed, given that the most illuminated areas – where molecules are more likely to be activated – are also those which are subjected to maximal bleaching effects, the balancing of the flux between brighter, more depleted areas and darker, more populated areas is enhanced by the bleaching process.

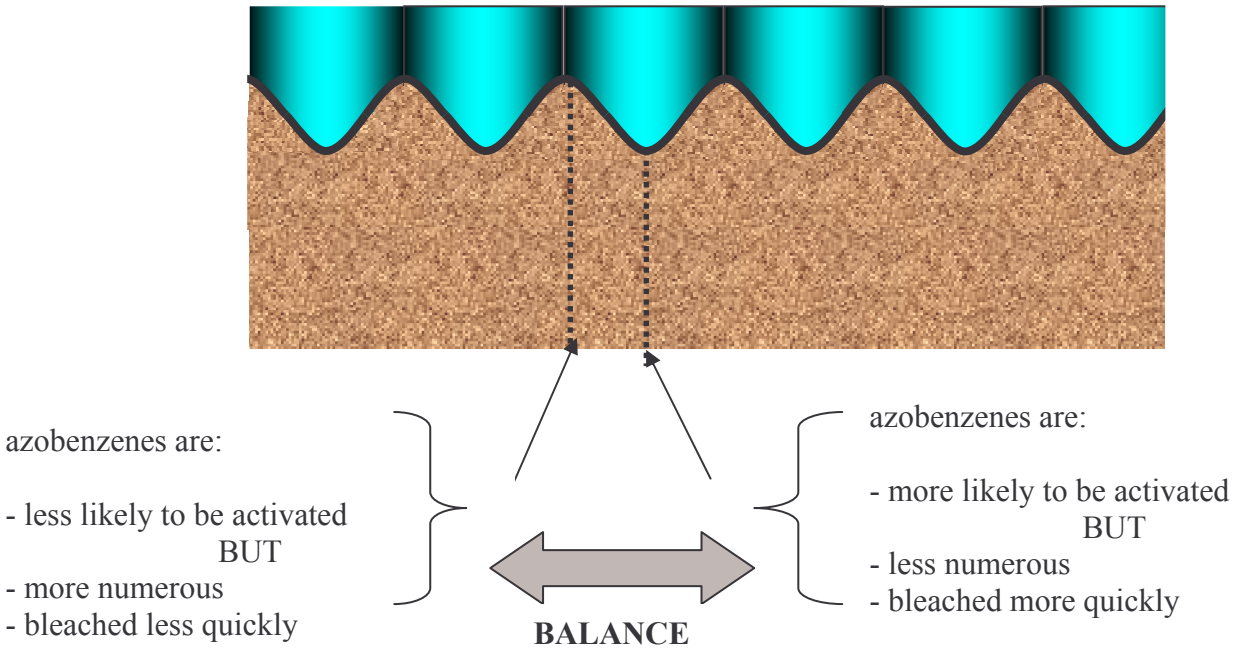

Fig. 45. Interpretation of the phenomenon of saturation as the result of the combination of the self-limited diffusion in the film enhanced by the bleaching process.

There are several experimental evidences that a phenomenon limiting the grating's growth in time is at work.

First, as we have already noted in section III.3.d., for an intensity of 1,5 mW / 10 mm^2, the amplitude at saturation is inferior (80 nm) to the one we get in similar conditions for an intensity of 15 mW / 10 mm^2 (120 nm). This means that the bleaching by itself cannot account Another evidence of that kind is brought by the work of Tripathy et al.[53] as well as that of Barrett et al. on the dependence of the surface grating's amplitude on the interference pattern spacing. Both works agree that, in similar conditions, the largest surface modulation is obtained for an interference pattern whose spacing is around 0,8 µm which means that the angle between the two interfering beams is around 40°.

This tends to show that « time is counted », otherwise in the long run the spacing should not matter and the amplitude reached at saturation should be the same. For, if the activity lifetime of the azobenzenes is limited in time, then the value reached at saturation will be all the greater since the process is fast. In section IV.3.2., we showed that our model gives a maximal recording rate at the origin for an angle of 45° between the two interfering beams, which is close from the 40° reported in the literature.

[53] Tripathy

IV.4. Furthering the model.

IV.4.a. Modulated polarization patterns.

IV.4.a.α Initial growth rate.

We have experimentally evidenced that – if not uniform – at least slightly modulated intensity patterns with periodically modulated polarisation direction give a surface relief grating that is similar to those observed when the light intensity is modulated.

The diffusion model presented here accounts for this observation.

Let us assume that the intensity is almost uniform and that the linear polarization direction rotates with a period $4\pi / K$ along the (Ox) axis as calculated in annex II.

Light intensity being uniform, the isomerization probability, thus the probability that a chromophore is put in motion, is the same at a given z for all abscissas x's in the layer.

However, the motion of the azobenzene chromophore is assumed to occur along the polarisation direction. This, the direction of the motion also varies periodically along the X axis.

Now, the effective motion that actually leads to the building of the grating is the one that occurs along the (Ox) axis. Thus, we can define an effective mean free path $l_x(x)$ along the (Ox) direction as we detail in annex II:

$$l_x(x) = l_0 . \cos(\frac{\alpha}{2}) . \left|\cos(\frac{Kx}{2})\right|$$

where $\frac{Kx}{2}$ is the angle formed by the polarization direction and the (Ox) axis.

$l(x)$ is a $\frac{2\pi}{K}$ periodic function.

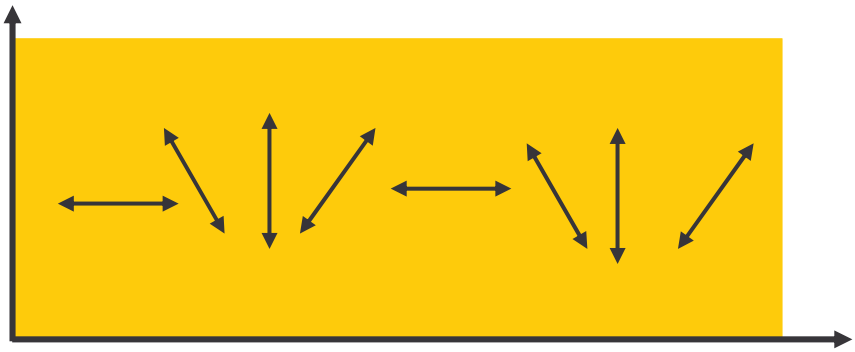

Fig. 46. Resulting pattern: light is (almost) uniform all over the sample. The linear polarization direction rotates periodically in the plane of the sample.

The following picture shows the polarization configuration resulting from the interference of counter-propagating circularly polarized beams at the surface of the film which defines a XY plane.

At these points where the polarization direction is along the X axis, matter is going away on both sides along the X axis, which leads to a depletion of the corresponding areas as opposed to these points where the polarization is along the Y axis and where globally matter remains there.

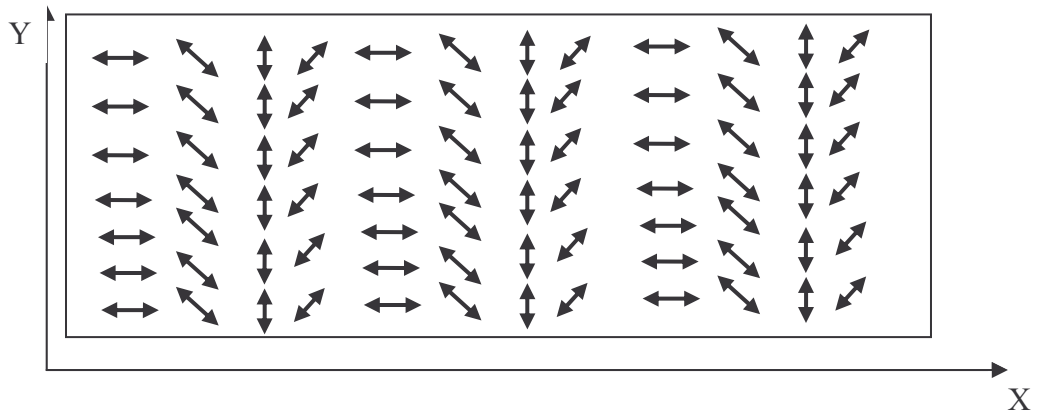

Fig. 47. Arrows indicating the configuration of the polarization direction in the XY plane of the film resulting from the superimposition of two counter-propagating beams. The flow of matter being assumed to be along the polarization direction, one can figure out that the net flux of matter is nil where the polarization is along the Y axis.

Quantitative approach.

The previous paragraph shows that, in this framework, the resulting non-zero molecular flux *J(x,t)*at abscissa x is due to the gradient of effective mean free path $l_X(x)$ along the X axis.

J(x,t) = 1/2 molec. activated between (x-l) and x- 1/2 molec. activated between x and (x+l)

$$J(x,t) = \frac{1}{2}\int_0^1 dy \int_{x-l}^{x} dX \int_0^{h(X,t)} dz \cdot n_v(X,z,t) - \frac{1}{2}\int_0^1 dy \int_{x}^{x+l} dX \int_0^{h(X,t)} dz \cdot n_v(X,z,t)$$

In this case, the number of activated molecules per unit volume and time is a constant.
What differs is the value of the effective mean free path $l_X(x)$.

$$J(x,t)=\frac{1}{2}\int_{x-l}^{x}dX\int_{0}^{h(X,t)}dz\cdot\phi\beta\frac{\lambda}{hc}I_0.e^{-\beta(h-z)}-\frac{1}{2}\int_{x-l}^{x}dX\int_{0}^{h(X,t)}dz\cdot\phi\beta\frac{\lambda}{hc}I_0.e^{-\beta(h-z)}$$

Integration along the X axis gives:

$$J(x,t)=\frac{1}{2}l(x-l)\int_{0}^{h(x-l,t)}dz\cdot\phi\beta\frac{\lambda}{hc}I_0.e^{-\beta(h-z)}-\frac{1}{2}l(x-l)\int_{0}^{h(x+l,t)}dz\cdot\phi\beta\frac{\lambda}{hc}I_0.e^{-\beta(h-z)}$$

$$J(x,t)=\frac{1}{2}\phi\frac{\lambda}{hc}I_0.l_x(x-l)(1-e^{-\beta h(x-l,t)})-\frac{1}{2}\phi\frac{\lambda}{hc}I_0.l_x(x+l)(1-e^{-\beta h(x+l,t)})$$

If we assume, as we did in section IV.2.a, that the mean free path *l* is small compared to the characteristic distance of variations of the polarization (that is to say $\frac{4K}{\pi}$), the expression of the molecular flux *J(x,t)* can be linearized as:

$$J(x,t)=\frac{1}{2}\phi\frac{\lambda}{hc}I_0.(-2l_x(x)).\frac{\partial}{\partial x}\left(l_x(x)(1-e^{-\beta h(x,t)}\right)$$

As done in section IV.2.a., we write the conservation of matter for a slice of infinitesimal thickness *dx*, which gives:

$$\frac{\partial h}{\partial t}=-V.\frac{\partial J}{\partial x}$$

This way, we get as an evolution equation for the free surface *h(x,t)*:

$$\frac{\partial h}{\partial t}=\phi\frac{\lambda}{hc}.I_0.V.\frac{\partial}{\partial x}\left(l_x(x)\frac{\partial}{\partial x}.[(l_x(x).(1-e^{-\beta h(x,t)})]\right)$$

As underlined in annex II, the absolute value in the expression of the mean free path *l(x)* leads to a discontinuity of its derivative. We will stick to one period for which we shall solve the equation. This enables us to write:

$$l_x(x)=l_0\cos(\frac{\alpha}{2}).\cos(\frac{Kx}{2})$$

The evolution equation of the local surface height *h(x,t)* can be written:

$$\frac{\partial h}{\partial t}=\phi\frac{\lambda}{hc}.I_0.V.l_0^2.\cos^2(\frac{\alpha}{2})\frac{\partial}{\partial x}\left(\cos(\frac{Kx}{2}).\frac{\partial}{\partial x}\left(\cos(\frac{Kx}{2}).\left(1-e^{-\beta h(x,t)}\right)\right)\right)$$

At this point, and given the experimental result presented in section III.4. for such a configuration, we find it interesting to calculate the expression of the initial growth rate $\frac{dh_1}{dt}(0)$ in the pure polarization modulation case. Then, we will compare this result to the initial growth rate computed in section IV.2.b.α. for intensity modulated patterns.

As we did in section IV.2.a., we can assume that at the beginning of its formation, the grating has a sine shape. So, for t small we can write:

$$h(x,t) = h_0 + h_1(t).\cos(Kx)$$

which we can introduce into the evolution equation.

With $D' = \phi\frac{\lambda}{hc}.I_0.V.l_0^2.\cos^2(\frac{\alpha}{2})$, the evolution equation can be expressed as:

$$\frac{dh_1}{dt}\cos(Kx) = D'^2\frac{\partial}{\partial x}\left(\cos(\frac{Kx}{2}).\frac{\partial}{\partial x}\left(\cos(\frac{Kx}{2})\left(1-e^{-\beta(h_0+h_1(t).\cos(Kx)}\right)\right)\right)$$

$$\frac{dh_1}{dt}\cos(Kx) = D'^2\frac{\partial}{\partial x}\left(\cos(\frac{Kx}{2}).\frac{\partial}{\partial x}\left(\cos(\frac{Kx}{2})\left(1-e^{-\beta h_0}\left(1-\beta h_1(t).\cos(Kx)\right)\right)\right)\right)$$

$$\frac{dh_1}{dt}\cos(Kx) = D'^2\frac{\partial}{\partial x}\left(\cos(\frac{Kx}{2}).\frac{\partial}{\partial x}\left(\left(1-e^{-\beta h_0}\right)\cos(\frac{Kx}{2})+\frac{\beta}{2}e^{-\beta h_0}h_1(t).\left(\cos(\frac{Kx}{2})+\cos(\frac{3Kx}{2})\right)\right)\right)$$

$$\frac{dh_1}{dt}\cos(Kx) = D'^2\frac{\partial}{\partial x}\left(\cos(\frac{Kx}{2}).\frac{\partial}{\partial x}\left(\left(1-e^{-\beta h_0}\right)\cos(\frac{Kx}{2})+\beta e^{-\beta h_0}h_1(t).\cos(\frac{Kx}{2}).\cos(Kx)\right)\right)$$

$$\frac{dh_1}{dt} = -\frac{D'K^2}{4}\left(\left(1-e^{-\beta h_0}\right)+\beta.e^{-\beta h_0}h_1(t)\right)$$

Thus, we get for the initial growth rate:

$$\frac{dh_1}{dt}(0) = -\frac{D'K^2}{4}\left(1-e^{-\beta h_0}\right)$$

That is to say:

$$\frac{dh_1}{dt}(0) = -\phi\frac{\lambda}{hc}.I_0.V.l_0^2.\cos^2(\frac{\alpha}{2})\frac{K^2}{4}(1-e^{-\beta h_0})$$

This expression differs from the one computed for intensity patterns which we computed in sectionIV.2.b.:

$$\frac{dh_1}{dt}(0) = -\phi \frac{\lambda}{hc} . I_0 . V . I_0^2 . \cos^2 \alpha . K^2 \left(1 - e^{-\beta h_0}\right)$$

The growth rate computed for polarization patterns differs from this one by a factor:

$$\frac{1}{4} . \left(\frac{\cos(\frac{\alpha}{2})}{\cos \alpha} \right)^2$$

For an angle α between the interfering beams equal to 32°, this factor is around 0,3.
Thus, in the context of the diffusion model developed here, we are expecting surface relief gratings obtained with modulated polarization configurations to grow about three times slower than when they are recorded with an intensity modulated pattern.
This could account for the growth rate experimentally found for a polarization grating configuration and reported in section III.4. where it appears to be at least three times slower.

IV.4.a.β. Saturation amplitude.

On the same graph which depicts the amplitude of the surface grating versus time, we noted that the saturation occurred much later. The grating is growing slowly and saturates only after one hour of exposure.
The model developed above provides an explanation for this. Indeed, if we assume as we did in section IV.3.c. that the saturation results from a combination between the diffusion mechanism and the bleaching process which, then we are expecting the surface grating to saturate later. Indeed, the illumination being almost uniform all over the film's surface, areas which are depleted and where each motion in efficient become optically inactive at the same rate as these areas where there is more matter and each motion is less efficient. This means that the self-balance inherent to the diffusion process is not enhanced by a contrast in bleaching.
This leads us to think that in this case it is purely the effect of bleaching – and not its coupling to the diffusion mechanism – which leads to the saturation of the grating.
This is also suggested by the experimental grating's growth presented in section III.4. where we can see that the characteristic saturation time – which is around one hour –happens to be close to the characteristic bleaching time for a layer exposed to a laser at a similar intensity.

IV.4.b. Erasing attempts.

For erasing attempts, the evolution equation of the free surface $h(x,t)$ becomes:

$$\frac{\partial h}{\partial t} = D\frac{\partial^2}{\partial x^2}(1 - e^{-\beta h(x,t)})$$

One can figure out how difficult erasing a surface relief grating can get by considering a layer of initial thickness h_0 previously exposed to an interference pattern for T seconds in order to record a surface relief grating. The free surface equation is $h_0+h_1(x,0)$ as the erasing attempt is about to begin at $t=0$.

As for the absorption coefficient, a long enough exposure causes it to decrease from β_0 to $\beta(T) = \beta_0 e^{-T/\tau} + \beta_\varepsilon$ If we assume T big enough compared to the characteristic lifetime activity τ, then the absorption factor β is small enough to allow us to write a development of $exp(-\beta(h_0+h_1(x,t))$: $e^{-\beta 0}(1- \beta h_1(x,t))$.

The evolution equation for $h_1(x,t)$ becomes:

$$\frac{\partial h_1}{\partial t} = D\beta(T)e^{-\beta h_0}\frac{\partial^2 h_1}{\partial x^2}$$

At the beginning of the erasing attempt the absorption coefficient has already dropped down to $\beta(T)$ due to the bleaching during the exposure. Thus:

$$\frac{\partial h_1}{\partial t}(x,0) = D\beta(T)e^{-\beta h_0}\frac{\partial^2 h_1}{\partial x^2}(x,0)$$

This is a diffusion equation which leads to h_1 tending to 0.

Nevertheless, the diffusion coefficient $D\beta e^{-\beta h_0}$ makes us expect a very slow decay for the amplitude of the grating.

This can be seen on the erasing experiment presented at the end of section III.5. where we noted the slowness of the erasing process.

We can relate this slowness to the value of the diffusion coefficient $D\beta e^{-\beta h_0}$ even prior to any bleaching.

Assuming that the surface grating has a sine form, writing $h(x,t) = h_0 + h_1(t).cos(Kx)$ in the diffusion equation above leads to:

$$\frac{dh_1}{dt}(0) = -DK^2 e^{-\beta h_0} \beta(T) h_1(0)$$

for the initial decay rate.

In similar conditions, except for the intensity that was twice smaller, we have calculated in section IV.3.a. that $D \approx 2{,}5.10^{-23}$ U.S.I. So, here D should be around 5.10^{-23} USI.

With $K = 7{,}5.10^6$ m^{-1}, β equal to a few μm^{-1} , $h_0 = 275$ nm and $h_1(0)$ around 40 nm, we get:

$$\frac{dh_1}{dt}(0) \approx \text{a few } 10^{-3} \text{ nm.s}^{-1}.$$

This small value corresponds to the experimental value given by the erasing experiment exposed in section III.5.:

$$\frac{dh_1}{dt}(0) \approx 7.10^{-3} \text{ nm.s}^{-1}.$$

This may explain why we had such a hard time erasing gratings. It also explains why it proved impossible for us to erase gratings that had been recorded for a long time. Indeed, in this case bleaching can divide the value of the factor $\beta.e^{-\beta h_0}$ – which is part of the diffusion coefficient D – by a factor from 5 to 10 (depending on the initial thickness h_0) if β decreases from 4,5 μm^{-1} to 0,4 μm^{-1} as it was shown to evolve in section III.1.c.

Thus, after bleaching, we are expecting an initial erasing rate even ten times slower, that is to say less than 10^{-3} nm.s^{-1}.

Moreover, as Kumar et al. reported, it is all the more difficult to flatten an initially structured grating as the film is initially thick.

This trend is suggested by the factor $e^{-\beta h0}$, which makes the diffusion quite small as the initial thickness h_0 is big.

IV.5. Links with the theory of molecular motors.

It is somewhat tempting to consider the assumptions formulated in section IV.1. in the light of the theory of « thermal ratchet » molecular motors developed by Magnasco as well as by Prost et al.[54]

In the framework of this theory, a particle is submitted alternatively to two periodic and asymmetrical potentials of periodicity L, or equivalently a particle alternate between two

[54] Prost, J. ; Chauwin, J. F. ; Peliti, L. ; Adjari, A. *Phys. Rev. Lett.* **1994**, *72*, 2652.

states, thus alternatively undergoing two potentials which need to be L periodic and asymmetrical. The possibility of a motion lies on the existence of a spatial asymmetry of the periodic potential to which each state is subjected. It also requires a temporal symmetry breaking. This latter is introduced by an optical or a chemical pumping which breaks the balance between the occupation probabilities of the two states. In this framework, thermal fluctuations are turned into work.

However, this model does not provide a suitable description for the light-induced motion of azobenzene-containing materials. Indeed, there is no physical reason why the interaction potential between the chromophore dipole and the electromagnetic field should be asymmetrical.
Even if it were so, it would lead to an outright nonsensical value for the mean free path *l*. Indeed, the periodicity of the interaction potential should be that of the electric field, that is to say around one micrometer. The associated « thermal ratchet » motion should have the same periodicity, which means that the azobenzene chromophore's step should be around one micrometer.

Nevertheless, we shall retain from this model the necessity of both a space and time symmetry breaking.
The existence of a displacement of step *l* for each isomerisation cycle could be explained by those trans-cis-trans cycles performed in a dissymmetric way: trans to cis isomerization through a given photonic path followed by a back photo-isomerization to the trans form following a different path as suggested by the picture below.

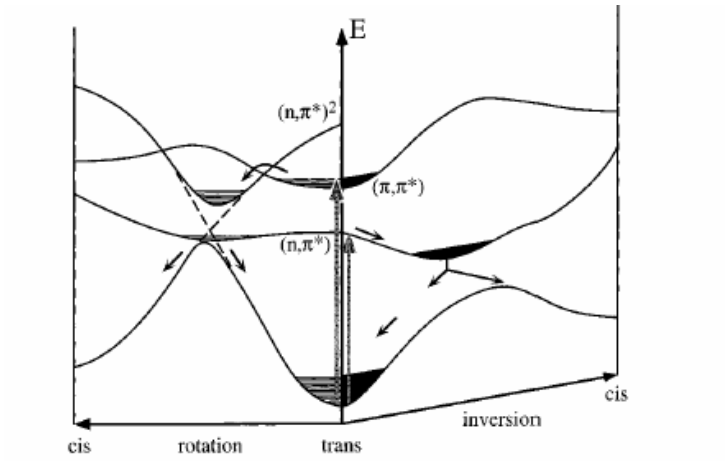

Fig. 48. The trans to cis photo-excitation can follow two different paths. The possibility for an azobenzene function to follow two different paths during a trans-cis-trans cycle(to reach the

cis state and to go back to the trans) provides an insight as to what the spatial asymmetry could be.

We also figure that thermal back isomerizations that occur in less than one second following the excitation to the cis form also take part in the motion process.
We hardly figure out how a molecule going back to the trans form through an identical path that is to say in a way symmetrical to the excitation, could be put in motion.
The motion also requires an interaction with its environment, the substrate for instance, that is to say a dissipation process which breaks the time symmetry.

CHAPTER V

The consequences of the model and its limits to account for our observations.

After having applied the model – which belongs to the "individual motion" category – to dense environments such as films in the previous chapter, we shall stick for a while to a single molecule. Our purpose is to apply the results obtained above in order to assess whether – in the context of our model –the attempt at trying to observe the motion of a unique azobenzene-containing molecule makes sense.

Then, we shall go back to dense environments. The presentation of several puzzling experimental results on azobenzene-containing films will call into question the diffusion model developed above.

V.1. Can the light-induced motion of a single molecule be observed ?

As underlined in section II.2., observing the light-induced motion of isolated molecules is quite tricky. It requires a mastery over the substrate / molecule interaction that has not been reached yet.

Besides, the order of magnitude of the shift step, the rate at which a molecule is moved and its lifetime are crucial parameters.
This is why we propose an estimation of the distance crossed by the chromophore during the optical activity lifetime.
To serve this purpose, we consider a chromophore deposited on a surface with which it can interact. The chromophore is located in the field of a linearly polarized laser whose intensity is equal to 15 mW / 10 mm^2. The polarization direction is comprised in the surface on which the chromophore is deposited.

Distance crossed by the chromophore versus time.

-In the framework of the model presented above, and using the order of magnitude drawn in section IV.3.1., each step *l* performed by the chromophore is around a few nanometres.
- The rate at which a molecule is shifted by a step l can be found out by dividing the number of isomerized molecules by unit volume and by unit time n_d by the density of molecules.

As shown in annex I, the number of molecules per unit volume and per unit time n_d which undergo diffusion motion is:

$$n_d = \phi\beta \frac{\lambda}{hc} I$$

As already mentioned, we have:
Φ = 0,05; λ = 473 nm; I = 15 mW / 10 mm^2; and the absorption coefficient β resulting from the fast orientation upon exposure to linearly polarized light is around 4,5 μm^{-1}.
In these conditions, we calculate:

$n_d \approx 5.10^{17}$ azobenzene functions moving every second per cubic millimetre.

Besides, the density of PMMA DR1 is equal to 1,1 which means that one cubic decimetre contains $1{,}1.10^3$ g of PMMA DR1.
The mass of one mole of statistical unit of PMMA DR1 is 178 g. This means that there are:

$\frac{1{,}12.10^3}{178} = 6{,}3$ mol of statistical units of PMMA DR1 for one cubic decimetre.

The molar composition of a statistical unit of PMMA DR1 consists in 30 % of DR1 and 70 % of PMMA.
The azobenzene functions being contained by the DR1, it means that there are:

$\frac{30}{100} \times 6{,}3$ mol = 1,9 mol of azobenzene functions for one cubic decimetre.

That is to say:

One cubic decimetre contains10^{24} azobenzene functions.

So, the concentration of azobenzene functions is: 10^{18} functions per cubic millimetre.

Since we estiamated that around $n_d = 5.10^{17}$ azobenzene functions are put in motion every second per cubic millimetre, we can estimate that each azobenzene chromophore undergoes diffusion motion every two second.

So, after t seconds, the azobenzene chromophore has undergone $N = \frac{t}{2}$ random-walk movements.

If we follow assumption **(A3)** formulated in section IV.1., the azobenzene chromophores perform a one-dimensional random-walk of mean free path l along the polarization direction.

Thus, after N shifts, the azobenzene function has covered a distance equal to $\sqrt{N}l$, typical of a random-walk.

This means that at time t, the distance covered by the chromophore is: $\sqrt{\frac{t}{2}}.l$

Distance covered by the chromophore during its optical activity lifetime.

For a 15 mW / 10 mm^2 intensity linearly polarized laser beam, we have estimated the lifetime activity to be around 40 minutes, that is to say T = 2400 seconds in section III.1.c.

From the value of l computed in the previous paragraph and the evaluation of the distance crossed t seconds after the beginning of the exposure, we can assess the distance covered by the azo-chromophore during its optical activity lifetime, considered in that example to be T = 2400 s:

distance covered during the optical activity lifetime = $\sqrt{\frac{T}{2}}.l \approx$ a few hundreds of nanometres

In the framework of the model that we developed in the previous chapter, it does make sense that a single molecule motion may be experimentally difficult to observe.

After having turned to isolated molecules, which was the very purpose of our "individual motion" oriented work, we would like to stick back to the environment of films in order to highlight unexpected observations that we came across.

Although marginal, these observations call into question the light-driven / bleaching-limited random-walk model that we developed above.

Unless, as we shall underline, limited control and knowledge over the experimental set-up and its consequences on the structure of the electric field lead to these few puzzling observations.

V.2. The limits of the model.

Some real-time experiments have brought a wealth of unexpected information. Paragraphs V.2.b. and V.2.*c*. of this section give two examples of deformation of an initially growing surface relief grating. This suggests that competing processes may be at work.
But another photo-responsive behaviour which suggests that the diffusion model does not encompass the whole phenomenon is brought by the behaviour of a PMMA DR1 layer subjected to an enhanced near-field under a tip. This is shown in the first paragraph.

V.2.a. Near field induced mass motion.

We generate an evanescent wave in a PMMA DR1 film through total reflection of a laser beam on the glassy backside of the sample. This field is enhanced using a platinum AFM tip. This way, we generate an electric field whose polarization direction is orthogonal to the surface and whose amplitude can reach 10^5 times the initial amplitude around the tip.

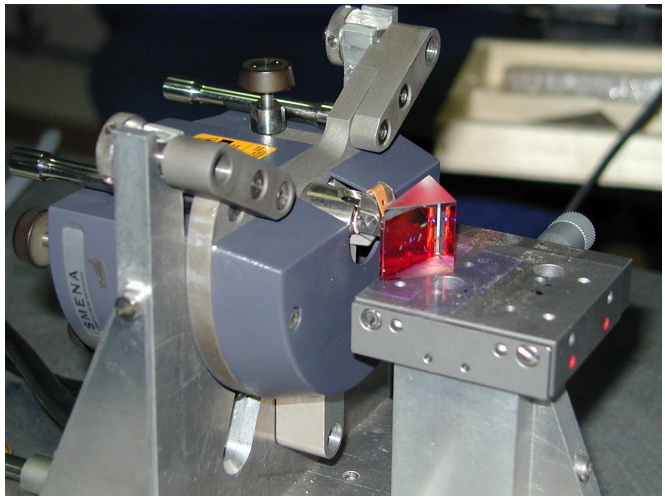

Fig. 49. AFM tip scanning the surface of the azo-film which is stuck to the prism by a refractive matching liquid.

We worked with a platinum tip of angular opening around 20° and, using the approach system of the AFM, we placed it what we estimate to be 20 nm from the film's surface.
Thus, the evanescent light was shone on the tip through the layer for about one minute.

AFM images performed after the exposure show that matter has piled up where the tip was. The piling up consists in a 80 nm bump whose lateral extension is 100 nm by100 nm.

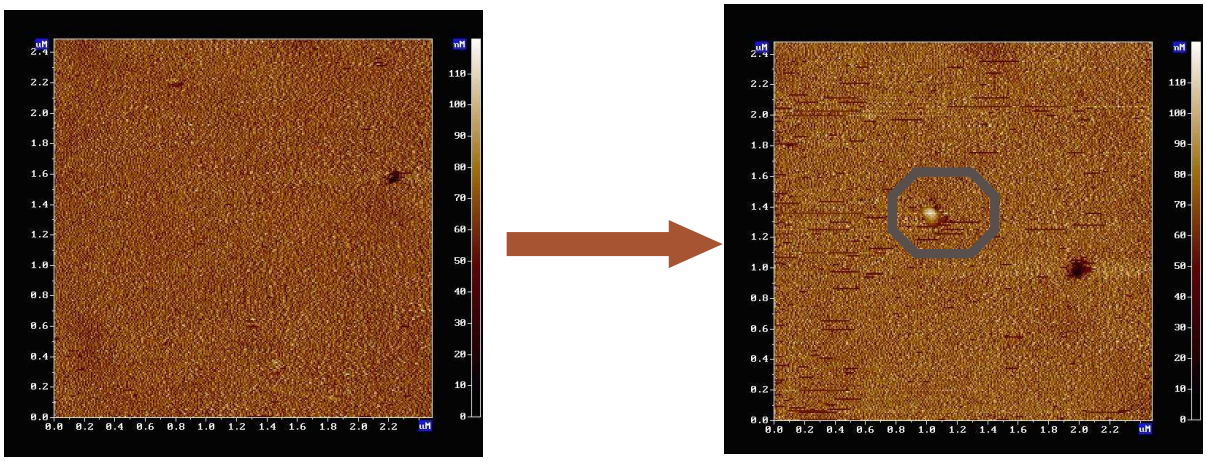

Fig. 50. AFM images before and after the film was subjected to an enhanced field under a metallic tip: matters piles up under the tip. It forms a 80 nm bump. There is an offset between the two images. The hole on the right can be used as a point of reference.

The mass motion that we observe here differs from the surface alterations that appeared for the interferential set-up at lower intensities.

In this case, the matter flows from the least exposed peripheral areas and converges towards the tip where the intensity of light is maximal.

The main difference in that experiment from those carried out with an interferential set-up is that we expect the electric field intensity to be much greater here.

This suggests that the molecular motion depends on the intensity of light.

Peretti et al. show that, depending on the light intensity, a "metallic tip facing a sample" device can lead to different results. At low intensity, they observe holes at the point to the vertical of which the tip was placed, which is what we would expect from the layers studied above. At high intensity, they observe bumps which also indicate a quite different behaviour.

Nevertheless, the structure of the electric field greatly differs from that used in the previous experiments. The exact structure of a field which is enhanced by a metallic tip remains a tangle question.

This change in behaviour depending on the intensity of light has been observed by Bian et al[55]in a situation where the polarization state is fully known. A linearly polarized Gaussian

[55] Bian, S. ; Williams, J. M.; Kim, D. Y.; Li, L.; Balasubramanian, S.; Kumar, J.; Tripathy, S. *J. Appl. Phys.* **1999**, *86*, 4498

beam is cast on a PMMA DR1 film. AFM images show that at intensities well below 1 mW / cm^2 the beam creates a hole as opposed to intensities around 1 mW / cm^2 which generate a bump.

Research groups from Laboratoire de Physique de la Matière Condensée, Ecole Polytechnique and Laboratoire de Nanotechnologie et d'Instrumentation Optique in Troyes[56] assume that there is a competition between two kinds of field components. As explained in their joint article, the electric field in the vicinity of the tip can be decomposed in a continuous spectrum of plane waves. The evanescent components correspond to the light scattered by the high spatial frequencies of the tip and are predominant over the lateral field components. In their opinion, the former is more energetic and tends to lift up matter as opposed to the lateral components which tend to create a hole as we would have expected.

What should be underlined at this point is the possibility to generate a mass transport at a sub-wavelength scale: the lateral extension of the bump on the AFM image is less than a tenth of a micrometer.

The importance of such a sub-wavelength mass transport has been highlighted as since 2001 by the joint work of research groups from the University of Potsdam, Queen's University of Kingston, Canada and WITec GmbH of Ulm, Germany[57,58].

The samples for their experiments were spin-coated films on glass consisting of side-chain azobenzene containing material, poly{(4-nitrophenyl)[4-[[2-(methacryloyloxy)-ethyl] ethylamino] phenyl]diazene} (pDR1M). They used near-field light, which was located in areas much smaller than the wavelength in order to generate nanometre large structures.

The applied optical near-fields were produced in two ways. First by the enhanced light around the illuminated gold nanoparticles and second by light which tunnels through the nanometric aperture of a SNOM tip. This special near-field light was directly used for influencing the surface profile.

---

[56] Landrau, N.; Peretti, J.; Chaput, F.; Lampel, G. ; Boilot, J.P. ; Lahlil, K. ; Bachelot, R. ; H'Dhili, F. ; Barchiesi, D. ; Lerondel, G. ; Fikri, R. ; Royer, P. *J. Appl. Phys.* **2003**, *94*, 2060.

[57] P. Karageorgiev, B. Stiller, D. Prescher, B. Dietzel, B. Schultz, L. Brehmer, Langmuir **16** (13), 5515-5518 (2000)

[58] Th. Geue, M. Schultz, J. Grenzer, U. Pietsch, A. Natansohn, P. Rochon, J. Appl. Phys. 87 (11), 7712 (2000)

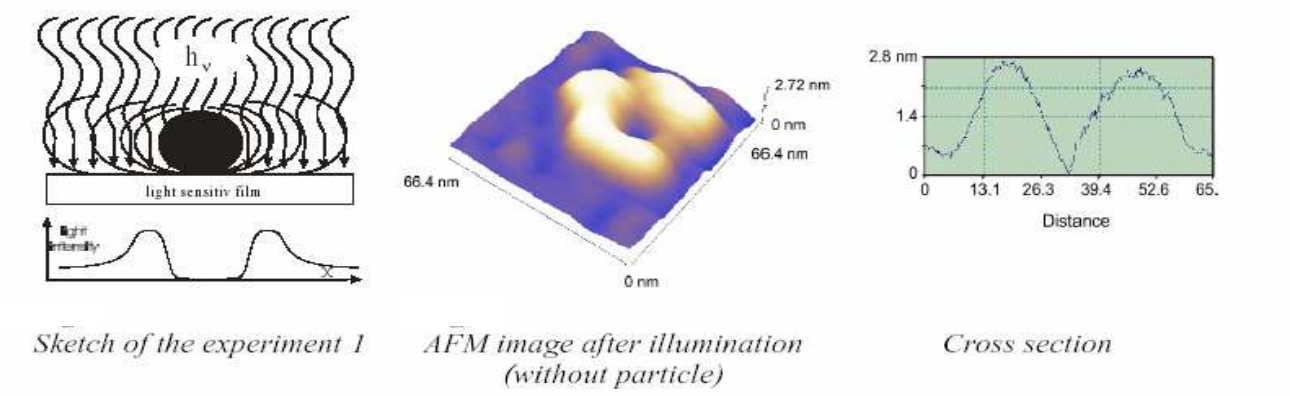

Sketch of the experiment 1 *AFM image after illumination (without particle)* *Cross section*

Fig. 51. Enhanced light around a gold nanoparticle leads to an optical near-field that generates an accumulation of matter where the intensity is maximal. Cf. references 3 and 4.

V.2.b.Phase inversion of the surface relief grating.

This change in behaviour depending on the intensity profile also seems to depend on the total amount of energy that the layer has received.

In section III.3.a, we have shown how a large part of the surface relief gratings obtained through the « real time » set-up for PMMA DR1 and GMO dendrimer films end up altogether blurred after a few minutes of backside exposure. However, other experiments carried out in the same conditions on some PMMA DR1 films display a totally different behaviour. In addition to the surface relief grating that is first built a second one appears, in phase opposition with it. Progressively, the first grating gives way to the second way, which results in a global π phase-change of the grating.

The four images presented below evidence the evolution of a surface relief grating while it is recorded on a PMMA DR1 film by the "real time" method.

The AFM progressively sweeps the surface of the PMMA DR1 film and displays a doubling of the grating's frequency followed by an inversion: the maxima and the minima are switched.

This is indicated by the bunch of three defects which appear on the AFM images. One should not be misled by the fact that the brightest one is always on a bump and thus conclude that there was no π change in the phase of the grating. Indeed, each of the three defects appears brighter when located on a bump and much less prominent when it is in a trough just because in the first case it is better rendered by the AFM tip. Keeping this in mind, we can see that the defect located on the left and that was on a bump on picture A ends up in a trough on picture D.

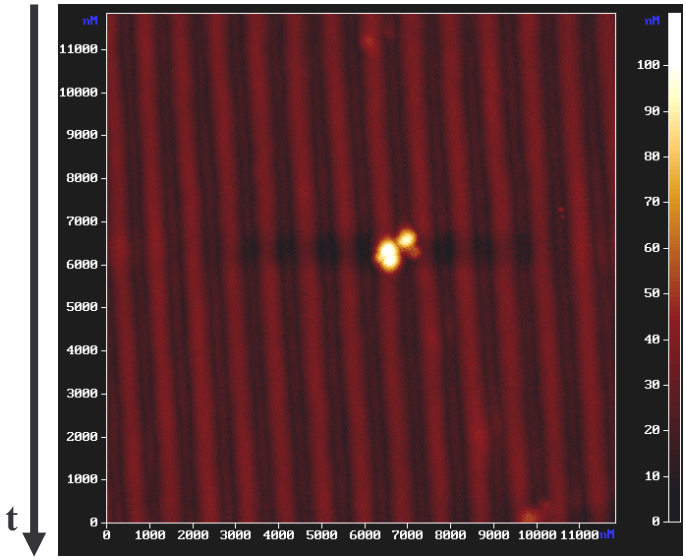
t
nM
11000
10000
9000
8000
7000
6000
5000
4000
3000
2000
1000
0
0 1000 2000 3000 4000 5000 6000 7000 8000 9000 10000 11000 nM
100
90
80
70
60
50
40
30
20
10
0

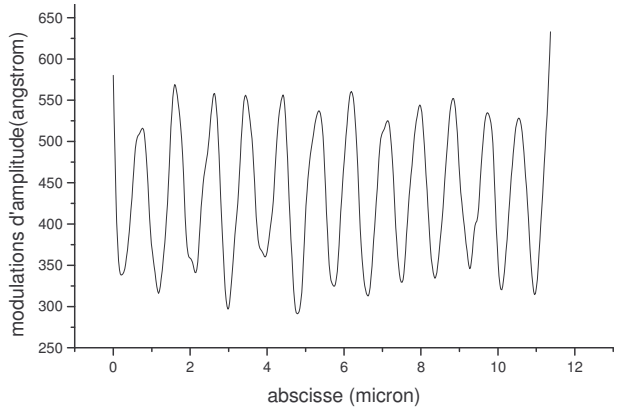
modulations d'amplitude(angstrom)
650
600
550
500
450
400
350
300
250
0 2 4 6 8 10 12
abscisse (micron)

A.

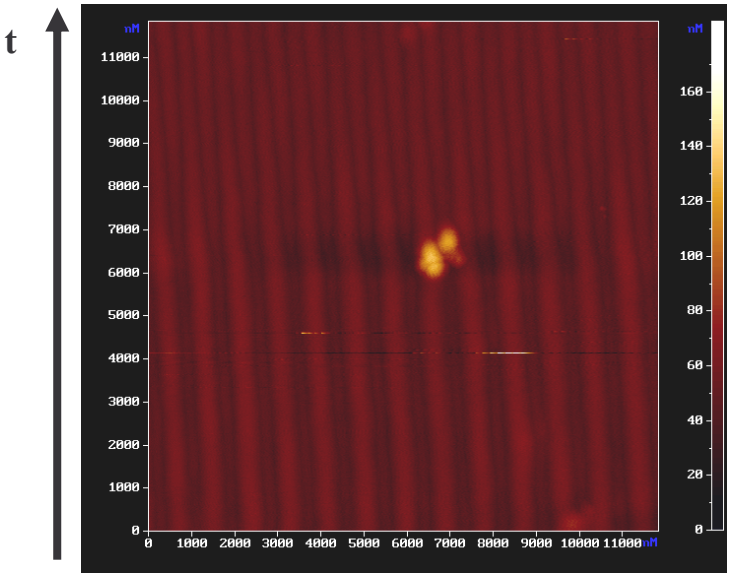
t
nM
11000
10000
9000
8000
7000
6000
5000
4000
3000
2000
1000
0
0 1000 2000 3000 4000 5000 6000 7000 8000 9000 10000 11000 nM
160
140
120
100
80
60
40
20
0

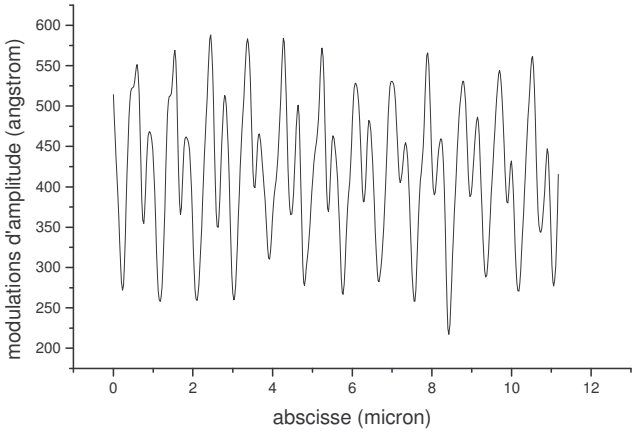
modulations d'amplitude (angstrom)
600
550
500
450
400
350
300
250
200
0 2 4 6 8 10 12
abscisse (micron)

B.

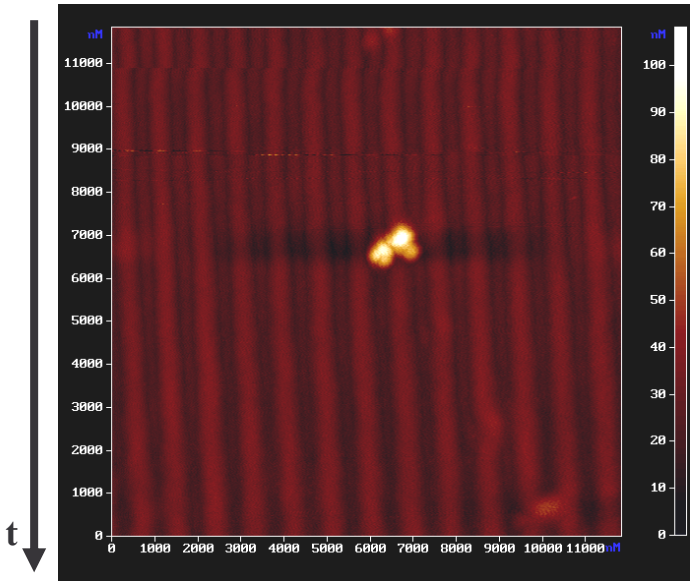
t
nM
11000
10000
9000
8000
7000
6000
5000
4000
3000
2000
1000
0
0 1000 2000 3000 4000 5000 6000 7000 8000 9000 10000 11000 nM
100
90
80
70
60
50
40
30
20
10
0

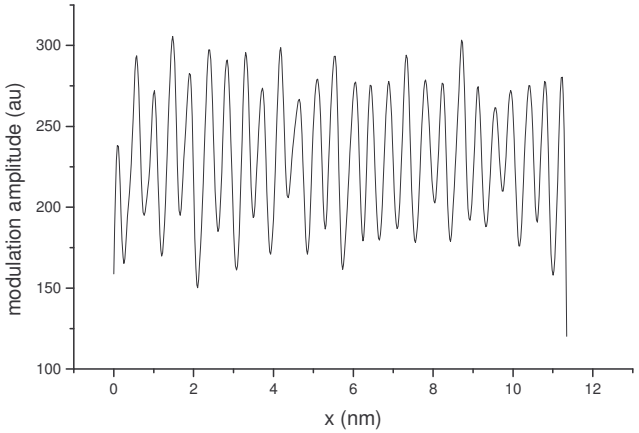
modulation amplitude (au)
300
250
200
150
100
0 2 4 6 8 10 12
x (nm)

C.

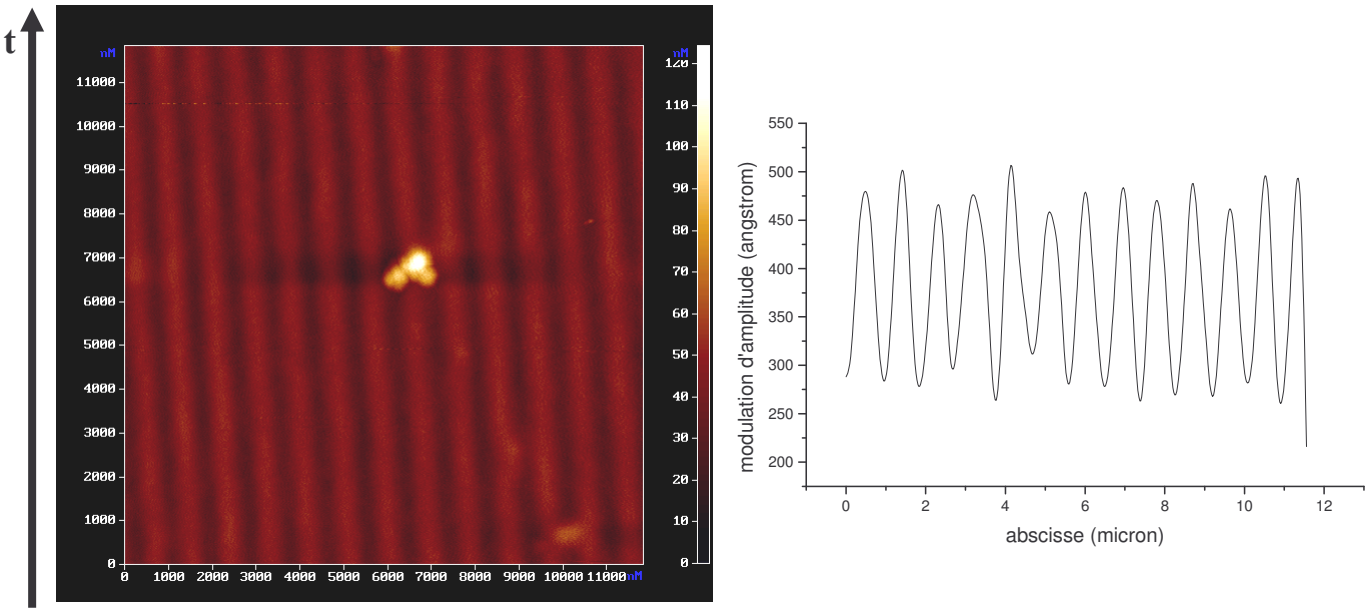

D.

Fig.52. Successive AFM images : A,B,C, D are images of a surface alternatively scanned upwards and downwards by an AFM tip as an interference patern is cast on the film. We can see the progressive formation of a double frequency grating on image B which then disappears to lead to a π change in the phase of the surface grating. This is evidenced by the defect located on the left and that was on a bump on picture A ends up in a trough on picture D.

This π phase difference of the surface relief grating has been observed by Perretti et al. with a set-up which allows them to monitor the phase relation between the light intensity grating cast on the surface and the surface relief grating that is being recorded. They show that after a few hours, the surface grating which was initially in phase opposition with the intensity pattern becomes in a matter of minutes in phase with it. They also evidence a decrease of the amplitude of modulation of the grating.

We also observe this decrease of the amplitude on some of the curves obtained with the in situ method and associated with such a change in phase.

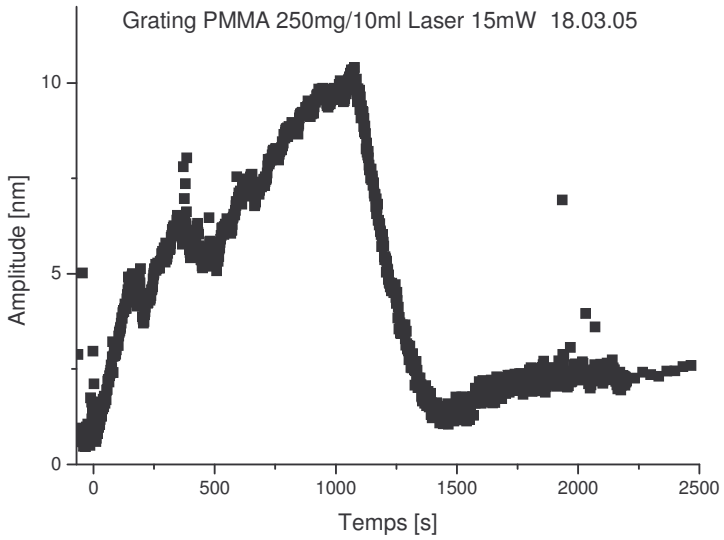

Fig. 53. Some grating's dynamics obtained with the real-time method display a sudden and drastic decrease of the amplitude of modulation.

These results suggest that the light-driven diffusion model proposed in the previous chapter does not account for all the phenomena that occur.

It may be in competition with a process such as the « field-dipole interaction » model proposed by Kumar et al. or such as the orientation gradient mechanism presented by Pedersen et al. for which the dipoles pile up at the points where the intensity is maximal.

However, as we noted in the previous section, maybe it is not the processes at work that should be called into question but only the structure of the electric field inside the film.

Lagugné-Labarthet et al. do not observe a π phase shift but they obtain a doubled frequency surface grating. Their interpretation is that the field in the layer is not just the result of the interfering beams. They assign, as the cause of the doubled frequency, the interference between the main beams and the first-order diffracted beam.

V.2.c. Formation of a spurious grating at a given angle.

The real-time observation of the formation of a surface relief grating also evidenced several times the formation of a spurious grating in a direction which makes an angle with the initial grating.

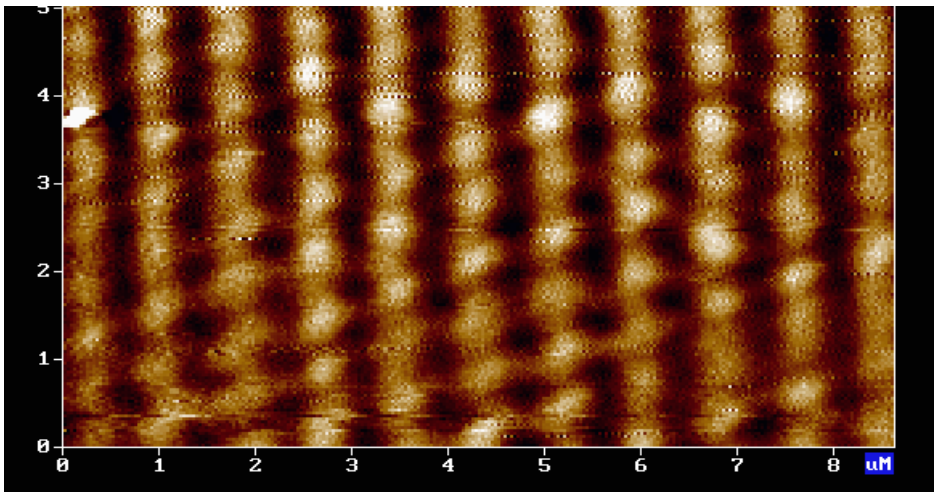

Fig. 54. AFM image of the surface of a PMMA DR1 film exposed to an intensity modulated interference pattern. After a few minutes of exposure, in addition to the expected vertical grating appears a second grating forming an angle with the fist one.

Once again, this may be a spurious effect due to the limited knowledge that we have of the actual electric field. This grating could be induced by the intensity pattern resulting from the interference caused by the AFM tip.

CONCLUSION AND PERSPECTIVES

Following the experiments carried out by other groups since the mid nineties, we have shown that the light-induced motion of azobenzene-containing materials cannot be reduced to a purely thermal phenomenon.

The polarization of light plays a major role in the process: matter is dragged along its direction, provided there is a non-zero intensity gradient along it.

Azobenzene-containing polymers are not the only azo-molecules to manifest such behaviour. Azobenzene-containing dendrimers proved to be highly photo-responsive materials.

The intensity of light and the thickness of the film come into play in the rate at which the matter is moved so that the essential parameter appears to be the total dose absorbed by the film.

This is adequately rendered by a light-driven diffusion model where molecules are assumed to perform a one-dimensional random-walk motion along the polarization direction.

This model also accounts for the effects of uniform light patterns where polarization only is modulated.

We showed that the saturation phenomenon cannot be explained by the diffusion alone. The bleaching of the azobenzene functions which leads to a loss of their optical activity plays a role in the limitation of the mass motion.

In the framework of this individual motion description, we can contemplate observing the shifts of isolated molecules, or groups of molecules, provided their interaction with the substrate on which they are deposited is well controlled.
Nevertheless, several observations suggest that competing phenomena may be at work.
First, real-time observations of the growth of surface gratings display a π change in their phase which takes place in a matter of minutes and which is often associated to a sudden decrease of the amplitude of the grating. Unless the electric field is drastically altered in the film, our model does not account for such a change.

The work presented in this memoir is focused on azobenzene containing polymers and dendrimers.
Nevertheless, it is important to conclude by underlining that light-induced motion is not restricted to azobenzene containing compounds. It also manifests itself in acrylate-rich hybrid glass materials exposed to UV light as evidenced by Pelissier et al.[59] in 1999, where matter also appears to flow from bright areas to darker ones.
In 2000, Srarnek et al.[60] observed a volume expansion under bandgap illumination in fluorozirconate of chalcogenide glasses.

A short run perspective is to replace the AFM that we used by a laser-free AFM Indeed, the red laser – which is reflected on the AFM scanning tip and which renders the surface topography – may induce spurious changes in the orientation of the chromophores. This unexpected effect of a red light on a liquid crystalline polyester – which absorbs at a shorter wavelength – was reported as early as 1993 by Ramanujam et al[61]. One year later, Kulinna et al.[62] from the same group evidenced a "biphotonic" phenomenon: azobenzenes first exposed to a 488 nm and then to a 633 nm laser end up parallel to the second writing beam. 488 nm photons are necessary to have a population of cis isomers and the role of the red laser is to photo-induce the cis-trans isomerization of the excess isomers[63].This phenomenon also comes

[59] Pelissier, S. ; Blanc, D. ; Andrews, M. P. ; Najafi, S.I. ; Tishchenko A.V. ; Parriaux, O. *Appl. Opt*., **38**, 6744-6748 (1999).

[60] R. Sramek, F. Smektala, W.X. Xie, M. Douay, P. Niay, *J. Non-Cryst. Solids*, **2000**, *277*, 39

[61] Ramanujam, P.S. ; Hvilsted, S. ; Andruzzi, F. *Appl. Phys. Lett.* **1993**, *62*, 1041.
[62] Kulinna, C. ; Zebger, I. ; Hvilsted, S.; Ramanujam, P.S.; Siesler, H. W. *Macromol. Symp.* **1994**, *83*, 161.
[63] Ramanujam, P.S. ; Hvilsted, S. ; Zebger, I.; Siesler, H. W. *Macromol. Rapid. Commun.* **1995**, *16*, 455.

into play in other materials such as methyl orange dispersed in poly(vinyl alcohol)[64] or methyl yellow in PMMA[65,66].

In addition to the spurious orientation that may generate the red laser of the AFM head, the scanning tip is also likely to diffract the blue laser in a "real-time" configuration.

Thus, in order to avoid any interaction between the red laser of the AFM and the layer, as well as any diffraction of the blue laser from the AFM tip, the group in which I worked is developing a laser-free device consisting in a vibrating vertical fork whose changes in the capacitance are used as the feed-back signal.

Another reason for developing such a device is that it opens perspectives of enhancing the optical field under the vertical tip which could lead to a focusing of the field on a surface as small as 10 nm by 10 nm.

As an introduction, we underlined that photo-responsive materials conjure up perspectives of miniaturization. By way of a conclusion, we would like to stress that the interest of light-controlled mass motion lies on the possibility of going beyond the limits of lithography. This requires focusing the electric field beyond the diffraction limit and can be achieved through near-field enhancement, provided we have a good understanding of the enhanced field.

This way, the light-induced control of nano-objects could be regarded as a "fine tuning" at scales that are beyond the scope of usual lithography.

---

[64] Liu, Y. ; Wang, H. ; Tian, M. ; Lin, J. ; Kong, X. ; Huang, S. ; Yu, J. *Opt. Lett.* **1995**, *20*, 1495.

[65] Bach, H. ; Anderle, K. ; Fuhrmann, T.; Wendorff, J.H. *J. Phys. Chem.* **1996**, *10*, 4135.

[66] Wu, P. ; Zu, B. ; Wu, X. ; Xu, J. ; Gong, X.; Zhang, G. Tang, G.; Chen, W. *Appl. Phys. Lett.* **1997**, *70*, 1224.

Annex I: density of activated molecules per unit time.

Let us consider a slice of PMMA DR1 film of infinitesimal thickness *dz* exposed to a laser beam of intensity I_0 propagating along the Z axis, perpendicular to the surface of area *S* of the film.

The number of photons that are absorbed in such a slice of area *S* and of thickness *dz* is equal to the energy absorbed divided by the energy of one photon.

The energy *dE* which is absorbed by a slice of surface *S* and of thickness *dz* during a given time *dt* can be expressed by using the definition of the absorption coefficient β.

Indeed, the intensity *dI* which is absorbed when the beam is going through *dz* is:

$$dI_{abs} = \beta.I.dz$$

Thus, the energy *dE* that is absorbed by a film of surface *S* during *dt* is:

$$dE = dI_{abs}.S.dt$$

$$dE = \beta.I.S.dz.dt$$

The energy of one photon of wavelength λ is:

$$\frac{hc}{\lambda}$$

So, the number of photons that are absorbed by the slice of volume *S.dz* during *dt* is equal to:

$$\frac{dE}{\frac{hc}{\lambda}} = \beta.I.\frac{\lambda}{hc}.S.dz.dt$$

This means that the number of photons absorbed per unit volume and unit time is:

$$\beta.I.\frac{\lambda}{hc}$$

A fraction of the azobenzenes that absorb a photon is isomerized from the trans form to the cis form. All the azobenzene-containing molecules being part of the pseudostilbene category as defined in section III.1., they come back to the trans form quite quickly either by absorbing a second photon or via thermal back isomerization.

The fraction of the molecules that perform a trans-cis-trans cycle is written Φ. It will be referred to as the quantum efficiency of the process.

Along with these isomerization cycles, the molecules undergo translation diffusion by an average amount l

Finally, the number of activated molecules which are put in motion per unit volume and unit time is:

$$n_d = \phi.\beta.\frac{\lambda}{hc}.I$$

Annex II: calculation of the interference pattern

In this annex, we calculate the resulting intensity and polarization patterns for two interfering beams with various states of polarization.

This interference pattern is formed on a layer.

The two interfering beams define a plane. The intersection of this plane with the layer defines the X axis.

The axis perpendicular to the plane defined by the beams is the Y axis which is in the plane of the layer.

The set of orthogonal axes is completed by the Z axis which is orthogonal to the plane of the layer.

As depicted below, we associate to each beam an orthogonal basis.

$\vec{k}_1$ and $\vec{k}_2$ are the wave vectors respectively associated to the beams (1) and (2)

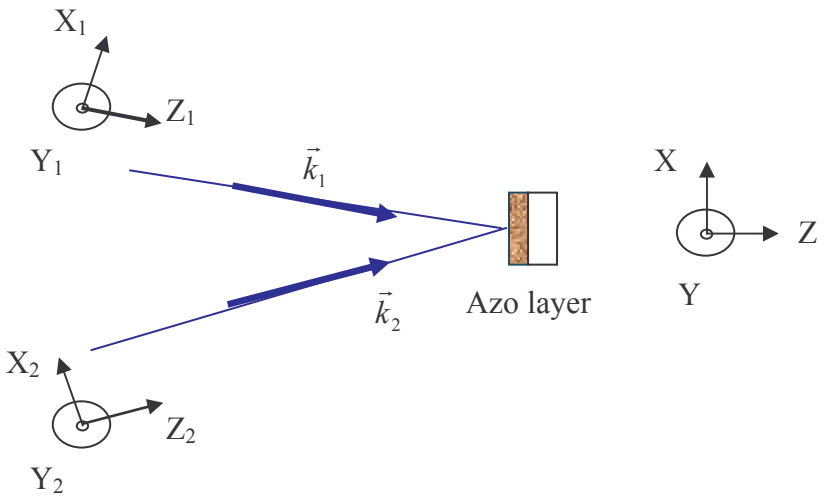

Fig. 55. Wave vectors and their associated basis interfering on an azo-layer.

In the (X,Y,Z) basis, their components are:

$$\vec{k}_1 = \frac{2\pi}{\lambda}\begin{bmatrix} \sin(\frac{\alpha}{2}) \\ 0 \\ \cos(\frac{\alpha}{2}) \end{bmatrix} \qquad \vec{k}_2 = \frac{2\pi}{\lambda}\begin{bmatrix} -\sin(\frac{\alpha}{2}) \\ 0 \\ \cos(\frac{\alpha}{2}) \end{bmatrix}$$

I. Circular polarization.

I.a. Fields rotating opposite ways.

The two interfering fields can be written:

$$\vec{E}_1 = \frac{E_0}{\sqrt{2}}\begin{bmatrix}1\\ i\\ 0\end{bmatrix}.e^{i(\vec{k}1.\vec{r}-\omega.t)} \qquad \vec{E}_2 = \frac{E_0}{\sqrt{2}}\begin{bmatrix}1\\ -i\\ 0\end{bmatrix}.e^{i(\vec{k}2.\vec{r}-\omega.t)}$$

Where $\vec{E}_1$ is expressed in the orthogonal basis (X_1,Y_1,Z_1) associated to beam (1) and $\vec{E}_2$ is expressed in the orthogonal basis (X_2,Y_2,Z_2) associated to beam (2).

The scalar products $\vec{k}_1.\vec{r}$ and $\vec{k}_2.\vec{r}$ can be computed by taking into account the fact that we are interested in the fields superposition on the plane defined by the free surface of the film, that is to say in the plane whose equation is *z = 0*.

Thus, $\vec{r} = \begin{bmatrix}x\\ y\\ 0\end{bmatrix}$. This way, we can write:

$$\vec{k}_1.\vec{r} = \frac{2\pi}{\lambda}\sin(\frac{\alpha}{2}).x \text{ and } \vec{k}_2.\vec{r} = -\frac{2\pi}{\lambda}\sin(\frac{\alpha}{2}).x\,.$$

Projected in the same (X,Y,Z) basis, the two electric field can be summed:

$$\vec{E}_{TOT} = \vec{E}_1 + \vec{E}_2 = \frac{E_0}{\sqrt{2}}\begin{bmatrix}\cos(\frac{\alpha}{2})\\ i\\ -\sin(\frac{\alpha}{2})\end{bmatrix}.e^{i(k\sin\frac{\alpha}{2}x-\omega.t)} + \frac{E_0}{\sqrt{2}}\begin{bmatrix}\cos(\frac{\alpha}{2})\\ -i\\ \sin(\frac{\alpha}{2})\end{bmatrix}\cdot e^{i(-k.\sin\frac{\alpha}{2}x-\omega.t)}$$

$$\vec{E}_{TOT} = \frac{E_0}{\sqrt{2}}\begin{bmatrix}2.\cos(\frac{\alpha}{2}).\cos(\frac{K}{2}x)\\ -2.\sin(\frac{K}{2}x)\\ -2i.\sin(\frac{\alpha}{2}).\sin(\frac{K}{2}x)\end{bmatrix}\cdot e^{-i\omega.t}$$

Thus, the resulting field is:

$$\vec{E}_{TOT} = \frac{E_0}{\sqrt{2}} \begin{bmatrix} 2.\cos(\frac{\alpha}{2}).\cos(k.\sin(\frac{\alpha}{2})x) \\ -2.\sin(k.\sin(\frac{\alpha}{2})x) \\ -2i.\sin(\frac{\alpha}{2}).\sin(k.\sin(\frac{\alpha}{2})x) \end{bmatrix} \cdot e^{-i\omega.t}$$

where $k = \frac{2\pi}{\lambda}$.

We can introduce the expression of the wave number K which appears in the intensity modulated pattern obtained for two linearly polarized interfering beams.

We showed that:

$$K = \frac{4\pi.\sin(\frac{\alpha}{2})}{\lambda}$$

Thus, the resulting field that reaches the free surface of the film is:

The intensity pattern which results from this superposition is:

$$I = \frac{1}{2}\mathrm{Re}(\vec{E}.\vec{E}^*)$$

Which gives:

$$I = \frac{1}{2}\frac{E_0^2}{2}4\left(\cos^2\frac{\alpha}{2}.\cos^2\frac{Kx}{2} + \sin^2\frac{Kx}{2} + \sin^2\frac{\alpha}{2}.\sin^2\frac{Kx}{2}\right)$$

It can be rewritten:

$$I = E_0^2\left(1 - \sin^2\frac{\alpha}{2}\cos Kx\right)$$

For an angle α equal to 32° between interfering beams, the modulation factor $\sin^2\frac{\alpha}{2}$ is around 0,08.

Thus, the intensity on the sample is only slightly modulated. It can be considered to be uniform.

It is the polarization direction, that is to say the direction of the electric field $\vec{E}_{TOT}$ that is strongly modulated.

The unitary vector $\vec{u}$ giving the polarization direction is:

$$\vec{u} = \frac{1}{1-\sin^2\frac{\alpha}{2}.\cos Kx}\begin{bmatrix} \cos(\frac{\alpha}{2}).\cos(\frac{K}{2}x) \\ \sin(\frac{K}{2}x) \\ i.\sin(\frac{\alpha}{2}).\sin(\frac{K}{2}x) \end{bmatrix}$$

The azobenzene function is assumed to move of a distance *l* along the direction of $\vec{u}$.
Thus, the shift can be written as a vector:

$$\vec{l} = \frac{l_0}{1-\sin^2\frac{\alpha}{2}.\cos Kx}\begin{bmatrix} \cos(\frac{\alpha}{2}).\cos(\frac{K}{2}x) \\ \sin(\frac{K}{2}x) \\ i.\sin(\frac{\alpha}{2}).\sin(\frac{K}{2}x) \end{bmatrix}$$

The effective mean free path, defined in chapter IV as the component l_x of $\vec{l}$ along the X direction in our experimental conditions, is:

$$l_x(x) = l_0.\cos(\frac{\alpha}{2}).\left|\cos(\frac{K}{2}x)\right|$$

The frequency for the electric field component is $\frac{K}{2}$ but the mean free path is an absolute value of the cosine function, which means that its frequency is K, just as the intensity modulation pattern that we get with a similar angle α between the interfering beams.
This absolute value leads to a discontinuity of the first derivative of $l_x(x)$.

I.b. Fields rotating the same way.
In their respective basis, the two interfering fields can be written:

$$\vec{E}_1 = \frac{E_0}{\sqrt{2}}\begin{bmatrix} 1 \\ i \\ 0 \end{bmatrix}.e^{i(\vec{k}1.\vec{r}-\omega.t)}$$

$$\vec{E}_2 = \frac{E_0}{\sqrt{2}}\begin{bmatrix} 1 \\ i \\ 0 \end{bmatrix}.e^{i(\vec{k}2.\vec{r}-\omega.t)}$$

Where $\vec{E}_1$ is expressed in the orthogonal basis (X_1,Y_1,Z_1) associated to beam (1) and $\vec{E}_2$ is expressed in the orthogonal basis (X_2,Y_2,Z_2) associated to beam (2).

As in the previous paragraph, we have:

$$\vec{k}_1.\vec{r} = \frac{2\pi}{\lambda}\sin(\frac{\alpha}{2}).x \text{ and } \vec{k}_2.\vec{r} = -\frac{2\pi}{\lambda}\sin(\frac{\alpha}{2}).x$$

Projected in the same (X,Y,Z) basis, the two electric field can be summed:

$$\vec{E}_{TOT} = \vec{E}_1 + \vec{E}_2 = \frac{E_0}{\sqrt{2}}\begin{bmatrix}\cos(\frac{\alpha}{2})\\ i\\ -\sin(\frac{\alpha}{2})\end{bmatrix}.e^{i(k\sin\frac{\alpha}{2}x-\omega.t)} + \frac{E_0}{\sqrt{2}}\begin{bmatrix}\cos(\frac{\alpha}{2})\\ i\\ \sin(\frac{\alpha}{2})\end{bmatrix}\cdot e^{i(-k.\sin\frac{\alpha}{2}x-\omega.t)}$$

Thus, the resulting field is:

$$\vec{E}_{TOT} = \frac{E_0}{\sqrt{2}}\begin{bmatrix}2.\cos(\frac{\alpha}{2}).\cos(k.\sin(\frac{\alpha}{2})x)\\ 2i.\cos(k.\sin(\frac{\alpha}{2})x)\\ -2i.\sin(\frac{\alpha}{2}).\sin(k.\sin(\frac{\alpha}{2})x)\end{bmatrix}\cdot e^{-i\omega.t}$$

II. Linear polarization.

II.a. s polarized beams.

The electric fields are linearly polarized in the plane along the Y axis.

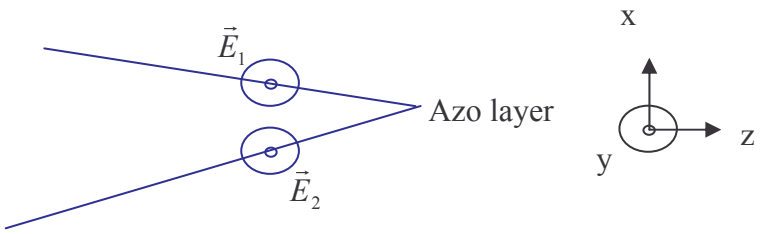

Fig. 56. s linearly polarized interfering beams.

The two interfering fields can be written:

$$\vec{E}_1 = E_0 \begin{bmatrix} 0 \\ 1 \\ 0 \end{bmatrix} . e^{i(\vec{k}1.\vec{r}-\omega.t)} \qquad \vec{E}_2 = E_0 \begin{bmatrix} 0 \\ 1 \\ 0 \end{bmatrix} e^{i(\vec{k}2.\vec{r}-\omega.t)}$$

Where $\vec{E}_1$ is expressed in the orthogonal basis (X_1,Y_1,Z_1) associated to beam (1) and $\vec{E}_2$ is expressed in the orthogonal basis (X_2,Y_2,Z_2) associated to beam (2).

The scalar products $\vec{k}_1.\vec{r}$ and $\vec{k}_2.\vec{r}$ can be computed by taking into account the fact that we are interested in the fields superposition on the plane defined by the free surface of the film, that is to say in the plane whose equation is *z = 0*.

Projected in the same (X,Y,Z) basis, the two electric field can be summed:

$$\vec{E}_{TOT} = \vec{E}_1 + \vec{E}_2 = E_0 \begin{bmatrix} 0 \\ 1 \\ 0 \end{bmatrix} . e^{i(k \sin\frac{\alpha}{2} x-\omega.t)} + E_0 \begin{bmatrix} 0 \\ 1 \\ 0 \end{bmatrix} \cdot e^{i(-k.\sin\frac{\alpha}{2} x-\omega.t)}$$

Thus, $\vec{r} = \begin{bmatrix} x \\ y \\ 0 \end{bmatrix}$. This way, we can write:

$$\vec{k}_1.\vec{r} = \frac{2\pi}{\lambda}\sin(\frac{\alpha}{2}).x \text{ and } \vec{k}_2.\vec{r} = -\frac{2\pi}{\lambda}\sin(\frac{\alpha}{2}).x .$$

Thus, the resulting field is:

$$\vec{E}_{TOT} = E_0 \begin{bmatrix} 0 \\ 2\cos(k.\sin(\frac{\alpha}{2})x) \\ 0 \end{bmatrix} \cdot e^{-i\omega.t}$$

where $k = \frac{2\pi}{\lambda}$.

The intensity pattern which results from this superposition is:

$$I = \frac{1}{2}\mathrm{Re}(\vec{E}.\vec{E}^*)$$

Which gives:

$$I = \frac{1}{2}E_0^2 4.\cos^2\left(k.\sin(\frac{\alpha}{2})x\right)$$

It can be rewritten:

$$I = E_0^2\left(1+\cos(Kx)\right).$$

Where:

$$K = \frac{4\pi}{\lambda}\sin\frac{\alpha}{2}$$

In this case, the visibility factor is equal to one.

II.b. p polarized beams.

The electric fields are linearly polarized in the plane along the Y axis.

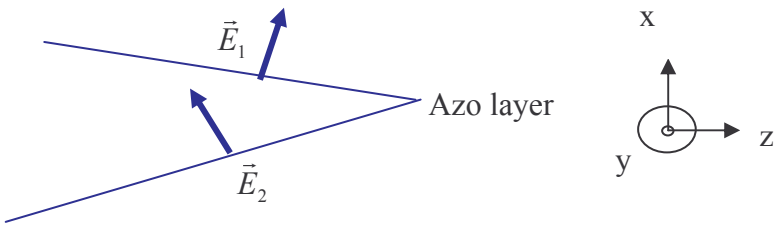

Fig. 57. p linearly polarized interfering beams.

The two interfering fields can be written:

$$\vec{E}_1 = E_0 \begin{bmatrix} 1 \\ 0 \\ 0 \end{bmatrix} . e^{i(\vec{k}1.\vec{r}-\omega.t)} \qquad \vec{E}_2 = E_0 \begin{bmatrix} 1 \\ 0 \\ 0 \end{bmatrix} e^{i(\vec{k}2.\vec{r}-\omega.t)}$$

Where $\vec{E}_1$ is expressed in the orthogonal basis (X_1,Y_1,Z_1) associated to beam (1) and $\vec{E}_2$ is expressed in the orthogonal basis (X_2,Y_2,Z_2) associated to beam (2).

The scalar products $\vec{k}_1.\vec{r}$ and $\vec{k}_2.\vec{r}$ can be computed by taking into account the fact that we are interested in the fields superposition on the plane defined by the free surface of the film, that is to say in the plane whose equation is $z = 0$.

Projected in the same (X,Y,Z) basis, the two electric field can be summed:

$$\vec{E}_{TOT} = \vec{E}_1 + \vec{E}_2 = E_0 \begin{bmatrix} \cos(\frac{\alpha}{2}) \\ 0 \\ \sin(\frac{\alpha}{2}) \end{bmatrix} . e^{i(k \sin\frac{\alpha}{2} x-\omega.t)} + E_0 \begin{bmatrix} \cos(\frac{\alpha}{2}) \\ 0 \\ -\sin(\frac{\alpha}{2}) \end{bmatrix} \cdot e^{i(-k.\sin\frac{\alpha}{2} x-\omega.t)}$$

Thus, $\vec{r} = \begin{bmatrix} x \\ y \\ 0 \end{bmatrix}$. This way, we can write:

$$\vec{k}_1.\vec{r} = \frac{2\pi}{\lambda}\sin(\frac{\alpha}{2}).x \text{ and } \vec{k}_2.\vec{r} = -\frac{2\pi}{\lambda}\sin(\frac{\alpha}{2}).x\,.$$

Thus, the resulting field is:

$$\vec{E}_{TOT} = E_0 \begin{bmatrix} 2\cos(\frac{\alpha}{2}).\cos(k\sin(\frac{\alpha}{2})x) \\ 0 \\ 2i\sin(\frac{\alpha}{2}).\sin(k\sin(\frac{\alpha}{2})x) \end{bmatrix} \cdot e^{-i\omega.t}$$

where $k = \frac{2\pi}{\lambda}$.

The intensity pattern which results from this superposition is:

$$I = \frac{1}{2}\mathrm{Re}(\vec{E}.\vec{E}^{*})$$

Which gives:

$$I = \frac{1}{2}E_0^2 4.\left(\cos^2(\frac{\alpha}{2}).\cos^2(k\sin(\frac{\alpha}{2})x) + \sin^2(\frac{\alpha}{2}).\sin^2(k\sin(\frac{\alpha}{2})x)\right)$$

It can be rewritten:

$$I = 2E_0^2\left(\left(\cos^2(\frac{\alpha}{2}) - \sin^2(\frac{\alpha}{2})\right).\cos^2(\frac{K}{2}x) + \sin^2(\frac{\alpha}{2})\right)$$

Where:

$$K = \frac{4\pi}{\lambda}\sin\frac{\alpha}{2}$$

$$I = 2E_0^2\left(\cos\alpha.\frac{1}{2}(1+\cos(Kx)) + \sin^2(\frac{\alpha}{2})\right)$$

Thus:

$$I = 2E_0^2(1+\nu\cos(Kx))$$

Where the visibility factor is:

$$\nu = \cos\alpha$$

The effective mean free path, as defined in section IV and in the configuration that we used is the component along the X axis.

So, we have: $l(x) = l_0\cos(\frac{\alpha}{2})$ where l_0 is the mean free path.

Annex III: mathematical relation between the first order diffraction peak and the amplitude of the surface relief grating.

The purpose of this annex is to show that the amplitude of the surface relief grating is not just proportional to the intensity of the first order diffraction peak that it leads to.

In the case of azobenzene-containing films exposed to an interference pattern, in addition to the sine shape topography grating there is a modulation of the refractive index of the layer resulting from the periodic variations of the ordering caused by polarized light.

In what follows, we neglect the effects of this modulation of index which would make the relation even more complex.

Thus, we consider a film whose free surface *h(x,t)* is defined by the equation:

$$h(x,t) = h_0 + h_1(t)\cos(Kx)$$

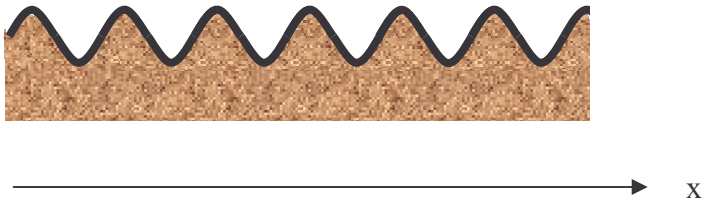

Fig. 58. The surface modulation is assumed to be periodic.

The resulting Fraunhofer intensity diffraction pattern is the square of the module of the amplitude. The amplitude is given by the Fourier Transform $\Im(T)$ of the transmittance *T(x,z)* of the film.

Taking into account both the absorption of the film through β and the change in phase resulting from the index difference between the film (*n* around 1,5) and the air (index close to 1), we write:

$$T(x,t) = \exp(-\beta h(x,t)).\exp\left(i\frac{2\pi}{\lambda}(n-1).h_1(x,t)\right)$$

In this case:

$$\Im(T) = \Im(\exp(-\beta h(x,t))) * \Im\left(\exp(i\frac{2\pi}{\lambda}(n-1).h_1(x,t))\right)$$

where $*$ is a convolution product.

Let us stick only to the part of the Fourier Transform related to the phase variation, that is to say the second part of the convolution product.

$\Im\left(\exp(i\frac{2\pi}{\lambda}(n-1).h_1(t).\cos(Kx)\right)$ gives a series of diffraction peaks.

The first order diffraction peak given by $\Im(a.\cos(Kx))$, where does not depend on x, is known to be proportional to $|J_1(a)|^2$. *$J_1(a)$* is the Bessel function (of the first kind) of order one.

So, the amplitude given by $\Im\left(\exp(i\frac{2\pi}{\lambda}(n-1).h_1(t).\cos(Kx)\right)$ leads, once we take the square of its module, to a first order diffraction peak whose intensity is proportional to:

$$\left|J_1\left(\frac{2\pi}{\lambda}(n-1).h_1(t)\right)\right|^2$$

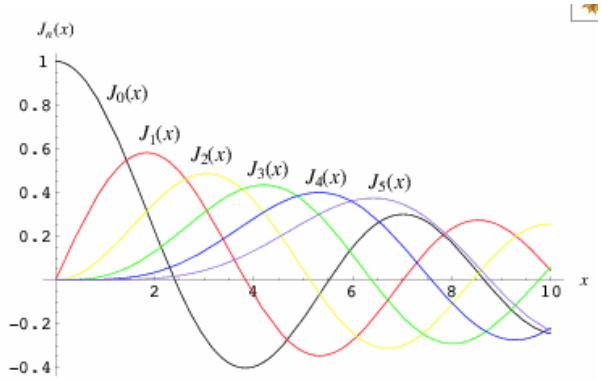

Fig. The red line is the Bessel function of order 1.

With λ = 473 nm, n = 1,5 for the PMMA DR1 film and h1(t) at least equal to 200 nm (since the modulation amplitude can reach this value for films of micronic thickness), we estimate the phase factor to be:

$$\frac{2\pi}{\lambda}(n-1).h_1 \approx 1{,}6$$

This means that $J_1\left(\frac{2\pi}{\lambda}(n-1).h_1\right)$ cannot be linearized. Indeed, a linearization would require a smaller value of the phase.

Even if we could linearize J_1, the intensity of the fist diffraction peak would be proportional to the square of the modulation amplitude h_1.

In all cases, the relation between the first order diffracted peak and the modulation amplitude is not straightforward.

It even becomes an issue for values the amplitude of which exceeds 300 nm.

BIBLIOGRAPHY

Rau, H. Photochemistry of azobenzenes. In: Rebek J., editor, *Photochemestry and Photophysics*, vol.2, Boca Raton, FL: CRC Press, 1990, p.119.

Kumar, G.; Neckers, D. Photochemistry of azobenzene-containg-polymers. *Chem. Rev.* 1989, 89, 1915.

Natansohn, A.; Rochon, P. Photoinduced motions in azobezene-based amorphous polymers: possible photonic devices. *Adv. Mat.* 1999, 11, 1387.

Delaire, J.; Nakatani, K. Linear and non-linear properties of photochromic molecules and materials. *Chem. Rev.* 2000, 100, 1817.

Labarthet, F.; Buffeteau, T., Sourisseau, C. Analyses of the diffraction efficiencies, birefringence, and surface relief gratings on azobenzene-containing polymer films. *J. Phys. Chem. B* 1998, 102, 2654.

Kim, D.; Lee, T.; Tripathy, S.; Jiang, X.; Li, L.; Kumar, J. Photo-fabrication of surface relief gratings on polymer films. *Macromol. Symp.* 1997, 116, 127.

Kumar, J.; Li, L.; Jiang, X.; Lee, T. ; Tripathy, S. Gradient force: the mechanism for surface relief grating formation in azobenzene functionalized polymers. *Appl. Phys. Lett.* 1998, 72, 2096.

Bian S, Li L, Kumar J, Kim D, Williams J, Tripathy S. Single laser beam-induced surface deformation on azobenzene polymer films. *Appl Phys Lett* 1998;73:1817.

Holme N, Nikolova L, Hvilsted S, Rasmussen P, Berg R, Ramanujam P. Optically induced surface relief phenomena in azobenzene polymers. *Appl Phys Lett* 1999;74:519.

Helgert M, Wenke L, Hvilsted S, Ramanujam P. Surface relief measurements in side-chain azobenzene polyesters with different substituents. *Appl Phys B* 2001;72:429.

Kim D, Li L, Jiang X, Shivshankar V, Kumar J, Tripathy S. Polarized laser induced holographic surface relief gratings on polymer films. *Macromolecules* 1995;28:8835.

Barrett C, Natansohn A, Rochon P. Mechanism of optically inscribed high-efficiency diffraction gratings in azo polymer films. *J. Phys. Chem.* 1996;100:8836.

Bian S, Williams J, Kim D et al. Photoinduced surface deformations on azobenzene polymer films. *J. Appl Phys* 1999;86:4498.

Fukuda T, Matsuda H, Shiraga T et al. Photofabrication of surface relief grating on films of azobenzene polymer with different dye functionalization. *Macromolecules* 2000;33:4220.

Naydenova I, Nikolova L, Todorov T, Holme N, Ramanujam P, Hvilsted S. Diffraction from polarization holographic gratings withsurface relief in side-chain azobenzene polyesters. *J Opt Soc Am B* 1998;15:1257.

Jiang X, Li L, Kumar J, Kim D, Shivshankar V, Tripathy S. Polarization dependent recordings of surface relief gratings onazobenzene containing polymer films. *Appl Phys Lett* 1996;68:2618.

Viswanathan N, Balasubramanian S, Li L, Tripathy S, Kumar J. Adetailed investigation of the polarization-dependent surface-relief-grating formation process on azo polymer films. *J Appl Phys* 1999;38:5928.

Jian X, Kumar J, Kim D, Tripathy S. Unusual polarization dependent optical erasure of surface relief gratings on azobenzene polymer films. *Appl Phys Lett* 1998;72:2502.

Srikhirin T, Laschitsch A, Neher D, Johannsmann D. Light-induced softening of azobenzene dye-doped polymer films probed with quartz crystal resonators. *Appl Phys Lett* 2000;77:963.

Andruzzi L, Altomare A, Ciardelli F, Solaro R, Hvilsted S, Ramanujam P. Holographic gratings in azobenzene side-chain polymethacrylates. *Macromolecules* 1999;32:448.

Barrett C, Rochon P, Natansohn A. Model of laser-driven mass transport in thin films of dye-functionalized polymers. *J Chem Phys* 1998;109:1505.

Sumaru K, Yamanaka T, Fukuda T, Matsuda H. Photoinduced surface relief gratings on azopolymer films: analysis by a fluid mechanics model. *Appl Phys Lett* 1999;75:1878.

Fukuda T, Sumaru K, Yamanaka T, Matsuda H. Photo-induced formation of the surface relief grating on azobenzene polymers analysis based on the fluid mechanics. *Mol Cryst Liq Cryst* 2000;345:587.

Bublitz D, Fleck B, Wenke L. A model for surface-relief formation in azobenzene polymers. *Appl Phys B* 2001;72:931.

Lefin P, Fiorini C, Nunzi J. Anisotropy of the photoinduced translation diffusion of azo-dyes. *Opt Mater* 1998;9:323.

Lefin P, Fiorini C, Nunzi J. Anisotropy of the photo-induced translation diffusion of azobenzene dyes in polymer matrices. *Pure Appl Opt* 1998;7:71.

Pedersen T, Johansen P, Holme N, Ramanujam P, Hvilsted S. Mean-field theory of photoinduced formation of surface reliefs in side-chain azobenzene polymers. *Phys Rev Lett* 1998;80:89.

Bian S, Liu W, Williams J, Samuelson L, Kumar J, Tripathy S. Photoinduced surface relief grating on amorphous poly(4-phenylazophenol) films. *Chem Mater* 2000;12:1585.

More specifically about molecular motors:

Feynman R. P., Leighton R.B., Sands M. *The Feynman Lectures on Physics* Addison-Wesley, Reading, MA, 1966) Vol.1, Ch. 46.

Adjari A, Prost J, *C.R. Acad. Sci. Paris II* 1993; 315:1635.

Magnasco M, *Phys. Rev. Lett.* 1993; 71:1477

Prost J, Chauvin JF, Peliti L, Ajari A, *Phys. Rev. Lett.* 1994 ; 72 :2652

Magnasco M, in *Flucuations and Order : The New Synthesis*, edited by MM Millonas, 1994, Springer-Verlag, Berlin.

Dolbeault J, Kinderlehrer D, Kowalczyk M, *Prétirage Ceremade no. 0244*, Hyke no. 2002-015, 19 pages.